

A NUMERICAL STUDY ON  
SPECIAL TRUSS MOMENT FRAMES

A THESIS SUBMITTED TO  
THE GRADUATE SCHOOL OF NATURAL AND APPLIED SCIENCES  
OF  
MIDDLE EAST TECHNICAL UNIVERSITY

BY

HARUN DENİZ ÖLMEZ

IN PARTIAL FULFILLMENT OF THE REQUIREMENTS  
FOR  
THE DEGREE OF MASTER OF SCIENCE  
IN  
CIVIL ENGINEERING

DECEMBER 2009

Approval of the thesis:

**A NUMERICAL STUDY ON SPECIAL TRUSS MOMENT FRAMES**

submitted by **HARUN DENİZ ÖLMEZ** in partial fulfillment of the requirements for the degree of **Master of Science in Civil Engineering Department, Middle East Technical University** by,

Prof. Dr. Canan Özgen  
Dean, Graduate School of **Natural and Applied Sciences**

Prof. Dr. Güney Özcebe  
Head of Department, **Civil Engineering**

Assoc. Prof. Dr. Cem Topkaya  
Supervisor, **Civil Engineering Dept., METU**

**Examining Committee Members:**

Prof. Dr. Mehmet Utku  
Civil Engineering Dept., METU

Assoc. Prof. Dr. Cem Topkaya  
Civil Engineering Dept., METU

Asst. Prof. Dr. Ayşegül Askan Gündoğan  
Civil Engineering Dept., METU

Asst. Prof. Dr. Afşin Sarıtaş  
Civil Engineering Dept., METU

Asst. Prof. Dr. Eray Baran  
Civil Engineering Dept., Atılım University

**Date:**

29.12.2009

**I hereby declare that all information in this document has been obtained and presented in accordance with academic rules and ethical conduct. I also declare that, as required by these rules and conduct, I have fully cited and referenced all material and results that are not original to this work.**

Name, Last name : Harun Deniz, Ölmez

Signature :

## ABSTRACT

### A NUMERICAL STUDY ON SPECIAL TRUSS MOMENT FRAMES

Ölmez, Harun Deniz  
M.Sc., Department of Civil Engineering  
Supervisor: Assoc. Prof. Dr. Cem Topkaya

December 2009, 92 pages

A three-phase numerical study was undertaken to address some design issues related with special truss moment frames (STMFs). In the first phase, the design approaches for distribution of shear strength among stories were examined. Multistory STMFs sized based on elastic and inelastic behavior were evaluated from a performance point of view. A set of time history analysis was conducted to investigate performance parameters such as the interstory drift ratio and the plastic rotation at chord member ends. The results of the analysis reveal that the maximum interstory drifts are not significantly influenced by the adopted design philosophy while considerable differences are observed for plastic rotations. In the second phase, the expected shear strength at vierendeel openings was studied through three dimensional finite element modeling. The results from finite element analysis reveal that the expected shear strength formulation presented in the AISC Seismic Provisions for Structural Steel Buildings is overly conservative. Based on the analysis results, an expected shear strength formula was developed and is presented herein. In the third phase, the effects of the load share and slenderness of X-diagonals in the special segment on the performance of the system were evaluated. Lateral drift, curvature at chord member ends, axial strain at X-diagonals and base shear were the investigated parameters obtained from a set of time history analysis. The results illustrate that as the load share of X-diagonals increases, the deformations decreases. Moreover, the slenderness of X-diagonals is not significantly effective on the system performance.

**Keywords:** Structural Steel, Truss, Moment Frame, Finite Element

## ÖZ

### MOMENT AKTARAN KAFES KİRİŞ SİSTEMLERİ ÜZERİNE BİR NÜMERİK ÇALIŞMA

Ölmez, Harun Deniz  
Yüksek Lisans, İnşaat Mühendisliği Bölümü  
Tez Yöneticisi: Doç. Dr. Cem Topkaya

Aralık 2009, 92 sayfa

Moment aktaran kafes kiriş sistemleri (STMF) ile ilgili bazı dizayn konularını ele almak için üç fazlı bir nümerik çalışmaya başlanmıştır. Birinci fazda, katlar arasındaki kesme dayanımının dağılımı için dizayn yaklaşımları incelenmiştir. Elastik ve inelastik davranışa göre boyutlandırılan çok katlı STMF sistemler performans açısından değerlendirilmiştir. Katlar arası ötelenme oranı ve başlık elemanları sonlarındaki plastik dönme gibi performans parametrelerini incelemek için bir takım zaman tanım analizleri yapılmıştır. Analiz sonuçları maksimum katlar arası ötelenmelerin uygulanan dizayn felsefesinden önemli derecede etkilenmediğini gösterirken, plastik dönmeler için önemli farklar gözlenir. İkinci fazda, üç boyutlu sonlu eleman modellemesi ile vierendeel açıklığında beklenen kesme dayanımı araştırılmıştır. Sonlu eleman analizlerinden elde edilen sonuçlar, AISC Çelik Yapılar için Sismik Şartname de bulunan beklenen kesme mukavemeti formülünün aşırı derecede güvenli tarafta kaldığını göstermektedir. Analiz sonuçlarına dayanılarak, bir beklenen kesme dayanımı formülü geliştirilmiş ve burada sunulmuştur. Üçüncü fazda, özel segmentteki X-diyagonallerin narinliğinin ve yük paylaşımının, sistemin performansı üzerindeki etkileri değerlendirilmiştir. Yatay ötelenme, başlık elemanı sonlarındaki eğrilik, X-diyagonallerdeki eksenel birim uzama ve taban kesme kuvveti, bir takım zaman tanım analizlerinden elde edilen ve incelenen parametrelerdir. Sonuçlar, X-diyagonallerin yük paylaşımının artması ile deformasyonlarda azalma olduğunu göstermektedir. Ayrıca, X-diyagonallerin narinliğinin sistemin performansı üzerinde önemli bir etkisi yoktur.

**Anahtar Kelimeler:** Çelik Yapı, Kafes, Moment Aktaran Çerçeve, Sonlu Eleman

To My Family and Gülnur

## **ACKNOWLEDGEMENTS**

I wish to express my deepest gratitude to my supervisor Assoc. Prof. Dr. Cem Topkaya for his invaluable support, guidance and insights throughout my research.

I wish to express my gratitude to my family, my love Gülnur and my friends for their understanding and invaluable support throughout my study.

This study was supported by a contract from the Scientific & Technological Research Council of Turkey (TÜBİTAK - 105M242). Also, the scholarship provided by TÜBİTAK during my graduate study is highly acknowledged.

## TABLE OF CONTENTS

ABSTRACT .....	iv
ÖZ .....	v
ACKNOWLEDGEMENTS .....	vii
TABLE OF CONTENTS .....	viii
LIST OF TABLES .....	x
LIST OF FIGURES .....	xi
CHAPTER	
1 INTRODUCTION .....	1
1.1 Description of Special Truss Moment Frames (STMFs) .....	1
1.2 Past Research on STMFs.....	4
1.3 Scope of the Thesis.....	11
2 MODELING ASSUMPTIONS AND VERIFICATION OF OPENSEES AND ANSYS SOFTWARE .....	12
2.1 Details of the Experimental Setup.....	12
2.2 Numerical Modeling Details – OPENSEES.....	13
2.2.1 Analysis Results.....	15
2.3 Numerical Modeling Details – ANSYS .....	19
3 AN EVALUATION OF STRENGTH DISTRIBUTION IN STMFs.....	21
3.1 Methodology and Design of STMFs .....	23
3.2 Static Pushover Analysis and Natural Periods .....	29
3.3 Time-History Analysis .....	36
3.3.1 Results of Time-History Analysis.....	38
3.3.1.1 Comparison with Pushover Analysis.....	38
3.3.1.2 Comparison of Different Designs .....	43
4 EVALUATION OF THE EXPECTED VERTICAL SHEAR STRENGTH FORMULATIONS .....	54
4.1 The Expected Vertical Shear Strength Formulations .....	54

4.2	Details of the Numerical Modeling .....	57
4.3	Evaluation of the Formulation Proposed by Chao and Goel (2008a) .....	59
4.4	The Proposed Formulation and Verification with the Analysis Results .....	61
5	AN EVALUATION OF SHEAR CONTRIBUTION BY X-DIAGONALS FOR STMF SYSTEMS .....	75
5.1	Methodology and Design of the Systems .....	75
5.2	Static Pushover Analysis and Natural Periods .....	79
5.3	Time-History Analysis .....	83
5.3.1	Results of Time-History Analysis .....	83
6	CONCLUSIONS .....	88
	REFERENCES .....	91

## LIST OF TABLES

### TABLES

Table 2.1: Section Properties of the Members .....	12
Table 2.2: Element Types of the Members .....	14
Table 3.1: Members outside the Special Segment .....	25
Table 3.2: Chord Member Sections .....	28
Table 3.3: Natural Periods of STMF Systems .....	35
Table 3.4: Details of Selected Ground Motion Records .....	37
Table 4.1: The Chord and Diagonal Sections Considered .....	58
Table 4.2: The Elastic Stiffness of the Chord Member for $2m L_s$ .....	60
Table 4.3: The Elastic Stiffness of the Chord Member for $2.5m L_s$ .....	60
Table 4.4: The Elastic Stiffness of the Chord Member for $3m L_s$ .....	61
Table 4.5: Comparison of Results for $2m L_s$ and A36 Type of Steel .....	65
Table 4.6: Comparison of Results for $2.5m L_s$ and A36 Type of Steel .....	66
Table 4.7: Comparison of Results for $3m L_s$ and A36 Type of Steel .....	67
Table 4.8: Comparison of Results for $2m L_s$ and A572-Gr50 Type of Steel.....	68
Table 4.9: Comparison of Results for $2.5m L_s$ and A572-Gr50 Type of Steel.....	69
Table 4.10: Comparison of Results for $3m L_s$ and A572-Gr50 Type of Steel.....	70
Table 4.11: Statistical Values for All Cases .....	74
Table 5.1: The Members outside the Special Segment.....	77
Table 5.2: The Members inside the Special Segment.....	78
Table 5.3: Natural Period and Mass of the STMF Systems.....	82
Table 5.4: The Average Values of the Results of Time History Analysis.....	84

## LIST OF FIGURES

### FIGURES

Figure 1.1: Typical Special Truss Moment Frames .....	1
Figure 1.2: Yielding Mechanism for STMFs .....	2
Figure 1.3: STMF with Piping and Duct Work .....	3
Figure 1.4: A Real Application of STMF .....	3
Figure 1.5: A Typical Load-Displacement Response for an STMF with Single Diagonals (Goel and Itani, 1994a) .....	5
Figure 1.6: A Typical Load-Displacement Response for an STMF with X-type Diagonals (Goel and Itani, 1994b) .....	5
Figure 1.7: A Typical Load-Displacement Response for an STMF with Vierendeel Segment (Basha and Goel, 1994) .....	6
Figure 2.1: The Dimensions of the Sub-assembly .....	13
Figure 2.2: Comparison of the Experimental Result with the Analytical Result Obtained for 1% Hardening .....	16
Figure 2.3: Comparison of the Experimental Result with the Analytical Result Obtained for 5% Hardening .....	16
Figure 2.4: Comparison of the Experimental Result with the Analytical Result Obtained for 10% Hardening .....	17
Figure 2.5: Details of Plastic Hinge Location .....	18
Figure 2.6: Comparison of Experimental Result with Numerical Result Obtained for Reduced Special Segment Length .....	18
Figure 2.7: Typical Finite Element Mesh .....	19
Figure 2.8: Comparison of Experimental Result with Finite Element Analysis Result .....	20
Figure 3.1: Geometrical Properties of the STMFs .....	23
Figure 3.2: Free Body Diagram – Same Strength in All Stories .....	24
Figure 3.3: Free Body Diagram – Shear Distribution from Elastic Analysis .....	26

Figure 3.4: Distribution of Shear Strength among the Stories (6 Story STMF) .....	27
Figure 3.5: Distribution of Shear Strength among the Stories (9 Story STMF) .....	27
Figure 3.6: Distribution of Shear Strength among the Stories (12 Story STMF) .....	28
Figure 3.7: Pushover Analysis Results for 6 Story STMF – Top Loading.....	29
Figure 3.8: Pushover Analysis Results for 6 Story STMF – Equal Lateral Loading.....	30
Figure 3.9: Pushover Analysis Results for 6 Story STMF – Inverted Triangular Loading .....	30
Figure 3.10: Pushover Analysis Results for 6 Story STMF – CGL Loading .....	31
Figure 3.11: Pushover Analysis Results for 9 Story STMF – Top Loading.....	31
Figure 3.12: Pushover Analysis Results for 9 Story STMF – Equal Lateral Loading...	32
Figure 3.13: Pushover Analysis Results for 9 Story STMF – Inverted Triangular Loading .....	32
Figure 3.14: Pushover Analysis Results for 9 Story STMF – CGL Loading .....	33
Figure 3.15: Pushover Analysis Results for 12 Story STMF – Top Loading.....	33
Figure 3.16: Pushover Analysis Results for 12 Story STMF – Equal Lateral Loading .....	34
Figure 3.17: Pushover Analysis Results for 12 Story STMF – Inverted Triangular Loading .....	34
Figure 3.18: Pushover Analysis Results for 12 Story STMF – CGL Loading .....	35
Figure 3.19: Response Spectra for the Selected Earthquake Records .....	36
Figure 3.20: Comparison of Pushover and Time-History Analysis Results for 6 Story STMF-PD.....	38
Figure 3.21: Comparison of Pushover and Time-History Analysis Results for 6 Story STMF-ED-IT .....	39
Figure 3.22: Comparison of Pushover and Time-History Analysis Results for 6 Story STMF-ED-CGL .....	39
Figure 3.23: Comparison of Pushover and Time-History Analysis Results for 9 Story STMF-PD.....	40

Figure 3.24: Comparison of Pushover and Time-History Analysis Results for 9 Story STMF-ED-IT .....	40
Figure 3.25: Comparison of Pushover and Time-History Analysis Results for 9 Story STMF-ED-CGL .....	41
Figure 3.26: Comparison of Pushover and Time-History Analysis Results for 12 Story STMF-PD .....	41
Figure 3.27: Comparison of Pushover and Time-History Analysis Results for 12 Story STMF-ED-IT .....	42
Figure 3.28: Comparison of Pushover and Time-History Analysis Results for 12 Story STMF-ED-CGL.....	42
Figure 3.29: Response of 6 Story STMF-PD.....	43
Figure 3.30: Response of 6 Story STMF-ED-IT.....	44
Figure 3.31: Response of 6 Story STMF- ED-CGL .....	44
Figure 3.32: Response of 9 Story STMF-PD .....	45
Figure 3.33: Response of 9 Story STMF-ED-IT.....	45
Figure 3.34: Response of 9 Story STMF-ED-CGL .....	46
Figure 3.35: Response of 12 Story STMF-PD .....	46
Figure 3.36: Response of 12 Story STMF-ED-IT.....	47
Figure 3.37: Response of 12 Story STMF-ED-CGL .....	47
Figure 3.38: Comparisons of Different Designs – 6 Story Systems .....	48
Figure 3.39: Comparisons of Different Designs – 9 Story Systems .....	49
Figure 3.40: Comparisons of Different Designs – 12 Story Systems .....	49
Figure 3.41: Ratio of Response Quantities – 6 Story Systems .....	50
Figure 3.42: Ratio of Response Quantities – 9 Story Systems .....	51
Figure 3.43: Ratio of Response Quantities – 12 Story Systems .....	51
Figure 4.1: Dimensions of the Numerical Model .....	57
Figure 4.2: The Normalized Moment Values versus Lateral Drift for A572-Gr50 Type of Steel .....	62
Figure 4.3: The Normalized Moment Values versus Lateral Drift for A36 Type of Steel.....	62

Figure 4.4: Ratio of Predicted to the Results of Analysis for Systems with A36 Type of Steel – 2m $L_s$ .....	71
Figure 4.5: Ratio of Predicted to the Results of Analysis for Systems with A36 Type of Steel – 2.5m $L_s$ .....	71
Figure 4.6: Ratio of Predicted to the Results of Analysis for Systems with A36 Type of Steel – 3m $L_s$ .....	72
Figure 4.7: Ratio of Predicted to the Results of Analysis for Systems with A572-Gr50 Type of Steel – 2m $L_s$ .....	72
Figure 4.8: Ratio of Predicted to the Results of Analysis for Systems with A572-Gr50 Type of Steel – 2.5m $L_s$ .....	73
Figure 4.9: Ratio of Predicted to the Results of Analysis for Systems with A572-Gr50 Type of Steel – 3m $L_s$ .....	73
Figure 5.1: Geometrical Properties of the Systems.....	76
Figure 5.2: Pushover Analysis Results for Systems Having X-Diagonals with Zero Slenderness.....	80
Figure 5.3: Pushover Analysis Results for Systems Having X-Diagonals with Infinite Slenderness.....	80
Figure 5.4: Cyclic Pushover Analysis Results for Systems Having X-Diagonals with Zero Slenderness .....	81
Figure 5.5: Cyclic Pushover Analysis Results for Systems Having X-Diagonals with Infinite Slenderness.....	82
Figure 5.6: Average Normalized Curvature Values for Different Design Types .....	84
Figure 5.7: Average Normalized Axial Strain Values for Different Design Types...	85
Figure 5.8: Average Base Shear Values for Different Design Types .....	85
Figure 5.9: Average Lateral Drift Values for Different Design Types.....	86

## CHAPTER 1

### INTRODUCTION

#### 1.1 Description of Special Truss Moment Frames (STMFs)

Special Truss Moment Frames (STMFs) can be used as a seismic load resisting system in buildings. STMFs can be thought of as a combination of moment resisting frames and eccentrically braced frames. In a typical STMF, girders are composed of trusses which have a weak special segment near the mid-span as shown in Figure 1.1.

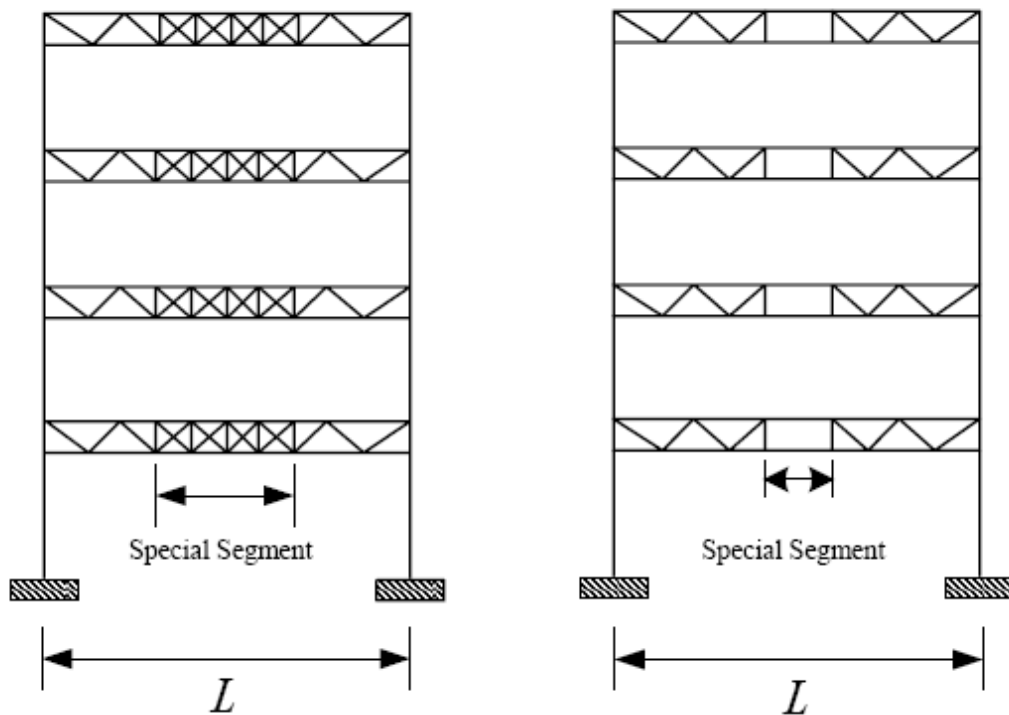


Figure 1.1: Typical Special Truss Moment Frames

The truss consists of top and bottom chord members, verticals, and diagonals. Like the eccentrically braced frames, a weak link called the special segment, is present in all STMFs. This weak region can be in the form of a vierendeel segment or a vierendeel with X-braces. The idea is that when earthquake forces act on the structure, high shear forces will develop at the mid-span of the truss leading to yielding in this region. For the vierendeel type systems plastic hinges form at the top and bottom chord ends. On the other hand, for vierendeel with X-braces, the braces yield under tension and buckle under compression, while plastic hinges form at the chord ends. A typical yielding mechanism for STMFs is given in Figure 1.2.

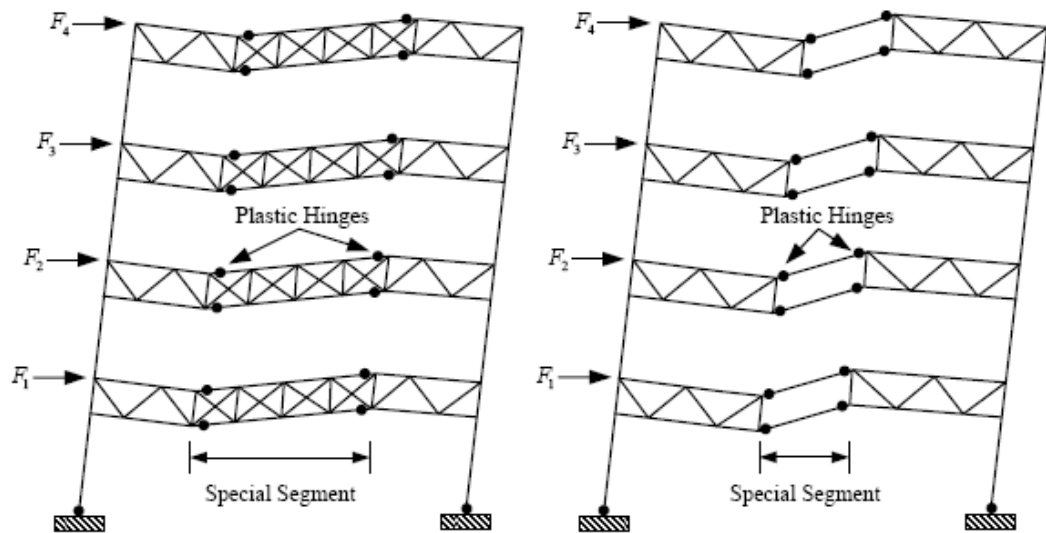


Figure 1.2: Yielding Mechanism for STMFs

There are various advantages of using STMF systems which can be summarized as follows:

- These systems require simple details for moment connections.
- These systems are more economical than solid web beam frames
- Being lighter the truss girders can be used for longer spans.
- These systems have greater overall structural stiffness due to deeper girders
- Web openings can be used for piping and duct work as shown in Figure 1.3.



Figure 1.3: STMF with Piping and Duct Work

There are design provisions for STMFs presented in the AISC Seismic Provisions for Steel Buildings. Unfortunately, no code provisions exist in Eurocodes. The development of STMFs is attributable to Professor Goel at The University of Michigan and his colleagues. The STMF system is relatively new and quite a few buildings in the United States utilize this type of framing as shown in Figure 1.4.



Figure 1.4: A Real Application of STMF

The following sections outline the research work conducted to date in chronological order to demonstrate the development of these systems.

## 1.2 Past Research on STMFs

### *Goel and Itani (1994a)*

This is the first paper published on STMFs. The authors aimed to develop an open-web truss-moment frame in this research. A prototype building was selected and designed according to 1988 UBC requirements. Based on the design, a total of three full-scale half-span truss column sub-assemblages were tested under large reversed cyclic displacements. The truss girders had single diagonal members. Under cyclic loading these single diagonals buckled and yielded. Because there was a single diagonal at each panel, the load carrying capacity decreased significantly after buckling. Representative load displacement diagram is given in Figure 1.5.

Apart from the experimental studies, the authors also conducted numerical analysis to investigate the earthquake performance of single diagonal systems. The authors concluded that the hysteretic behavior under cyclic loading is very poor because of buckling and early fracture of truss web members. In addition, the inelastic dynamic response analysis showed that such systems respond poorly to severe ground motions with large story drifts and excessive inelastic deformations of truss web members and columns.

### *Goel and Itani (1994b)*

In a companion paper, the authors investigated the potential of using an X-diagonal system for STMFs. After observing the poor behavior of single diagonals the authors decided to use an X-type system. This way when one of the diagonals buckles under compression the other diagonal is under tension and should be capable of carrying the shear forces. A one story sub-assemblage consisting of a full-span truss and two columns at the ends was tested. Two sub-assemblages were tested and the difference was the applied displacement protocol. In general, the specimens showed stable behavior. A representative load displacement behavior is given in Figure 1.6.

The authors conducted time-history analysis to investigate the performance of truss girders with X-type diagonals. The findings of this research showed that the

proposed system can be an excellent and efficient seismic resistant framing system for certain classes of building structures.

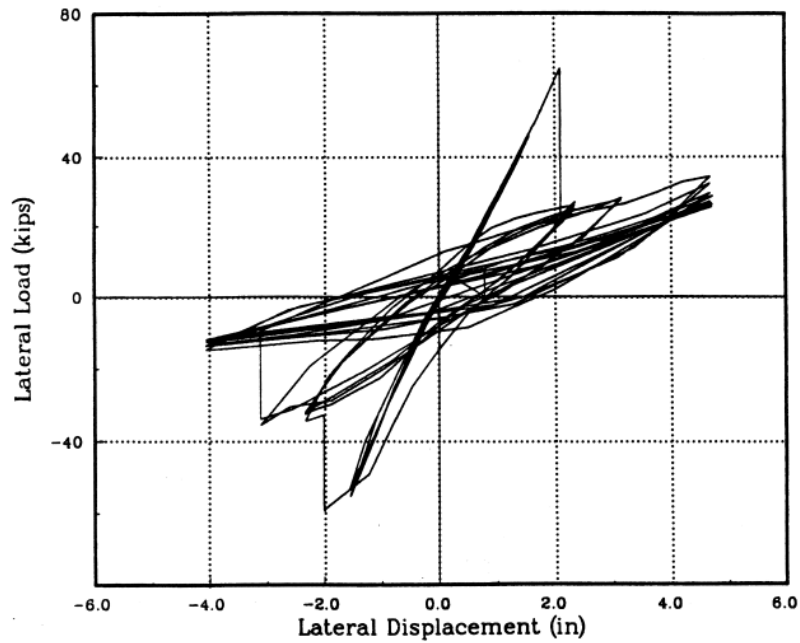


Figure 1.5: A Typical Load-Displacement Response for an STMF with Single Diagonals (Goel and Itani, 1994a)

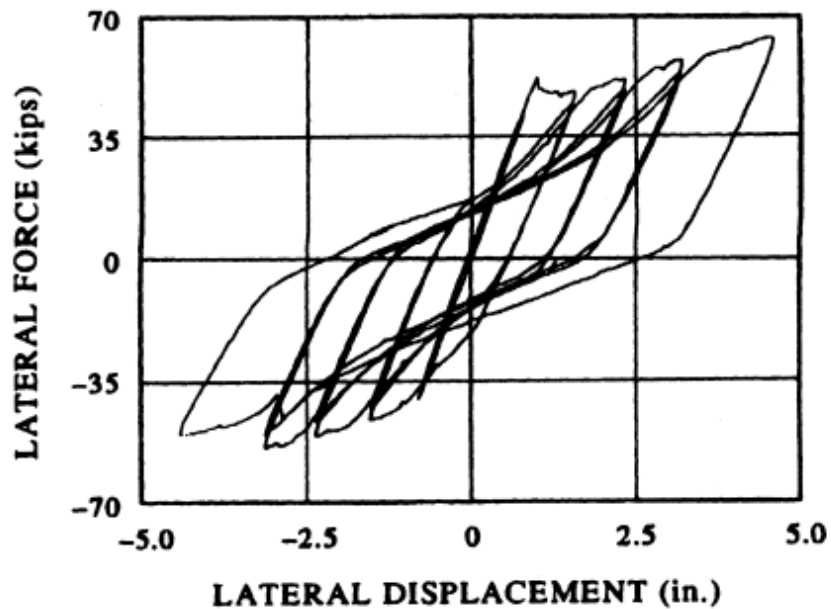


Figure 1.6: A Typical Load-Displacement Response for an STMF with X-type Diagonals (Goel and Itani, 1994b)

***Basha and Goel (1994)***

The authors investigated the potential use of a vierendeel segment for dissipating energy. The previous research work by Goel and Itani (1994a, 1994b) concentrated on using diagonals in the special segment. These diagonals may restrict the available space. In this study, a vierendeel panel was proposed as an alternative configuration of the special segment. The work consisted of an experimental program followed by a set of numerical analysis.

In the experimental program STMFs with and without gravity loading were studied. A representative floor plan was selected for a 4-story building and the STMF design was conducted according to 1991 UBC provisions. Based on the designed sections, a one-bay sub-assembly of a typical story was experimented. As mentioned before, the sub-assembly was first tested without the application of gravity loads. Two displacement histories were applied. Afterwards the same kind of a sub-assembly was tested under the presence of point loads that simulate gravity loading. All tests revealed that the sub-assembly provide stable hysteretic behavior as shown in Fig. 1.7.

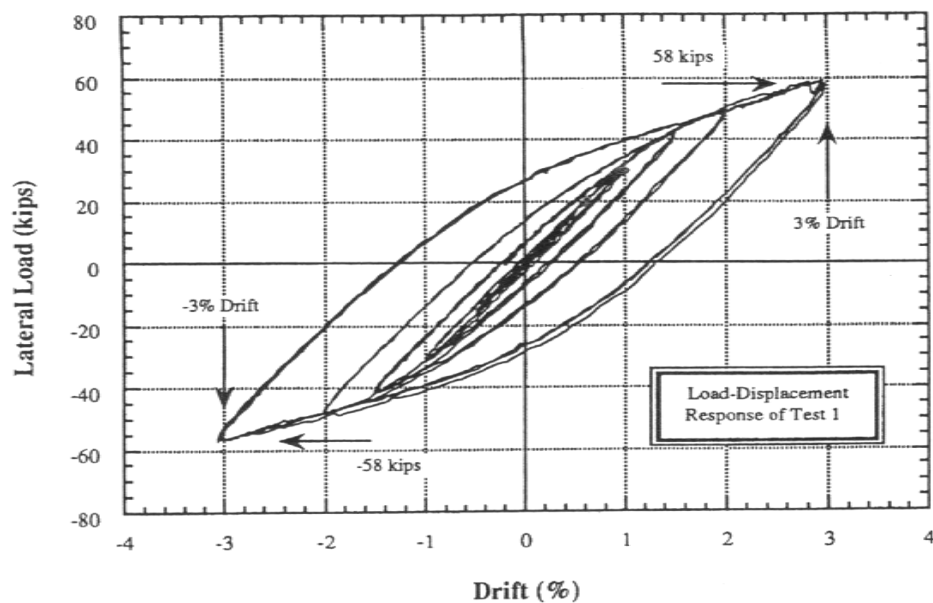


Figure 1.7: A Typical Load-Displacement Response for an STMF with Vierendeel Segment (Basha and Goel, 1994)

A detailed investigation of the specimen behavior is presented in Chapter 2. Therefore, the specimen details are presented later.

The authors concluded that the responses of the sub-assemblages under lateral loads alone as well as under combined gravity and lateral loads were full and stable with no pinching and degradation. A set of modeling recommendations were presented for systems with a vierendeel segment. The dynamic response from numerical studies was excellent.

***Goel, Rai, and Basha (1998)***

In this research report the authors present guidelines for the design of STMFs. The limit state design philosophy applied to STMFs was presented. The special segment of the STMF is expected to yield and dissipate energy, while the rest of the system remains elastic. Only yielding at the column bases is permitted. In this guide several rules based on limit state design were given to proportion the truss members that are outside the special segment. Design of STMFs with vierendeel segment and with X-bracing was explained by making use of examples. Both hand calculations and computer analysis were given. After presenting the design of the STMFs authors presented some analytical results on these representative designs. Basically, pushover analysis and nonlinear time history analysis were conducted to investigate the performance of these systems. The report concluded with a short set of design recommendations that was adopted by the 1997 UBC specification.

***Parra-Montesinos, Goel, and Kim (2006)***

In this research the authors studied the performance of steel double-channel built-up chords of STMF. Rather than experimenting the whole system, the researchers concentrated on the chord members. Back-to-back channel sections may be used to increase the base shear capacity for STMF with a vierendeel segment. In this experimental program, six cantilever double-channel members were subjected to reverse cyclic loading to observe their performance. The main parameters were the stitch spacing and lateral bracing for the channel members. The authors concluded that the current AISC requirements for stitch spacing and lateral bracing are not

adequate to ensure large rotation capacity in double channel built-up members. A new equation was proposed based on the test results.

***Chao and Goel (2008a)***

The primary goal of the researchers was to propose a modified expression for the expected shear strength of the special segment. Members outside of the special segment were proportioned using capacity design principles and the applied loads were derived based on the shear strength of the special segment. Over the years, Goel and his colleagues developed expressions for the expected shear strength and their developments lead to the code provisions. These expressions take into account the formation of plastic hinges at the chord ends, yielding of diagonals in tension, buckling of diagonals in compression, flexibility of chord members and etc. Chao and Goel identified that the expected shear strength expression presented in the AISC specification may lead to overdesign of the members if the moment of inertia of the member is large. In order to develop a modified expression, the authors conducted a set of nonlinear static and dynamic analyses. Based on the analyses results the authors concluded that the AISC equation significantly overestimates the expected shear strength. Based on the findings of the numerical analysis a more refined expression was developed.

***Chao and Goel (2008b)***

In this research, the authors developed a performance based plastic design methodology for STMFs. Before this research work, the STMFs were designed using elastic analysis methods. The use of elastic analysis to proportion the members lead to nonuniform distributions of story drifts and yielding in special segments along the height of the structure. In order to achieve a more uniform yielding and story drifts the authors developed a design methodology. The performance based plastic design approach is based on energy theorems and does not require the use of a response modification factor. The procedure is performance based, therefore, the target drift has to be known or determined in advance. The authors derived an expression for a modified base shear, based on energy concepts. The modified base shear is dependent on the target drift, preselected yield mechanism, and code-specified elastic

design spectral value for a given hazard level. The modified base shear actually corresponds to the base shear at the structural collapse level. Therefore, this base shear value can be directly used in the plastic design of the structure. The code specified base shear value is generally less than the modified base shear, and corresponds to the level at the first significant yield. The procedure uses a lateral load profile that was developed by Chao, Goel, and Lee (2007). This lateral load profile was developed based on different steel structural systems such as moment frames, concentrically braced frames, eccentrically braced frame, and STMFs.

The authors verified the proposed performance based design approach by a 9-story STMF subjected to SAC ground motions. The analysis results revealed that the design based on the proposed methodology resulted in uniform interstory drifts. In addition, the maximum amount of drift was less than the target value.

#### ***AISC Code Provisions for STMFs***

AISC Seismic Provisions for Structural Steel Buildings (2005) provide a few rules for the design of STMFs. The span length and depth of the truss is limited to 20m and 1.8m, respectively. Columns and truss segment outside the special segment should be designed to remain elastic during a seismic event. The length of the special segment should be between 0.1 to 0.5 times the truss span length. The length to depth ratio of the special segment should be kept between 1.5 and 0.67. The special segment can contain vierendeel panels or X-braced panels. For X-braced panels the bracing can be from flat bars that are connected at the intersection of braces.

The shear strength of the special segment shall be calculated as the sum of the available shear strength of the chord members through flexure, and the shear strength corresponding to the available tensile strength and 0.3 times the available compressive strength of the diagonal members, when they are used. The shear strength ( $V_n$ ) can be calculated as follows according to the AISC definition:

$$V_n = \frac{4M_{nc}}{L_s} + (P_{nt} + 0.3P_{nc}) \sin \alpha \quad \text{Equation (1.1)}$$

Where;

$M_{nc}$ : nominal flexural strength of a chord member of the special segment

$L_s$ : length of the special segment

$P_{nt}$ : nominal tensile strength of a diagonal member of the special segment

$P_{nc}$ : nominal compressive strength of a diagonal member of the special segment

$\alpha$ : angle of diagonal members with the horizontal.

For special segments with X-bracing, the top and bottom chord members shall provide at least 25 percent of the required vertical shear strength.

Strength of non-special segment members shall be determined from capacity design. The AISC Specification provides the following equation for calculating the expected shear strength of the special segment ( $V_{ne}$ ):

$$V_{ne} = \frac{3.75R_y M_{nc}}{L_s} + 0.075EI \frac{(L - L_s)}{L_s^3} + R_y (P_{nt} + 0.3P_{nc}) \sin \alpha \quad \text{Equation (1.2)}$$

Where;

$EI$ : flexural elastic stiffness of a chord member of the special segment

$L$ : span length of the truss

$R_y$ : ratio of the expected yield stress to the specified minimum yield stress.

Once the expected strength of the special segment is calculated from Equation 1.2, then forces on the columns and truss members outside the special segment can be calculated using this maximum amount of shear produced. The Equation 1.2 takes into account the increased moments at the chord member ends due to the strain hardening. In addition, the material overstrength is accounted for using the  $R_y$  factor. Recent research conducted by Chao and Goel (2008a) showed that Equation 1.2 provides overestimates of the expected shear strength. Authors proposed an alternative equation for replacement of the code equation.

AISC Specification mandates that the chord members and diagonal web members within the special segment must be seismically compact. In addition, lateral bracing should be provided at both ends of the top and bottom chord members.

### **1.3 Scope of the Thesis**

The thesis work consists of a three phase numerical study on STMFs. In the first phase the design philosophy for multistory STMFs were evaluated. The distribution of shear strength among the stories was studied through dynamic time-history analyses. In the second phase, the expected shear strength formulations for vierendeel segment were evaluated. The expected shear strength was studied through detailed three dimensional finite element models of one story STMFs. In the third phase the effect of load share between chord members and X-diagonals were studied taking into account different diagonal slenderness values. Time-history analyses were conducted to evaluate the response of single story systems in phase three.

The numerical analyses for phase 1 and 3 were conducted using OPENSEES while the finite element calculations were performed using ANSYS. In Chapter 2, the numerical models were verified against the experimental results. The details of the studies and results of phases 1, 2, and 3 are given in Chapters 3, 4, and 5, respectively. Finally, the conclusions are presented in Chapter 6.

## CHAPTER 2

### MODELING ASSUMPTIONS AND VERIFICATION OF OPENSEES AND ANSYS SOFTWARE

The verification of software was conducted by utilizing the experimental results presented by Basha and Goel (1994). Only STMFs with a vierendeel segment is treated herein.

#### 2.1 Details of the Experimental Setup

Basha and Goel (1994) conducted quasi-static experiments on a sub-assembly as shown in Figure 2.1. In this setup, lateral loading was applied to one of the columns using a hydraulic actuator. A link beam with pinned ends was connected to the column tops to transfer this lateral load to both columns. The specimen consisted of a truss member with a vierendeel segment. The sizes of the members are summarized in Table 2.1. All angles were A572 steel with a nominal yield strength of 50 ksi. The measured yield strength from coupon tests ranged between 60 to 63 ksi. All sandwich plates were A36 steel with a nominal yield strength of 36 ksi. The measured yield strength from coupon tests was 48 ksi. The sandwich plates were welded between the angles and were extended beyond the special segment to provide the development length of the built-up section.

Table 2.1: Section Properties of the Members

Member	Section	F <sub>y</sub> ksi
Chords within the Special Segment	2L 3x3x1/2	50
	PL 2-1/4x1	36
Chords outside the Special Segment	2L 3x3x1/2	50
Diagonals	2L 2-1/2x2-1/2x1/4	50
Verticals	2L 1-1/2x1-1/2x1/4	50

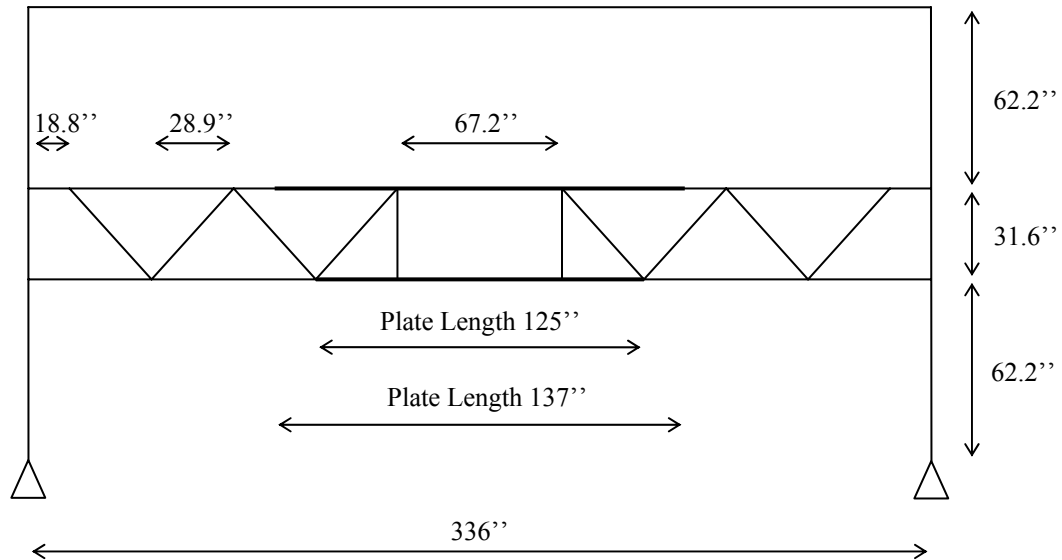


Figure 2.1: The Dimensions of the Sub-assembly

The loading history, which was applied to the sub-assembly during the experiment, was as follows:

- Two cycles of 0.5 % drift
- Two cycles of 1 % drift
- Two cycles of 1.5 % drift
- Two cycles of 2 % drift
- Three cycles of 3 % drift

## 2.2 Numerical Modeling Details – OPENSEES

A 2-D model of the sub-assembly was prepared in OPENSEES. Because out of plane deformations were prevented during the experiment, a 2-D model was sufficient to capture the response of the specimen. The element types used in modeling are summarized in Table 2.2. As shown from this table, chords inside the special segment were modeled with nonlinear beam-column elements, because significant inelastic behavior is expected in this region. Similarly the chords outside the special segment, the verticals and the diagonals were also modeled using nonlinear beam-column elements. Actually during the experiment, the researchers observed inelastic behavior in these members especially for the ones that were close

to the special segment. Actual yield strengths and the dimensions presented in Figure 2.1 were used in modeling. The link beam was modeled using a truss element and columns were modeled using elastic beam-column elements.

Table 2.2: Element Types of the Members

<b>Member</b>	<b>Element</b>
Chords within the Special Segment	nonlinearBeamColumn Element
Chords outside the Special Segment	nonlinearBeamColumn Element
Diagonals	nonlinearBeamColumn Element
Verticals	nonlinearBeamColumn Element
Columns	elasticBeamColumn Element
Link Beam	truss Element

All cross sections were modeled using fiber elements. The nonlinear material behavior of steel was modeled using a built-in material model named “steel02”. This material model is well suited for cyclic behavior of steel and accounts for the Bauschinger effect.

In the previous analytical studies conducted by Basha and Goel (1994), researchers used a lumped plasticity element to model the special segment chord members. This element requires the moment versus rotation behavior of plastic hinges at the member ends. Basha and Goel (1994) stated that the customary moment rotation relationships used for moment resisting frames are not suitable for modeling the STMFs. The key point here is the selection of a post yield slope to represent the strain hardening effects. In general a post yield slope of 5% is used for representing the moment rotation response for typical members in moment resisting frames. Basha and Goel (1994) have identified that using a 5% slope is inadequate for modeling the STMFs. Because the special segment lengths are rather short in these kinds of systems, the curvature and rotation demands are significantly different. By using a trial and error procedure, Basha and Goel (1994) concluded that using a 10% post yield slope is sufficient for modeling purposes.

The modeling technique adopted in this thesis is different than the one of Basha and Goel (1994). The nonlinear beam-column element, used in modeling the chord members, was combined with fiber sections to model the cross section behavior. The element requires inputting a material stress-strain law to convert the stresses to stress resultants. Therefore, an explicit moment-rotation behavior is not needed in these kinds of elements. The strain hardening behavior is treated at the material level by changing the hardening modulus value.

In order to calibrate the numerical model with the experimental results, three different hardening modulus values were considered in this study. These modulus values represent 1%, 5%, and 10% of the elastic modulus of steel.

### **2.2.1 Analysis Results**

The load displacement responses obtained using the OPENSEES software, were compared with the experimental results in Figures 2.2, 2.3, and 2.4. According to the comparisons, numerical modeling with a hardening modulus of 5% of the elastic modulus gives the best result among the three. The maximum amount of lateral load measured during testing was 58 kips. The maximum amount of lateral load from numerical analysis was 56.5 kips using a 5% post yield slope. Moreover, in all cases the elastic stiffness from the simulations was 20 kips/in which is identical to the experimentally observed value.

Although using a hardening modulus of 5% of the initial elastic modulus gives promising results, this assumption is not consistent with real observations on material behavior. Usually the hardening modulus from cyclic material tests ranges between 0.5 and 1 percent of the initial elastic modulus. Therefore, using 5% of the initial modulus is unrealistic and can have adverse effects on the analysis results. In fact preliminary analysis using a 5 percent slope showed significant amount of hardening for these systems. Because of these reasons, additional verification studies were conducted in this thesis to better simulate the system by using realistic hardening values.

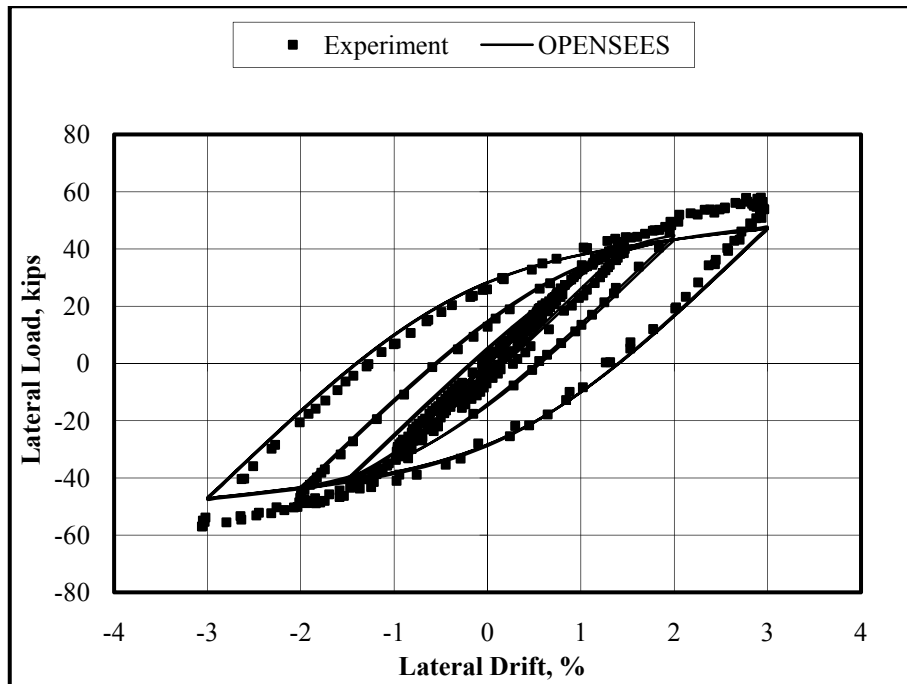


Figure 2.2: Comparison of the Experimental Result with the Analytical Result Obtained for 1% Hardening

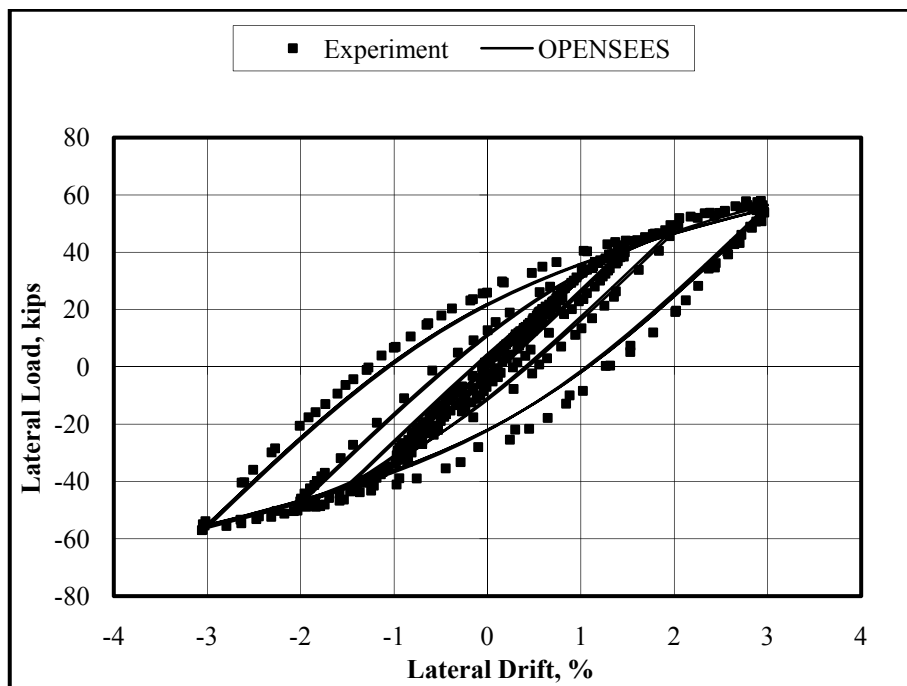


Figure 2.3: Comparison of the Experimental Result with the Analytical Result Obtained for 5% Hardening

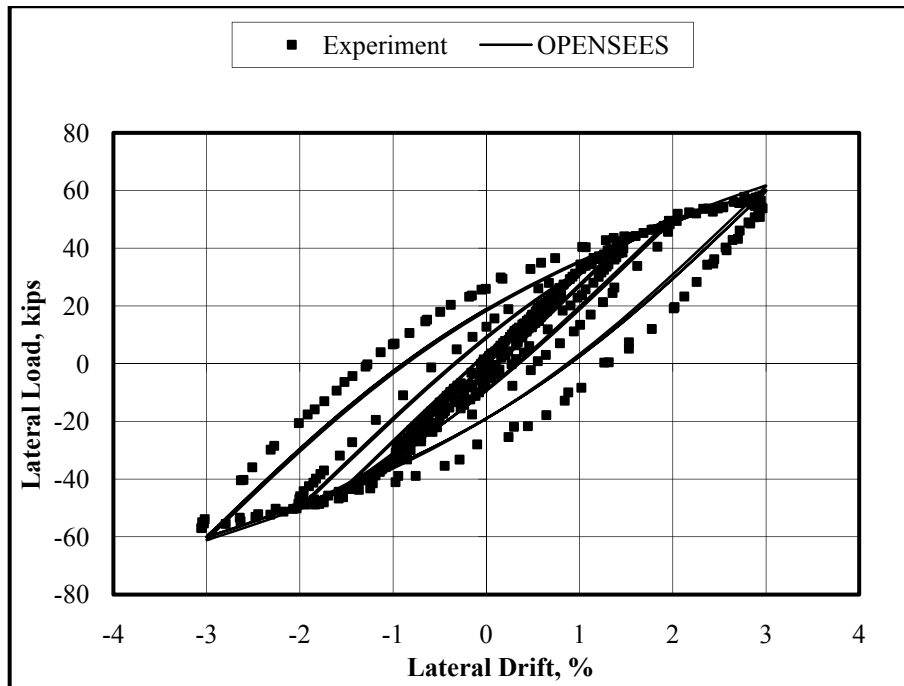


Figure 2.4: Comparison of the Experimental Result with the Analytical Result Obtained for 10% Hardening

A careful examination of the truss geometry as depicted by Basha and Goel (1994) indicated that the length of the special segment is 67.2 inches. This value corresponds to the distance between the centerlines of the two verticals that were placed at both ends of the chord members. A more accurate computer model should consider the clear distance between the verticals. In addition, during the formulation of the beam-column elements the integration is carried at the ends and these are the locations where the plastic hinges occur. In reality, however, plastic hinges penetrate into the member and can form further away from the ends. Usually the plastic hinges can form at a distance between half of the member depth to a full member depth. Taking these into account, a revised length equal to 61.2 inches was used in the computer modeling. As shown in Figure 2.5, this length was obtained by considering the clear distance between the verticals (i.e. subtracting the depth of verticals for the centerline distance value) and assuming that the plastic hinges will form at a distance equal to half of the chord member depth.

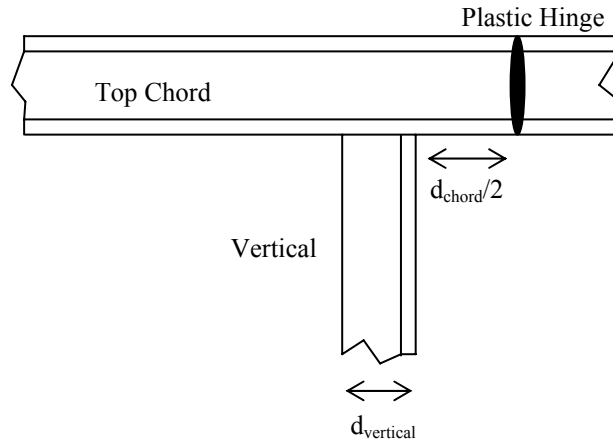


Figure 2.5: Details of Plastic Hinge Location

The same analysis was conducted using this reduced length for the special segment and utilizing a hardening modulus equal to 1 percent of the initial elastic modulus. The result is presented in Figure 2.6.

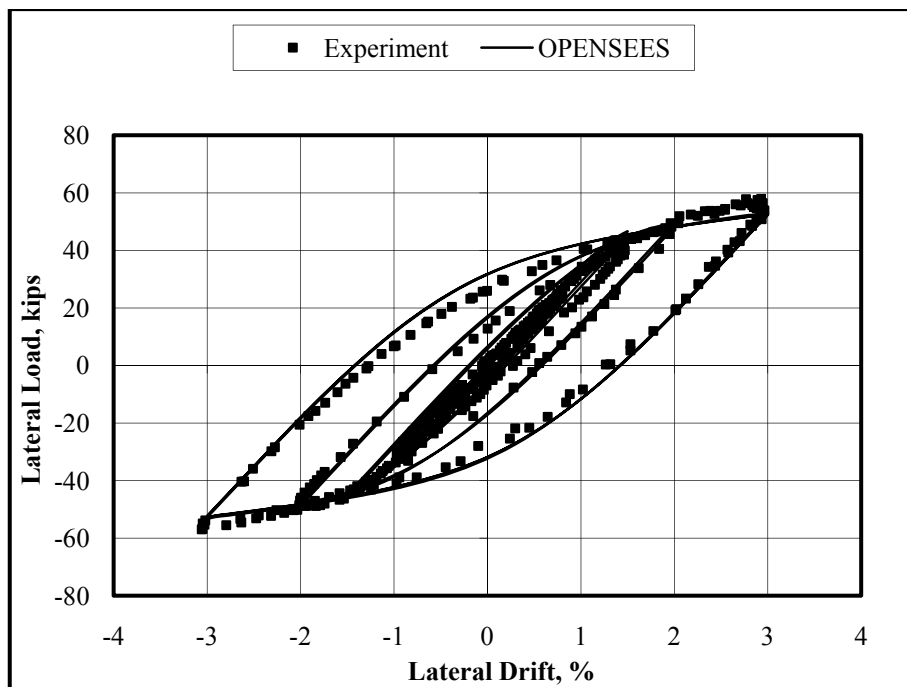


Figure 2.6: Comparison of Experimental Result with Numerical Result Obtained for Reduced Special Segment Length

According to the revised result it is evident that considering a reduced length with more realistic material properties was sufficient to capture the response. The use of a hardening modulus equivalent to 1 percent of the initial elastic modulus will be further justified in the following section on finite element analysis.

### 2.3 Numerical Modeling Details – ANSYS

A full three dimensional model of the specimen was prepared in ANSYS. All elements were modeled using 8-node shell elements (shell93). The link beam was modeled with truss elements (link8). Bilinear kinematic hardening with a slope of 1 percent of the initial elastic slope was utilized in the model. The same displacement history utilized in testing was applied to the model. The chord member ends were finely meshed to adequately model the inelastic behavior in these regions. A typical finite element mesh is given in Figure 2.7.

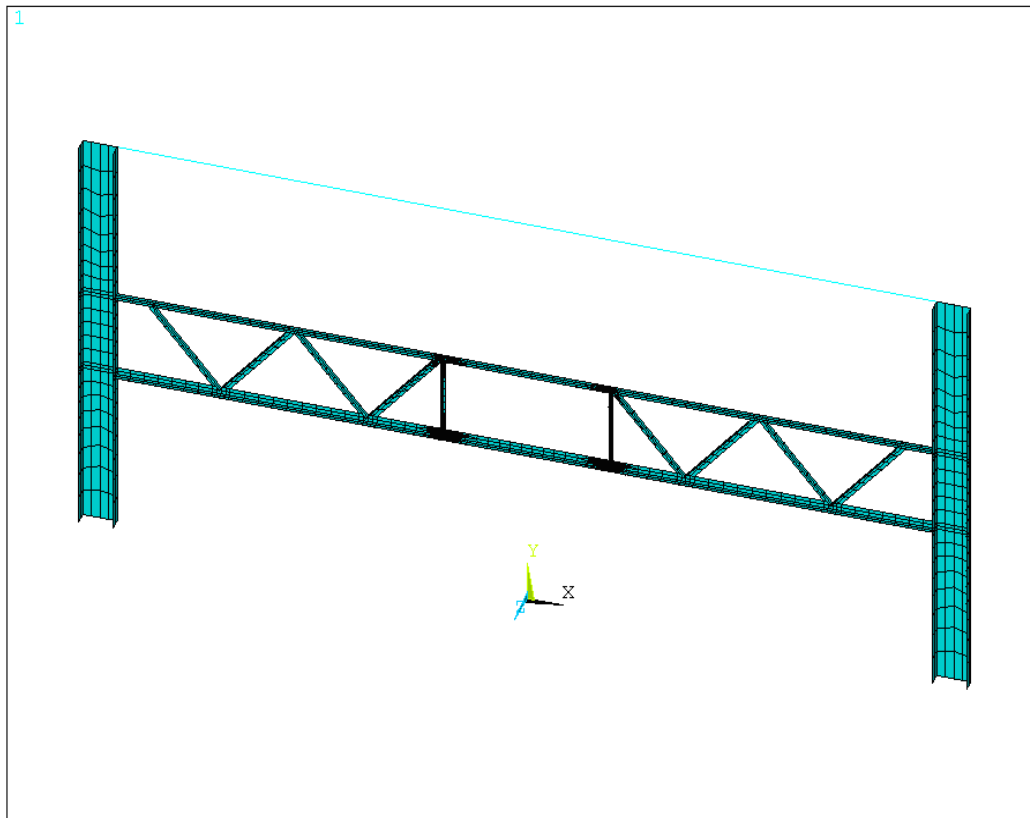


Figure 2.7: Typical Finite Element Mesh

The finite element model of the specimen was modeled using 192 nodes and 132 shell elements. The chord members were meshed into two in coarsely meshed regions and into six in finely meshed regions.

The comparison of load displacement response from the experimental result and numerical result is given in Figure 2.8. It is evident from the comparison that the finite element simulation is satisfactory in predicting the response of the specimen.

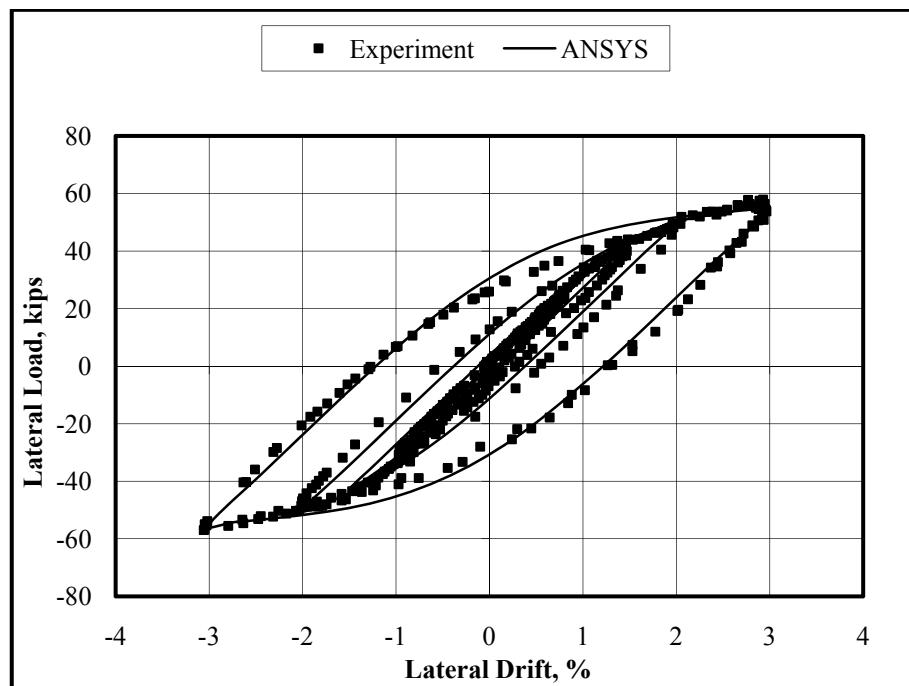


Figure 2.8: Comparison of Experimental Result with Finite Element Analysis Result

Simulations utilizing OPENSEES and ANSYS revealed that the specimen behavior can be predicted with reasonable level of accuracy using these software. Further numerical studies presented in this thesis employed the numerical details adopted in this chapter.

## CHAPTER 3

### AN EVALUATION OF STRENGTH DISTRIBUTION IN STMFs

Design of STMF systems presents a variety of challenges especially for earthquake loads. Engineers frequently utilize equivalent static load procedures to take into account the inertia forces produced during an earthquake. Regardless of the specification used and its recommended lateral load distribution, the problem of designing for strength at each story level arises. Engineers have options for the distribution of shear strength of special segment among the stories. First studies (Goel and Itani (1994b)) on design of STMFs recommended the use of same truss at all story levels leading to an equal distribution of shear strength among the stories. Some earlier studies suggested that the truss members can be sized based on the elastic shear force distribution. Recently, Chao and Goel (2008b) recommended that a special lateral force distribution developed by Chao, Goel, and Lee (2007) should be used in the design of STMF systems and the sizing should be based on the elastic shear forces produced by this lateral load distribution.

The lateral load distribution proposed by Chao, Goel, and Lee (2007) is calculated as follows:

$$F_i = (\beta_i - \beta_{i+1})F_n \text{ when } i = n, \beta_{n+1} = 0$$

$$F_n = V \left( \frac{w_n h_n}{\sum_{j=1}^n w_j h_j} \right)^{0.75T^{-0.2}} \quad \text{Equation (3.1)}$$

$$\beta_i = \frac{V_i}{V_n} = \left( \frac{\sum_{j=i}^n w_j h_j}{w_n h_n} \right)^{0.75T^{-0.2}} \quad \text{Equation (3.2)}$$

Where;

$\beta_i$ : shear distribution factor at level  $i$

$V_i, V_n$ : story shear forces at level  $i$  and at the top ( $n^{\text{th}}$  level), respectively

$w_j$ : seismic weight at level  $j$

$h_j$ : height of level  $j$  from the ground

$w_n$ : seismic weight of the structure at the top level

$h_n$ : height of roof level from the ground

$T$ : fundamental natural period

$F_i, F_n$ : lateral forces applied at level  $i$  and top level  $n$ , respectively

$V$ : design base shear.

This lateral load distribution takes into account the higher amounts of forces produced at top stories during an earthquake. Chao and Goel (2008b) proposed a performance based design methodology for STMFs that is based on this lateral load distribution and a target interstory drift level. These researchers concluded that the lateral drift and plastic rotation demands tend to be uniform if the proposed design methodology is adopted.

The aim of the study presented in this chapter is to explore the seismic behavior of STMFs designed using different lateral load distributions and special segment strength variations among the stories. The main objective of the study is to quantify the consequences of using same truss designs in all stories. This design philosophy is useful because it expedites the design and manufacturing of STMFs. Only a single type of truss needs to be designed and manufactured in this case. If a design based on elastic analysis is considered then several different truss designs should be conducted and the manufacturing should accommodate these different designs.

### 3.1 Methodology and Design of STMFs

In order to compare different designs and load distributions 6, 9, and 12 story STMFs with a vierendeel segment were considered. A single story portion of a typical STMF is given in Figure 3.1. As shown in this figure, a column height of 2.5m, a truss depth of 1m, a span length of 10m, and a special segment length of 2m were considered.

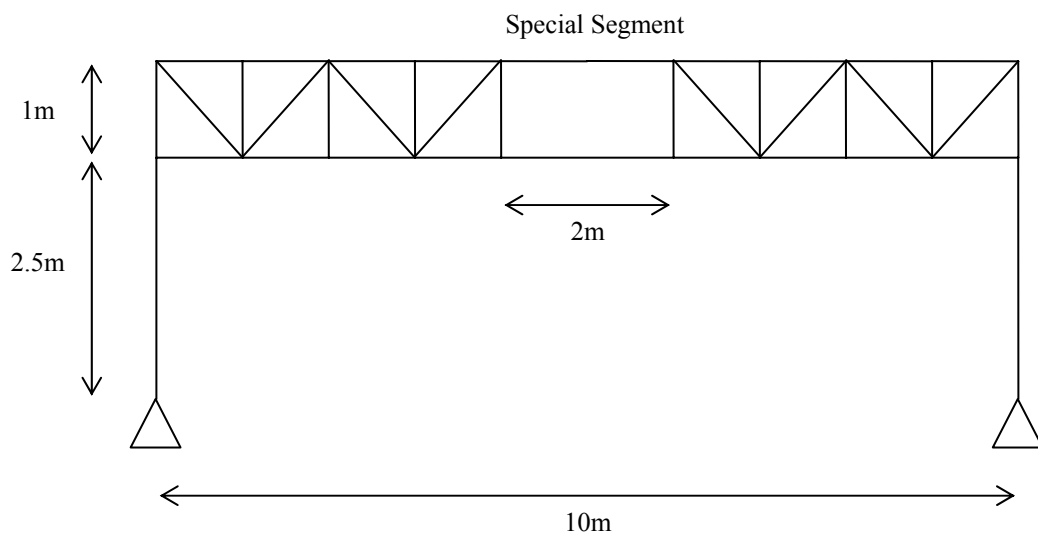


Figure 3.1: Geometrical Properties of the STMFs

In order to make a fair comparison between the designs, same sections were used for the members outside the special segment, in all cases. All members outside the special segment were modeled to behave elastically during the analysis and plastic behavior was constrained to the chord members in special segment. If the engineer chooses to utilize same section members in all stories then the strength is equally distributed along the height of the STMF as shown in Figure 3.2. In this type of a design, the distribution of lateral forces only has an influence on the sum of the shear strengths in all stories.

The relationship between the required strength of the special segment ( $V_{ss}$ ) and the base shear ( $V_{lateral}$ ) can be expressed as:

$$V_{ss} = \frac{V_{lateral} H_{eq}}{nL} \quad \text{Equation (3.3)}$$

Where;

$H_{eq}$ : equivalent height of the applied lateral load

$n$ : number of stories.

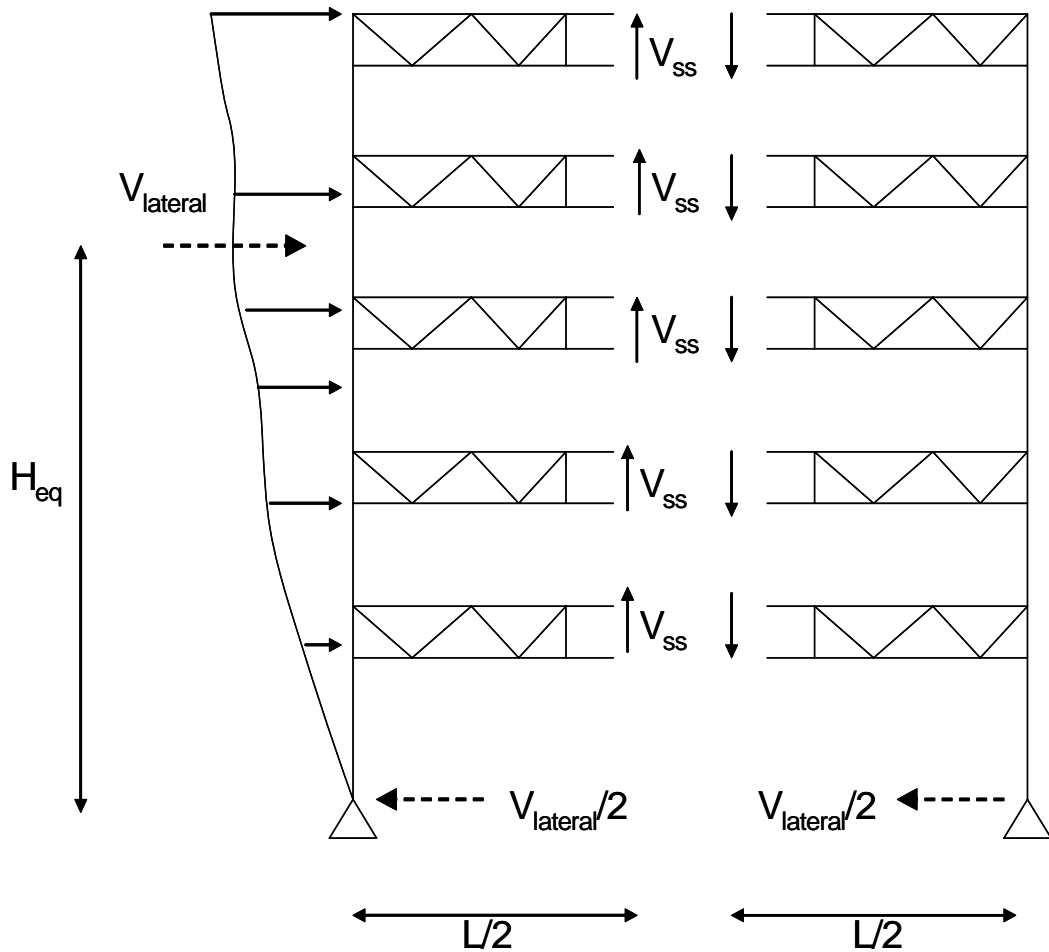


Figure 3.2: Free Body Diagram – Same Strength in All Stories

In the present study two C10x15.3 channel section chord members with a yield strength of 350 MPa were considered for the truss with same strength sections in all stories. The rest of the truss system was designed based on the strength of the special segment. The panel length for all trusses was 1m. The sections used for the members outside the special segment are given in Table 3.1.

Table 3.1: Members outside the Special Segment

Member	Section
Chord outside the Special Segment	2MC18x58
Diagonals	2L5x5x1/2
Verticals	2L4x4x7/16
Columns	W36x652

The sum of shear strengths of the special segments with 2C10x15.3 sections are equal to 2184kN, 3276kN, 4368kN for 6, 9, and 12 story STMFs, respectively. These strength values were kept constant and distributed according to the elastic load share of each story produced by a particular lateral load distribution. As shown in Figure 3.3, the distribution of the shear forces on the special segments varies if the design is based on elastic analysis. In order to keep the shear strength values the same, the following condition was applied:

$$nV_{ss} = \sum_i^n V_{ssi} \quad \text{Equation (3.4)}$$

Where;

$V_{ssi}$ : shear on special segment at the  $i^{\text{th}}$  level

Based on the elastic distribution of forces and the total shear strength requirement, the shear forces on special segments were determined. By considering these forces the chord members of the special segment were designed for lateral forces that correspond to inverted triangular distribution and Chao, Goel, and Lee (2007) distribution which is referred as CGL distribution hereafter.

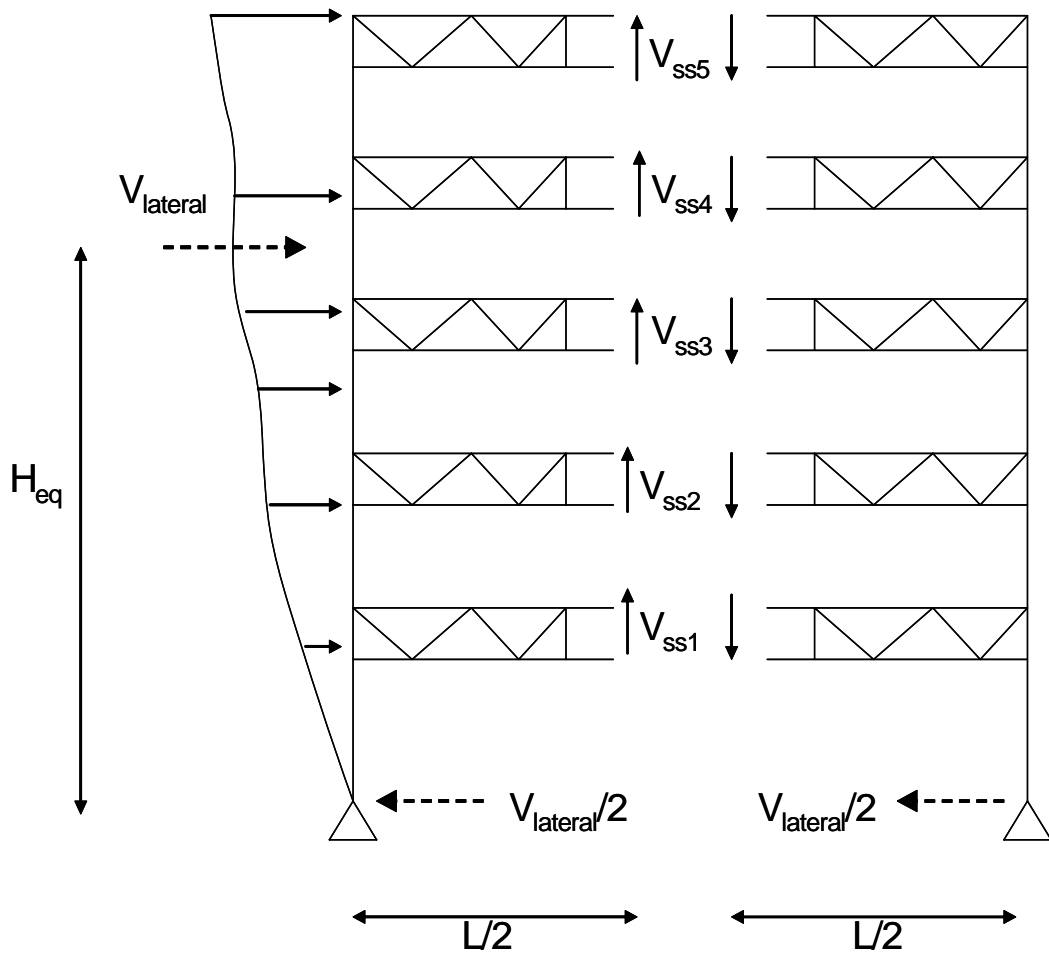


Figure 3.3: Free Body Diagram – Shear Distribution from Elastic Analysis

The design, where all trusses along the building height were the same, is termed as plastic design (PD). The design, where the trusses were designed based on elastic force distribution, is termed as elastic design (ED). There are two types of elastic design that was conducted namely, design based on inverted triangular distribution (ED-IT) and design based on CGL distribution (ED-CGL).

The required strength normalized by the total shear strength of all segments are plotted as a function of story number in Figures 3.4, 3.5, and 3.6 for 6, 9, and 12 story STMFs, respectively. The designed sections for each analysis or loading case are given in Table 3.2.

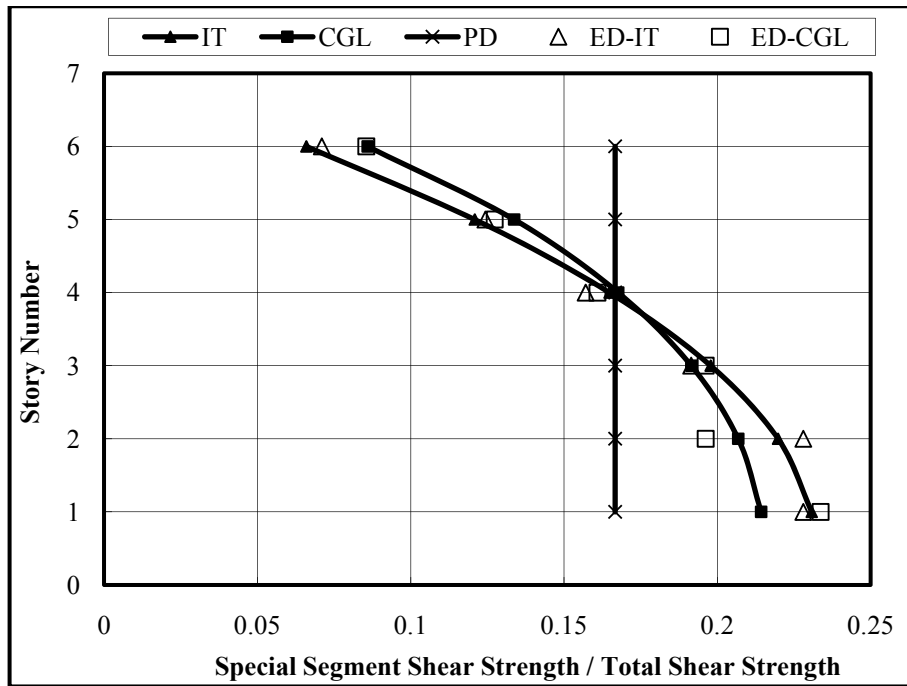


Figure 3.4: Distribution of Shear Strength among the Stories (6 Story STMF)

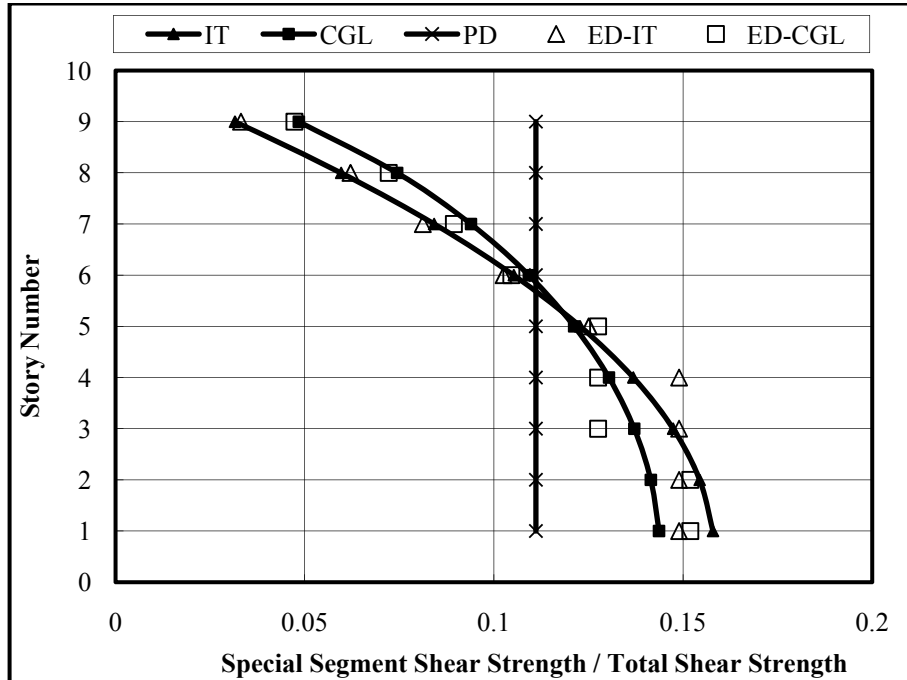


Figure 3.5: Distribution of Shear Strength among the Stories (9 Story STMF)

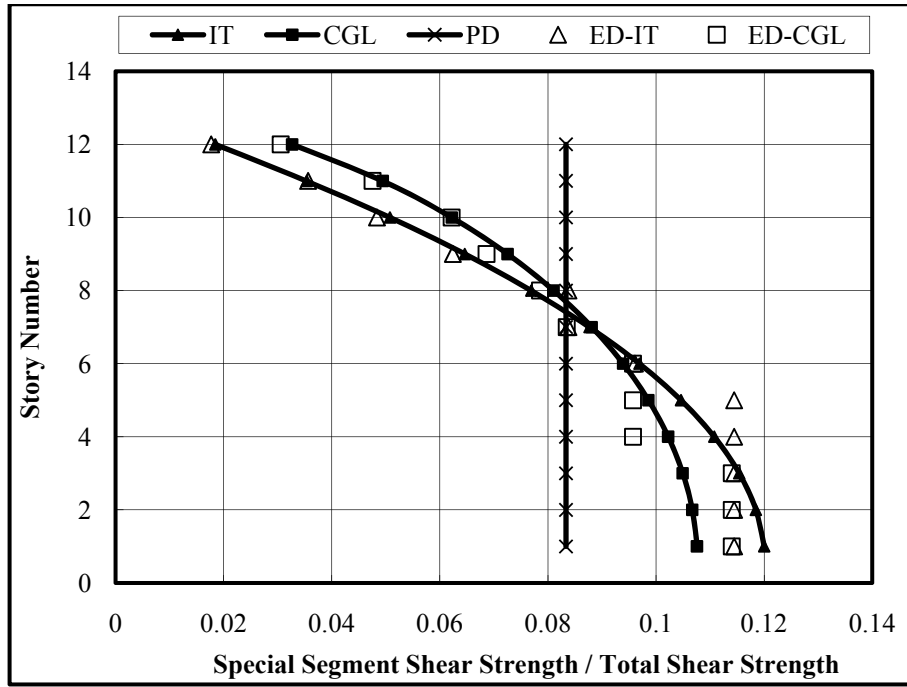


Figure 3.6: Distribution of Shear Strength among the Stories (12 Story STMF)

Table 3.2: Chord Member Sections

Story Number	Six Story		Nine Story		Twelve Story	
	Inverted Triangular	CGL	Inverted Triangular	CGL	Inverted Triangular	CGL
1	2C10x25	2C10x25	2C10x25	2C10x25	2C10x25	2C10x25
2	2C10x25	2C10x20	2C10x25	2C10x25	2C10x25	2C10x25
3	2C10x20	2C10x20	2C10x25	2C10x20	2C10x25	2C10x25
4	2C10x15.3	2C10x15.3	2C10x25	2C10x20	2C10x25	2C10x20
5	2C9x13.4	2C9x13.4	2C10x20	2C10x20	2C10x25	2C10x20
6	2C7x9.8	2C7x12.2	2C10x15.3	2C10x15.3	2C10x20	2C10x20
7			2C9x13.4	2C9x15	2C9x20	2C9x20
8			2C8x11.5	2C8x13.7	2C9x20	2C10x15.3
9			2C6x8.2	2C7x9.8	2C9x13.4	2C8x18.7
10					2C7x14.7	2C9x13.4
11					2C7x9.8	2C8x11.5
12					2C5x6.7	2C6x10.5

For dynamic analysis purposes it was assumed that the mass at every story is 125 tons. For all cases the members outside the special segment were kept the same in order not to introduce other variables.

### 3.2 Static Pushover Analysis and Natural Periods

In order to make sure that the different truss designs give similar base shear values, a set of pushover analysis were conducted on the STMF systems. Basically four different lateral load procedures were applied to obtain pushover responses. These four load profiles include a point load at the topmost story, equal lateral load, CGL load distribution, and inverted triangular load distribution. For all analyses a hardening modulus of 1 GPa was considered. Figures 3.7 through 3.18 present the findings of the pushover analysis results. As can be seen from these figures, the responses of the three different designs are similar. Essentially for all loading types the trusses designed using an elastic inverted triangular distribution and the CGL distribution display very similar responses. The response of the truss designed based on equal strength in all stories concept deviates slightly from the response of other two for equal lateral and inverted triangular loadings.

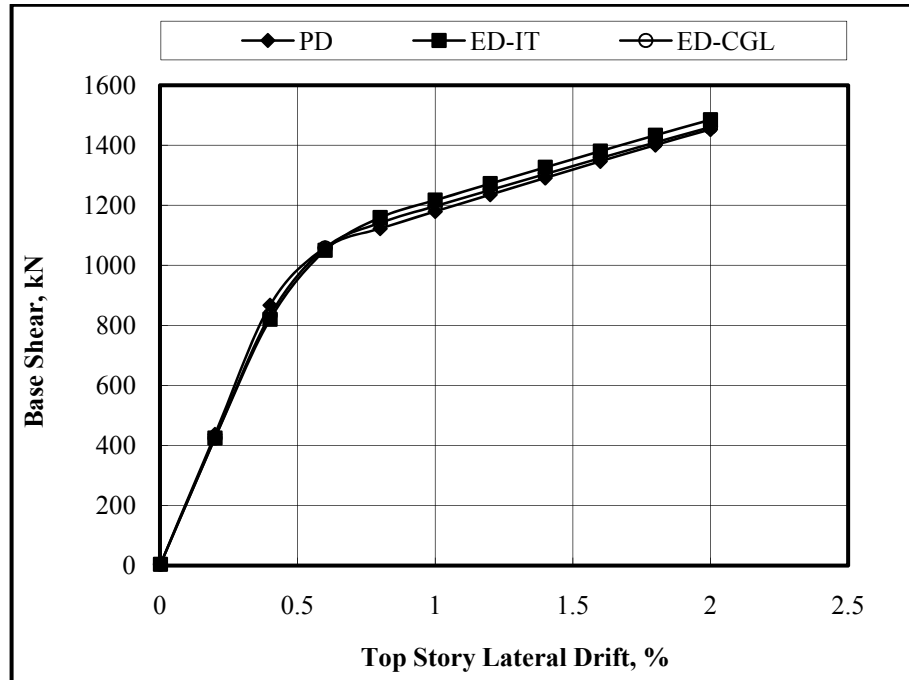


Figure 3.7: Pushover Analysis Results for 6 Story STMF – Top Loading

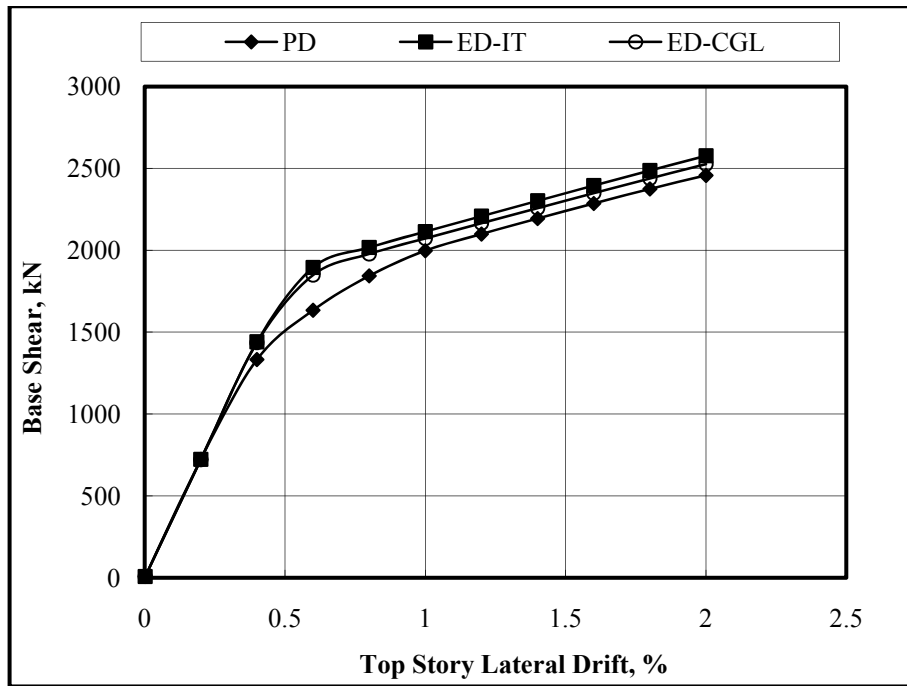


Figure 3.8: Pushover Analysis Results for 6 Story STMF – Equal Lateral Loading

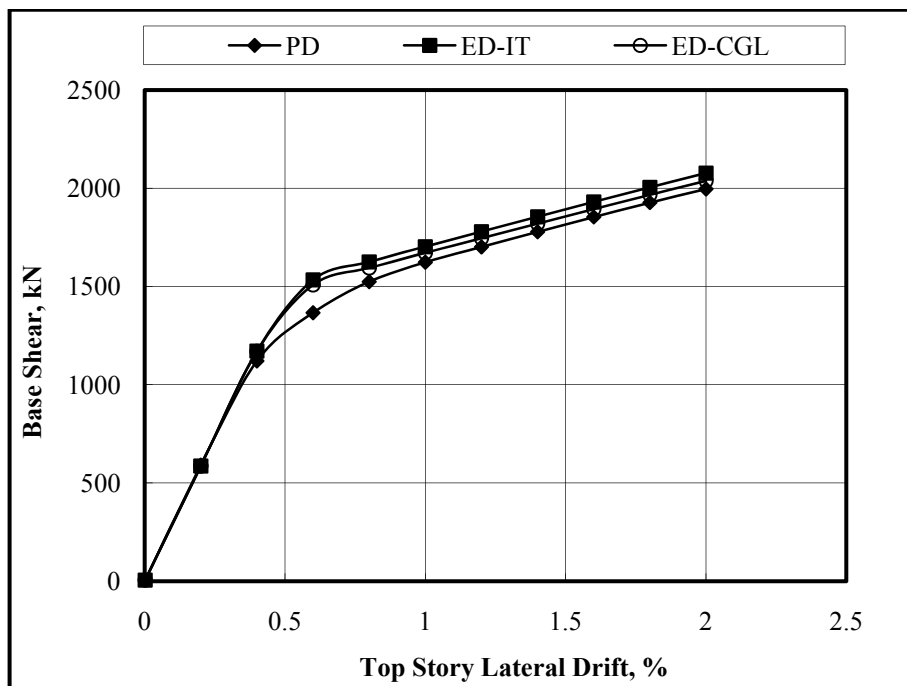


Figure 3.9: Pushover Analysis Results for 6 Story STMF – Inverted Triangular Loading

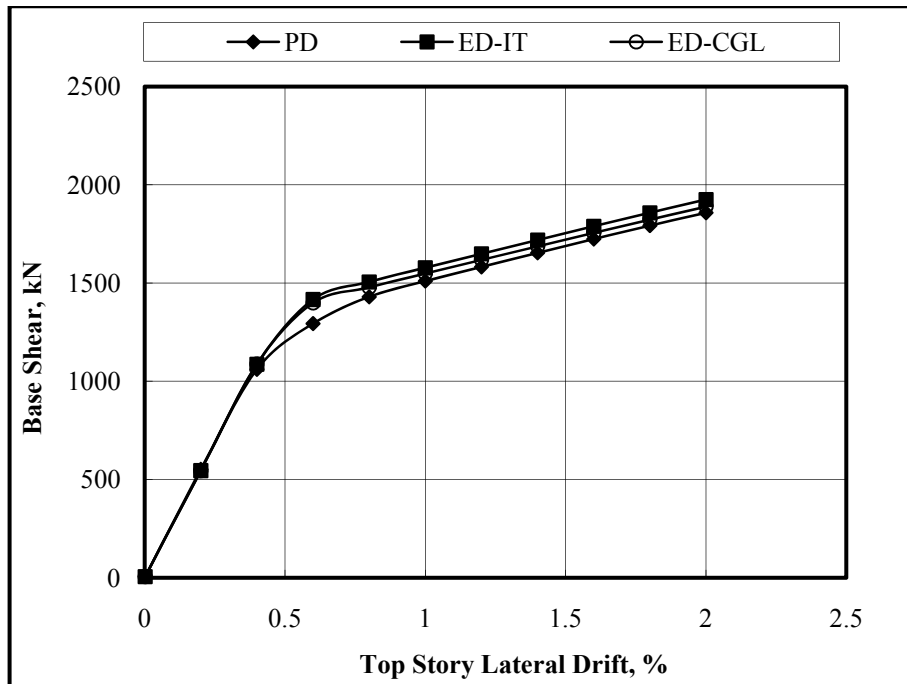


Figure 3.10: Pushover Analysis Results for 6 Story STMF – CGL Loading

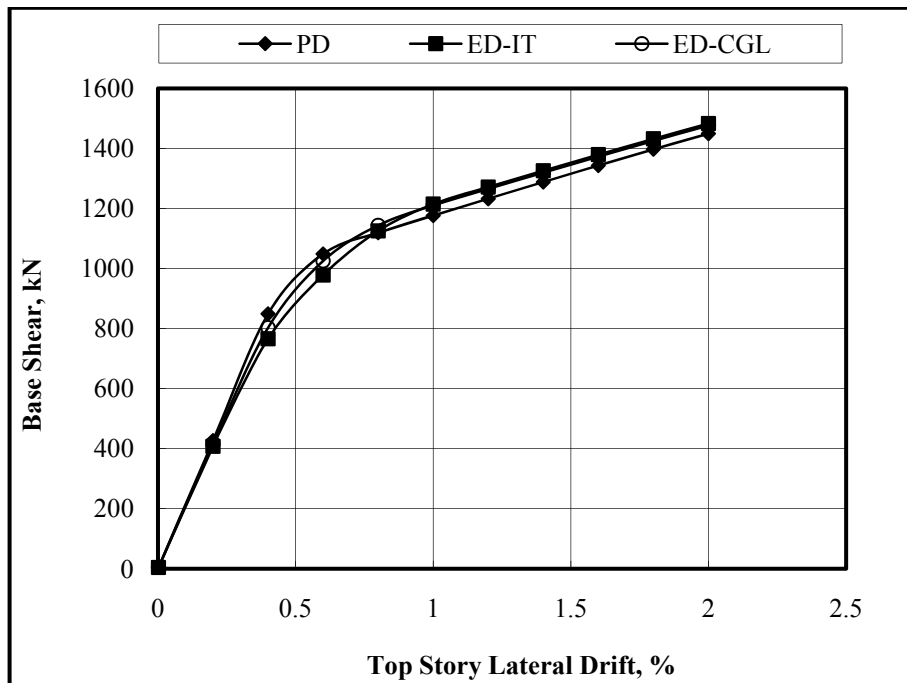


Figure 3.11: Pushover Analysis Results for 9 Story STMF – Top Loading

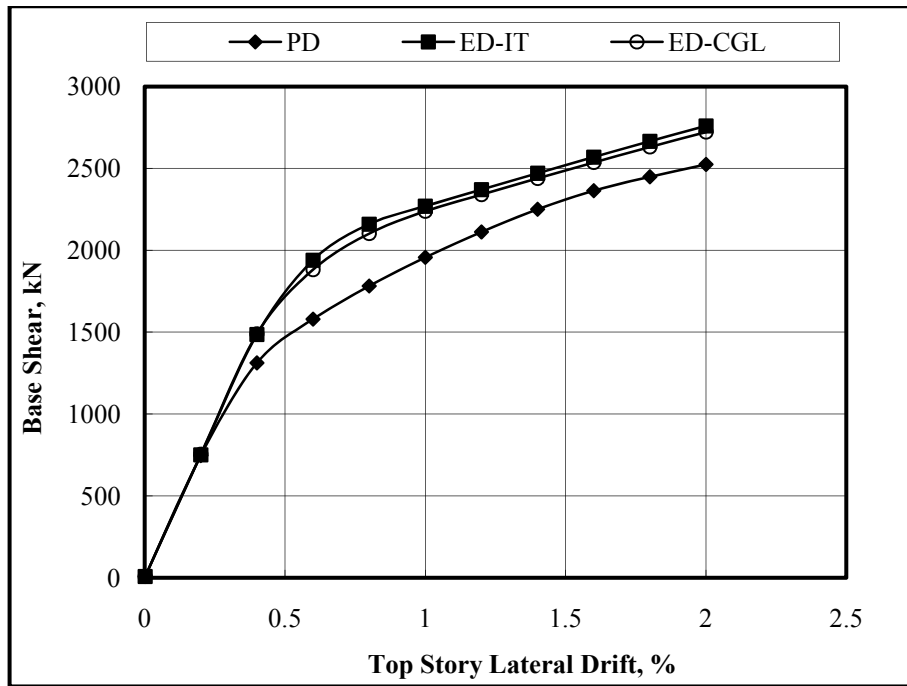


Figure 3.12: Pushover Analysis Results for 9 Story STMF – Equal Lateral Loading

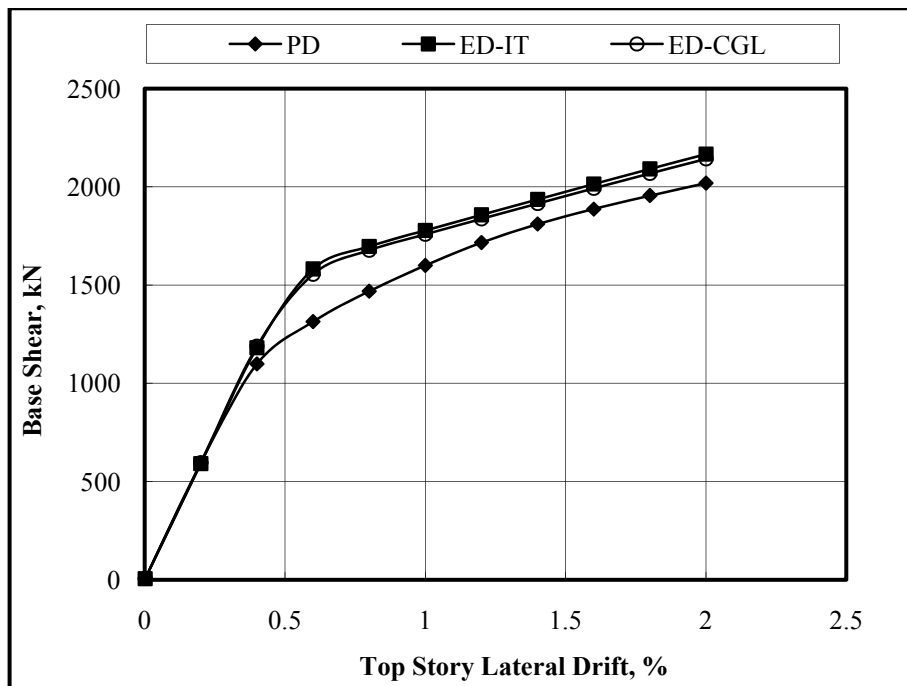


Figure 3.13: Pushover Analysis Results for 9 Story STMF – Inverted Triangular Loading

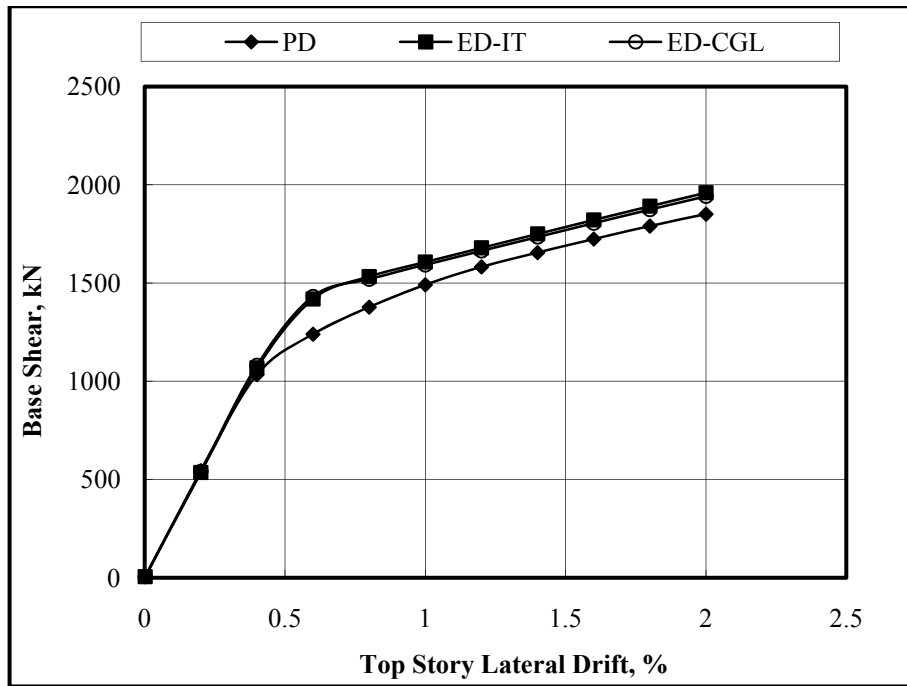


Figure 3.14: Pushover Analysis Results for 9 Story STMF – CGL Loading

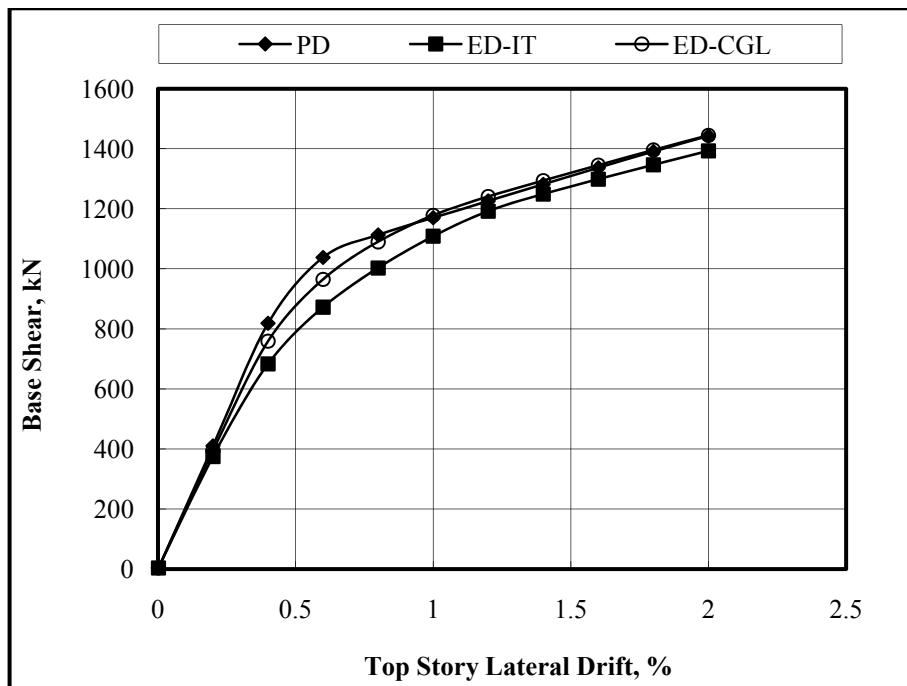


Figure 3.15: Pushover Analysis Results for 12 Story STMF – Top Loading

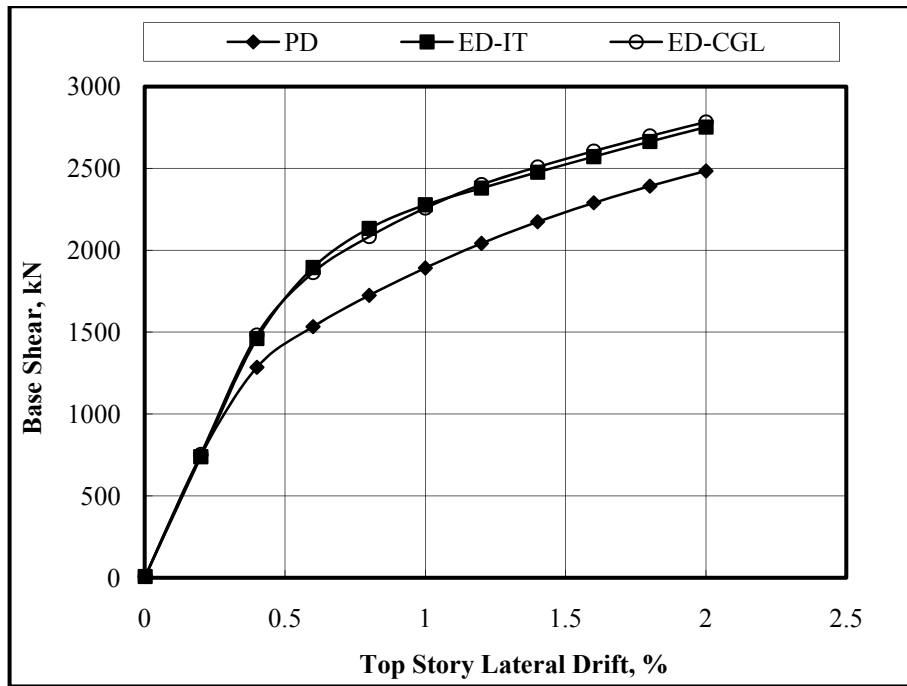


Figure 3.16: Pushover Analysis Results for 12 Story STMF – Equal Lateral Loading

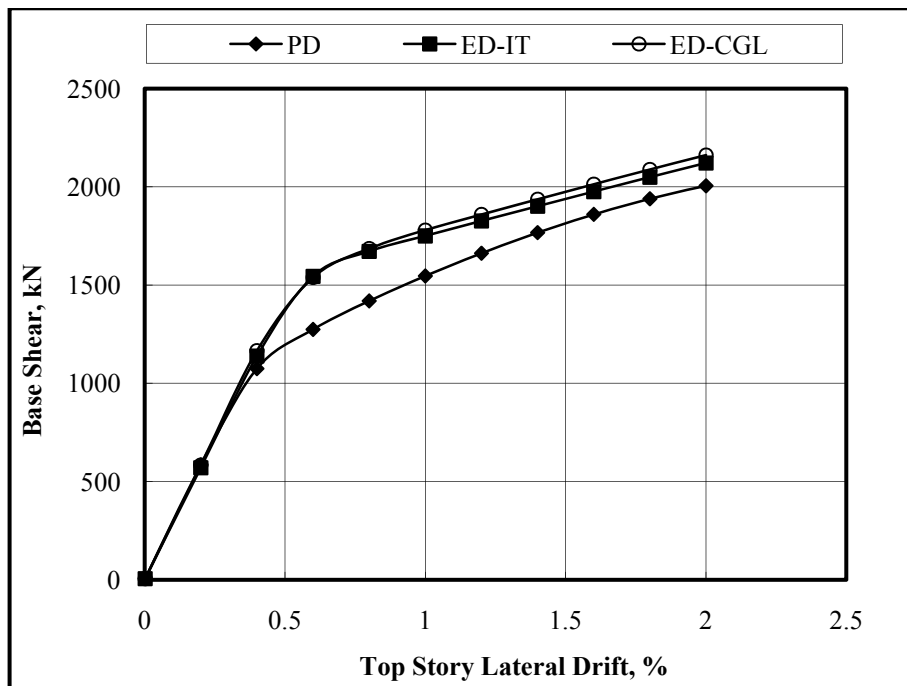


Figure 3.17: Pushover Analysis Results for 12 Story STMF – Inverted Triangular Loading

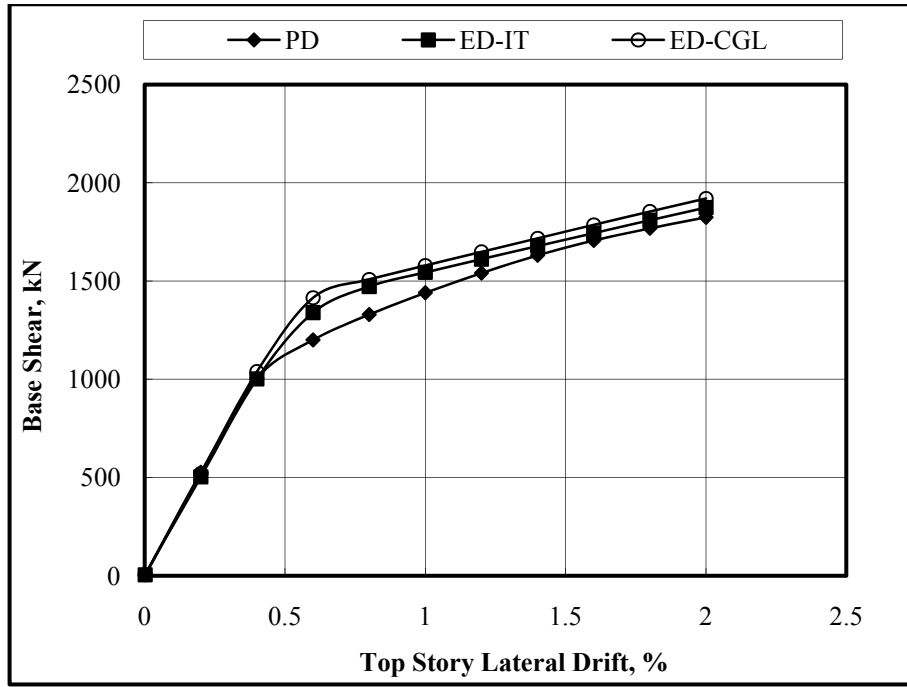


Figure 3.18: Pushover Analysis Results for 12 Story STMF – CGL Loading

Apart from pushover analysis, an eigenvalue analysis was conducted for each STMF to obtain the natural periods of the systems. Natural periods for the first three modes of vibration are given in Table 3.3. As shown in this table for a particular number of story, the fundamental natural periods of STMFs designed using different methods are close to each other.

Table 3.3: Natural Periods of STMF Systems

Number of Story	Period (sec)								
	1 <sup>st</sup> Mode			2 <sup>nd</sup> Mode			3 <sup>rd</sup> Mode		
	Plastic Design	Elastic Design (IT)	Elastic Design (CGL)	Plastic Design	Elastic Design (IT)	Elastic Design (CGL)	Plastic Design	Elastic Design (IT)	Elastic Design (CGL)
6	1.16	1.15	1.15	0.28	0.29	0.29	0.11	0.12	0.12
9	1.71	1.69	1.69	0.47	0.49	0.48	0.21	0.22	0.22
12	2.29	2.26	2.26	0.67	0.71	0.69	0.32	0.34	0.33

### 3.3 Time-History Analysis

A set of time-history analysis was conducted to study the behavior of STMFs under earthquake loading. All structures were subjected to a suite of ground motions that are listed in Table 3.4. These ground motions have a wide range of intensity and in general, force the STMF behavior into the inelastic range. Earthquake records with varying intensity were expected to produce different levels of drift demands so that the behavior of STMFs at various drift levels can be examined. For all structures a design base acceleration (DBA) was calculated by dividing the base shear at structural yield level to the total reactive mass. The 2% damped response spectra of the selected earthquakes and design base accelerations (DBAs) for 6, 9, and 12 story systems are given in Figure 3.19.

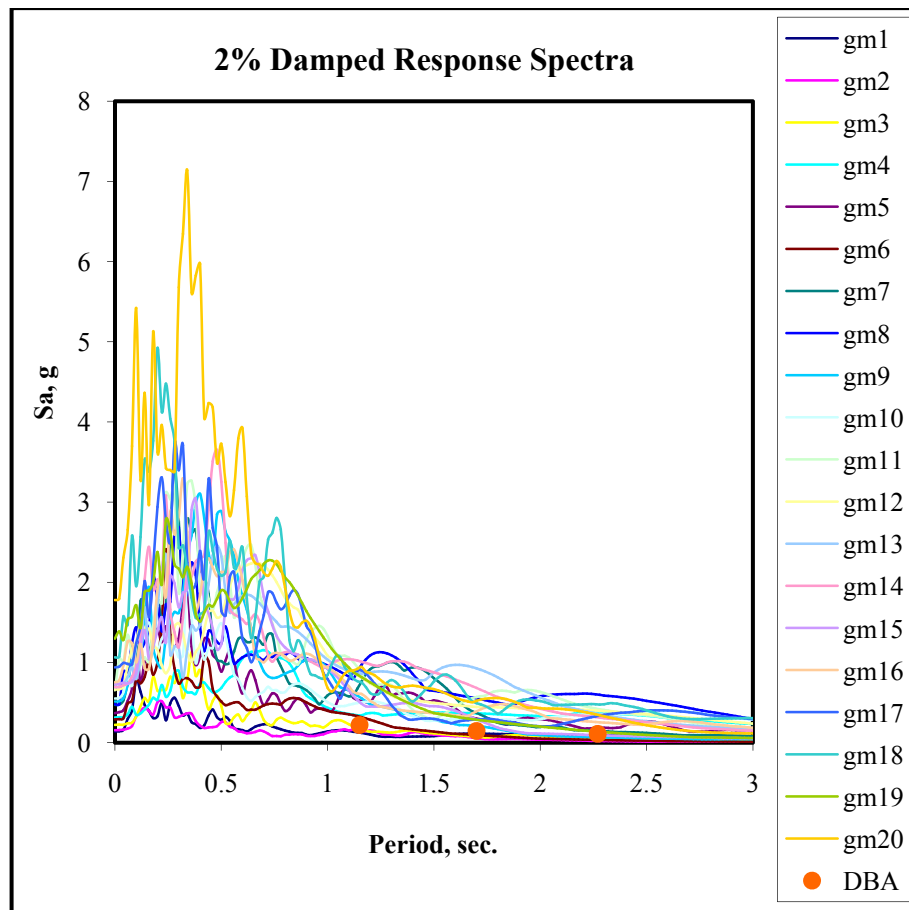


Figure 3.19: Response Spectra for the Selected Earthquake Records

Table 3.4: Details of Selected Ground Motion Records

GM #	Earthquake	Country	Date	Station Location	Site Geology	M <sub>w</sub>	PGA (g)
1	Imperial Valley	USA	15.10.1979	El Centro Array #1, Borchard Ranch	Alluvium	6.5	0.141
2	Morgan Hill	USA	24.04.1984	Gilroy Array #2 (Hwy 101 & Bolsa Rd)	Alluvium	6.1	0.157
3	Northridge	USA	17.01.1994	Downey County Maint. Bldg.	Alluvium	6.7	0.223
4	Imperial Valley	USA	15.10.1979	Meloland Overpass	Alluvium	6.5	0.314
5	Northridge	USA	17.01.1994	Saticoy	Alluvium	6.7	0.368
6	Whittier Narrows	USA	01.10.1987	Cedar Hill Nursery, Tarzana	Alluvium / Siltstone	6.1	0.405
7	Loma Prieta	USA	18.10.1989	Capitola Fire Station	Alluvium	7.0	0.472
8	Northridge	USA	17.01.1994	Rinaldi Receiving Station	Alluvium	6.7	0.480
9	Northridge	USA	17.01.1994	Katherine Rd, Simi Valley	Alluvium	6.7	0.513
10	Imperial Valley	USA	15.10.1979	El Centro Array #5, James Road	Alluvium	6.5	0.550
11	Chi Chi	Taiwan	20.09.1999	CHY028	USGS(C)	7.6	0.653
12	Cape Mendocino	USA	25.04.1992	Petrolia, General Store	Alluvium	7.0	0.662
13	Kobe	Japan	16.01.1995	Takarazu	USGS (D)	6.9	0.693
14	Kobe	Japan	16.01.1995	Takarazu	USGS (D)	6.9	0.694
15	Northridge	USA	17.01.1994	Katherine Rd, Simi Valley	Alluvium	6.7	0.727
16	Düzce	Turkey	12.11.1999	Bolu	USGS(C)	7.1	0.754
17	Northridge	USA	17.01.1994	Sepulveda VA Hospital	Alluvium	6.7	0.939
18	Tabas	Iran	16.09.1978	Tabas	Stiff Soil		1.065
19	Morgan Hill	USA	24.04.1984	Coyote Lake Dam	Rock	6.1	1.298
20	Northridge	USA	17.01.1994	Tarzana Cedar Hill Nursery	Alluvium	6.7	1.778

All 9 STMF systems were subjected to the ground motions listed in Table 3.4. A stiffness proportional damping equal to 2 percent of the critical damping was considered in all analysis. During a typical analysis drifts at story levels, curvatures at the chords of special segments, and the base shears were recorded. The curvature values were converted to plastic rotations after analysis. The curvature-plastic rotation relationship was derived by considering simple loading cases. A plastic hinge length of 5 percent of the length of the member was obtained from Gauss-Lobatto quadrature for five number of integration points. Taking into account this

plastic hinge length, a relationship between curvatures and plastic rotations can be easily developed.

### 3.3.1 Results of Time-History Analysis

#### 3.3.1.1 Comparison with Pushover Analysis

Time-history analysis results give useful information about the lateral loading profile during a seismic event. In general many modes contribute to the response of a system under dynamic loading. In this part of the study the time-history analysis results are correlated with the pushover analysis results that were presented earlier. Basically, the maximum absolute base shear and the maximum absolute top story drift were considered for each 20 time-history analysis and these values are plotted against the pushover curves obtained using different lateral load profile assumptions. The plots are given in Figures 3.20 through 3.28.

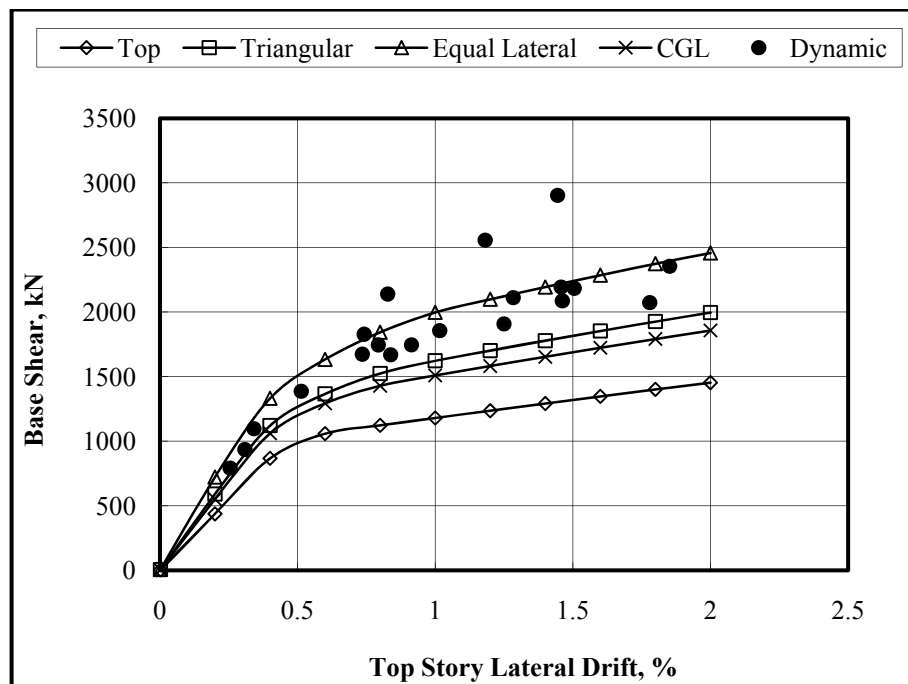


Figure 3.20: Comparison of Pushover and Time-History Analysis Results for 6 Story STMF-PD

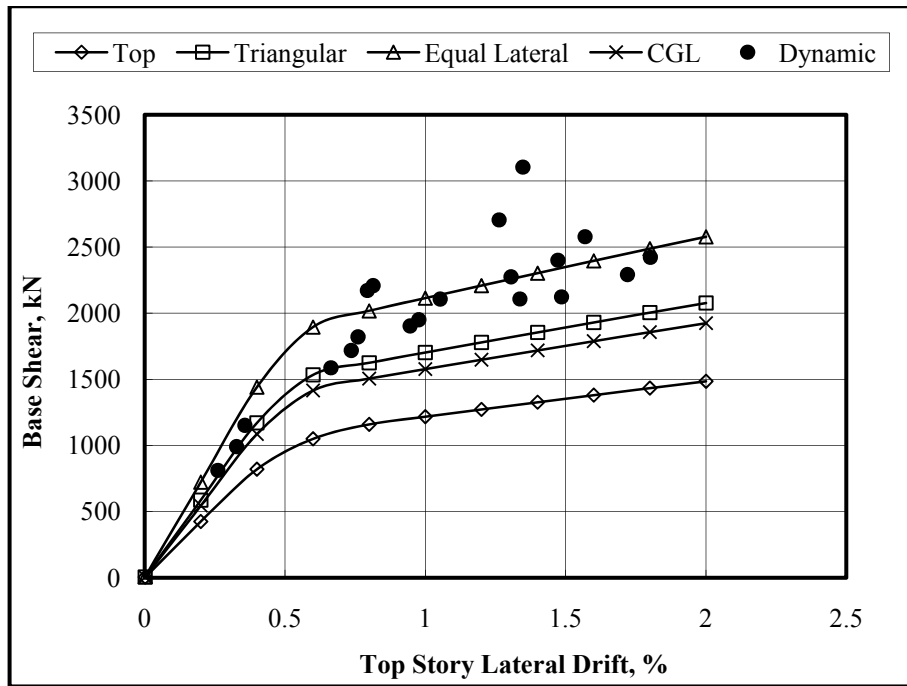


Figure 3.21: Comparison of Pushover and Time-History Analysis Results for 6 Story STMF-ED-IT

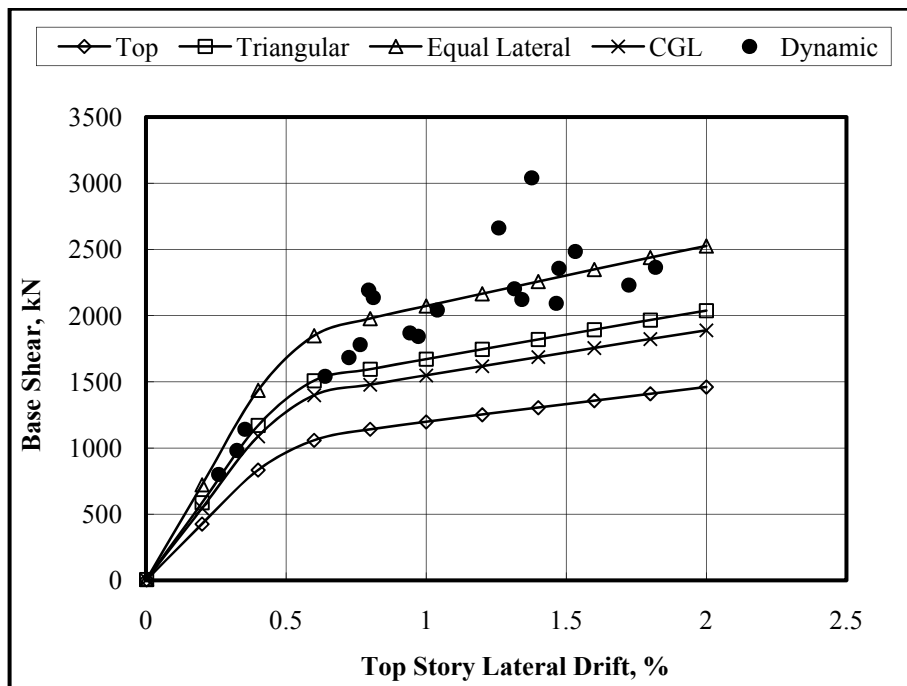


Figure 3.22: Comparison of Pushover and Time-History Analysis Results for 6 Story STMF-ED-CGL

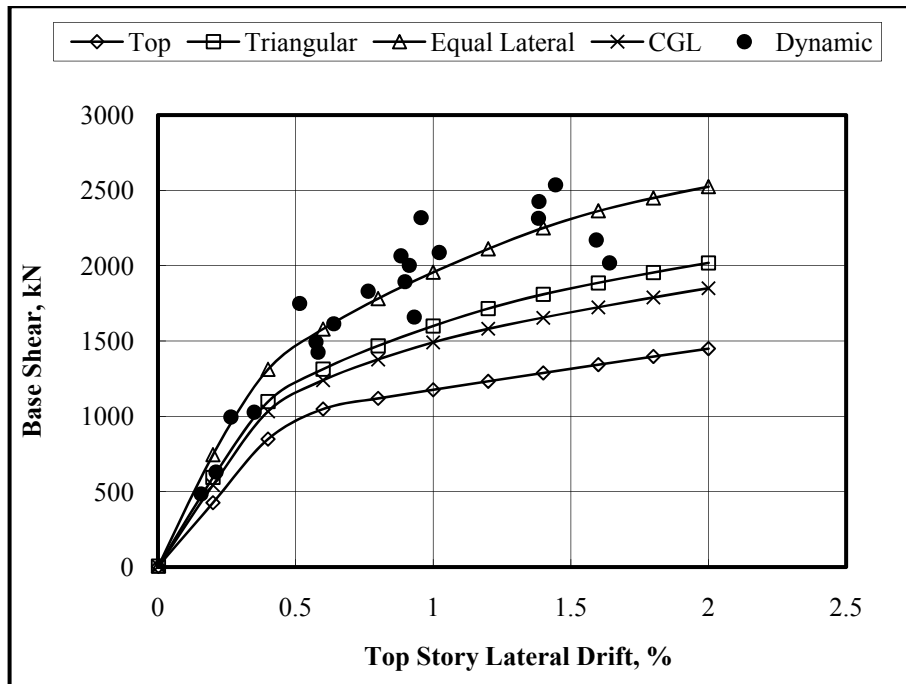


Figure 3.23: Comparison of Pushover and Time-History Analysis Results for 9 Story STMF-PD

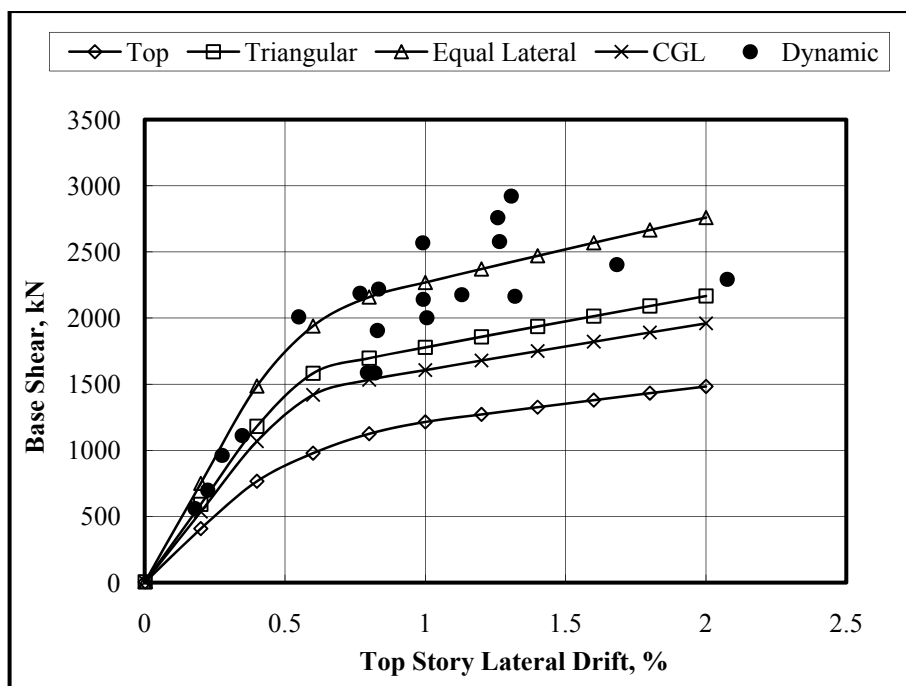


Figure 3.24: Comparison of Pushover and Time-History Analysis Results for 9 Story STMF-ED-IT

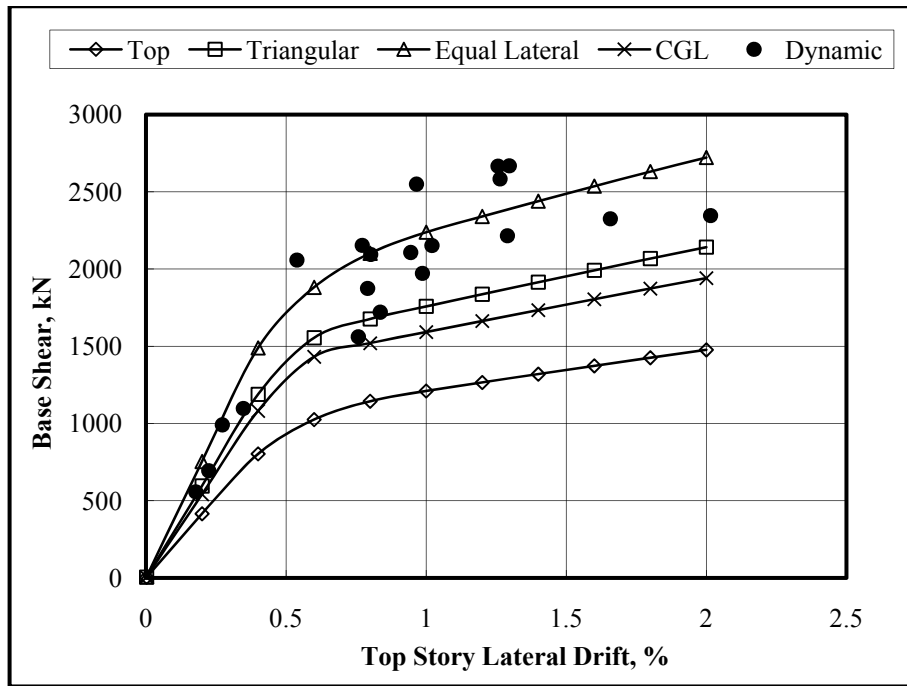


Figure 3.25: Comparison of Pushover and Time-History Analysis Results for 9 Story STMF-ED-CGL

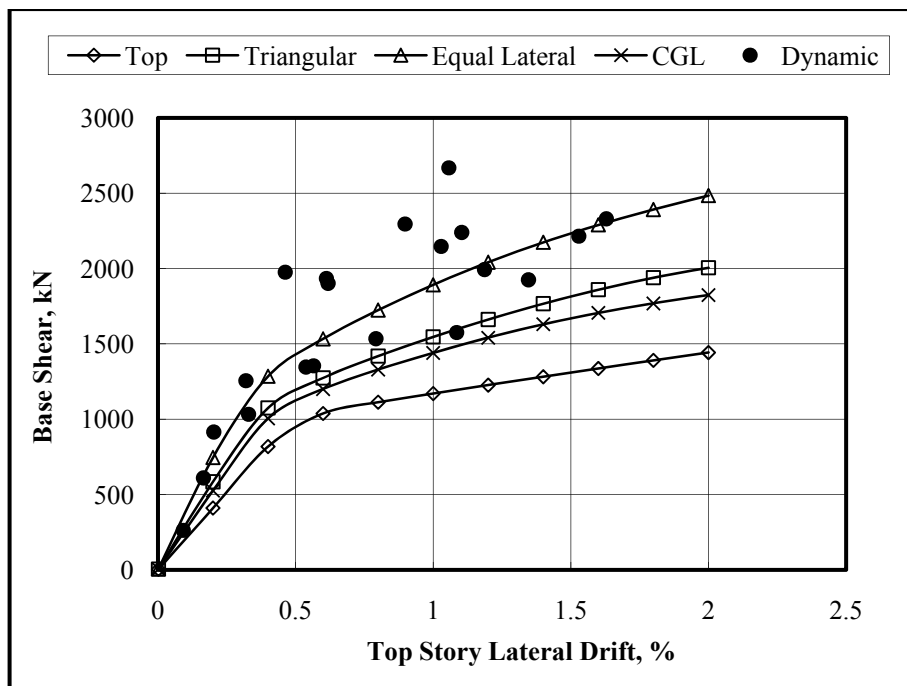


Figure 3.26: Comparison of Pushover and Time-History Analysis Results for 12 Story STMF-PD

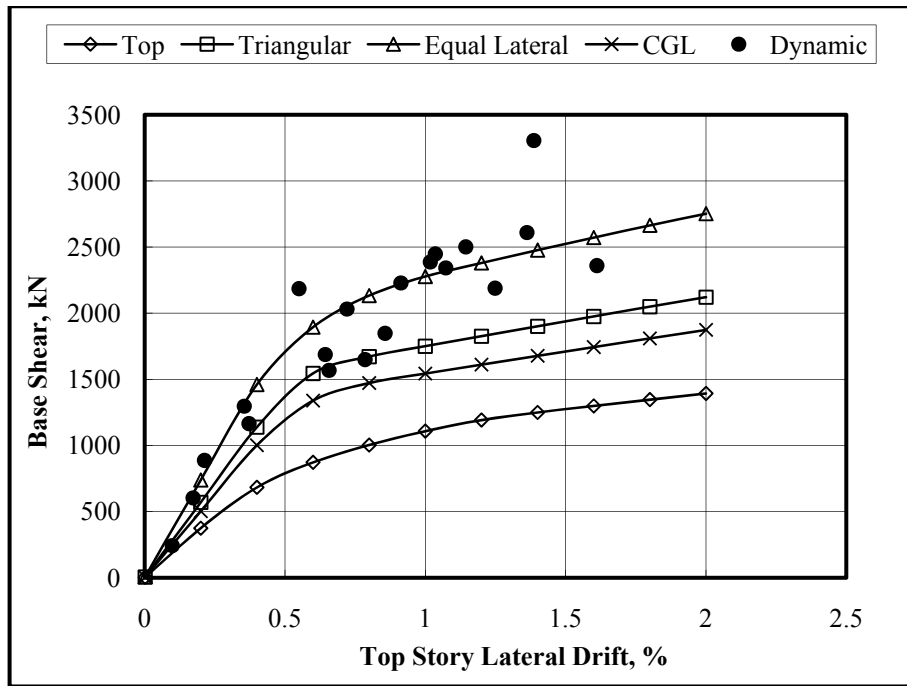


Figure 3.27: Comparison of Pushover and Time-History Analysis Results for 12 Story STMF-ED-IT

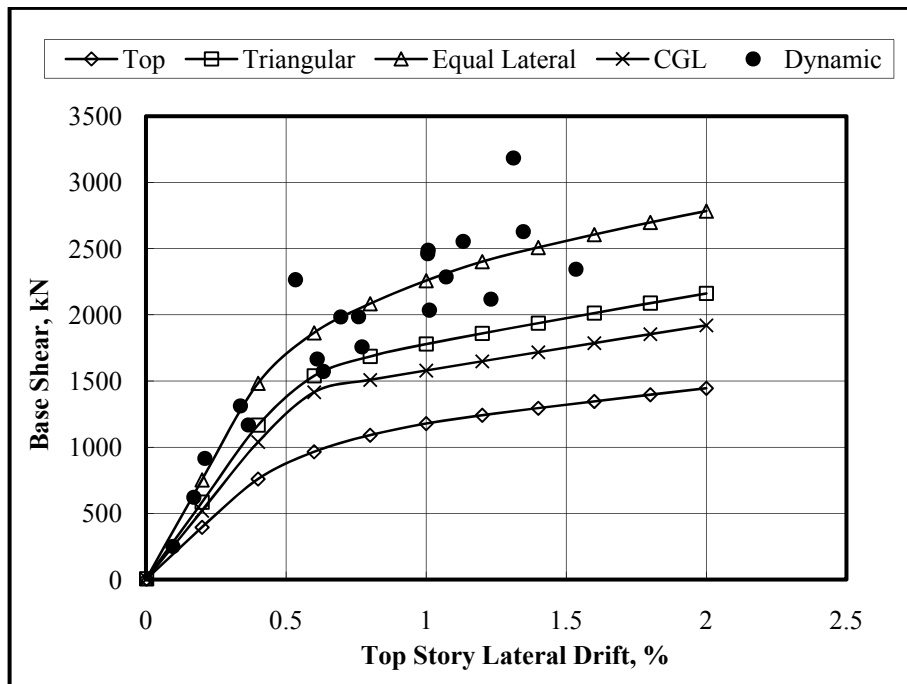


Figure 3.28: Comparison of Pushover and Time-History Analysis Results for 12 Story STMF-ED-CGL

It is evident from these figures that most of the earthquake records result in an inelastic activity in the systems. STMF systems remained elastic under the action of a few of the ground motions. The comparisons with pushover analysis reveal that the base shear versus top story drift can best be predicted using the equal lateral load distribution. This observation is valid for all types of designs and all heights considered.

### 3.3.1.2 Comparison of Different Designs

In this section the trusses designed based on three different approaches are compared in terms of their performance. As mentioned earlier, two measures are used to conduct the comparisons among the different designs. The maximum interstory drift at all stories and the maximum amount of plastic rotation at the chord member ends were recorded. For each STMF and 20 time-history analysis the results for these quantities are given in Figures 3.29 through 3.37.

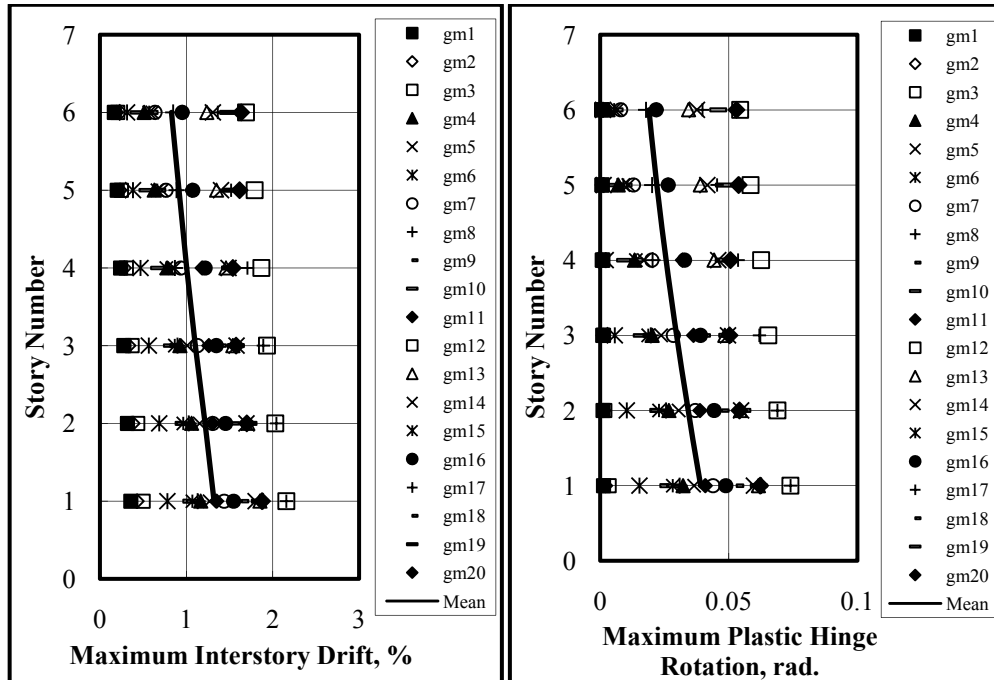


Figure 3.29: Response of 6 Story STMF-PD

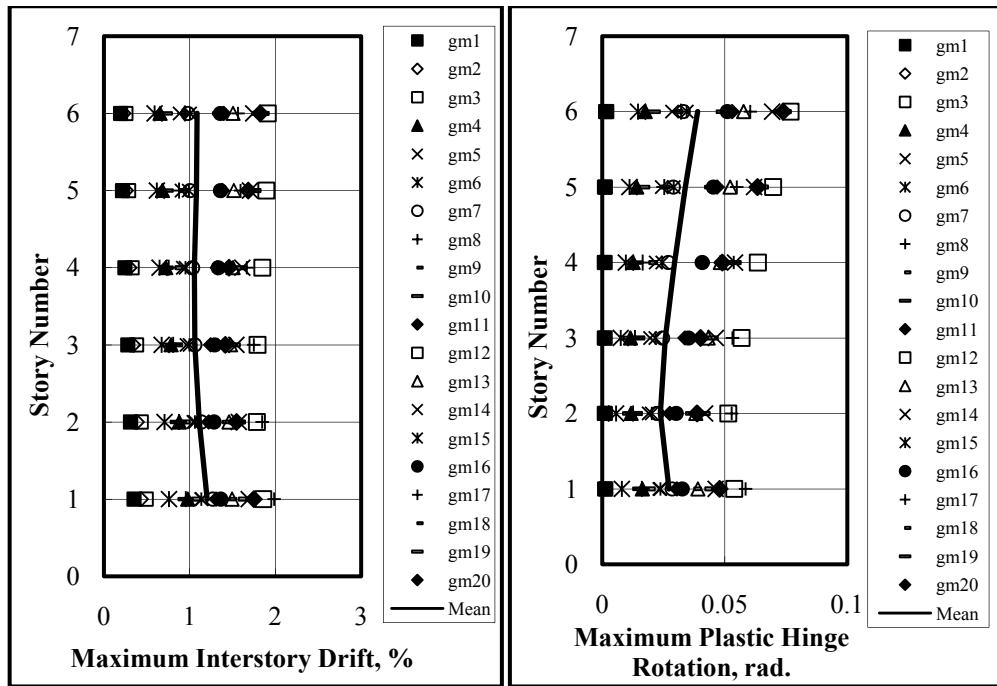


Figure 3.30: Response of 6 Story STMF-ED-IT

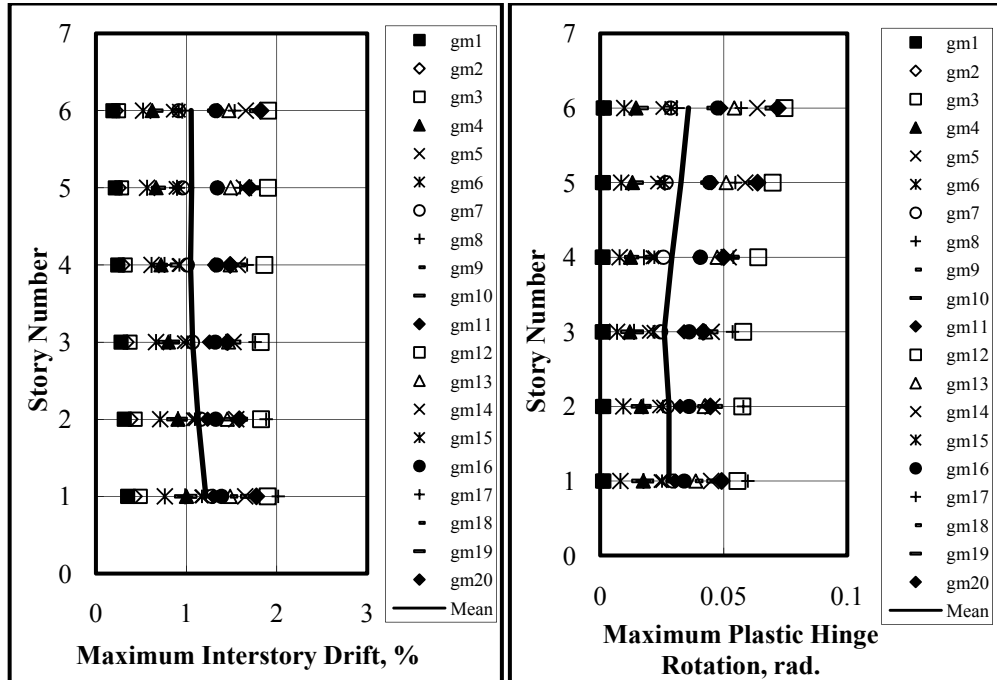


Figure 3.31: Response of 6 Story STMF-ED-CGL

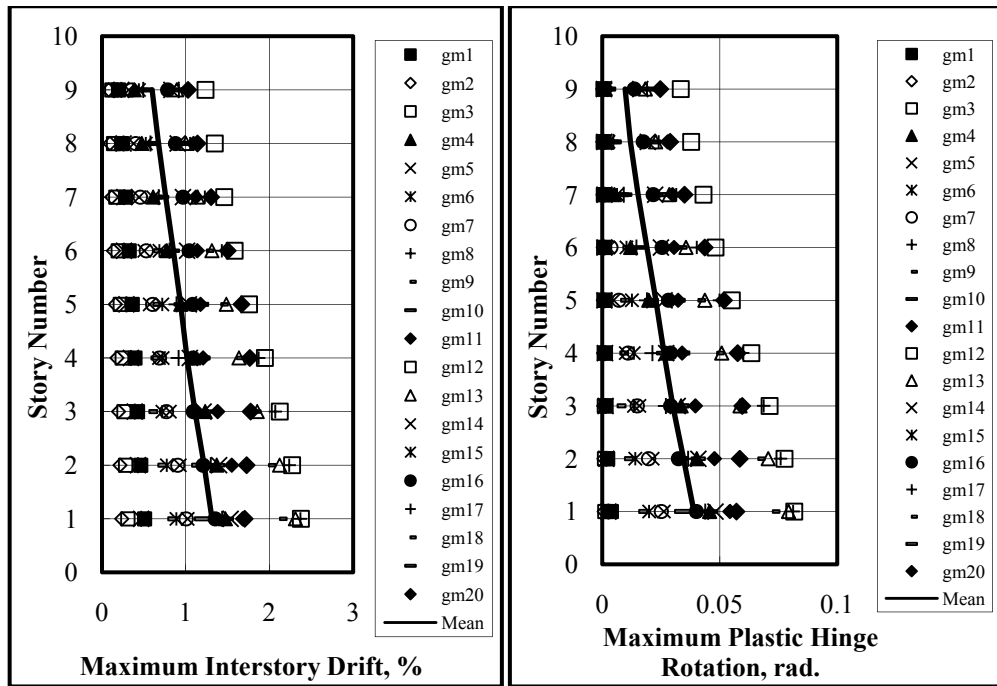


Figure 3.32: Response of 9 Story STMF-PD

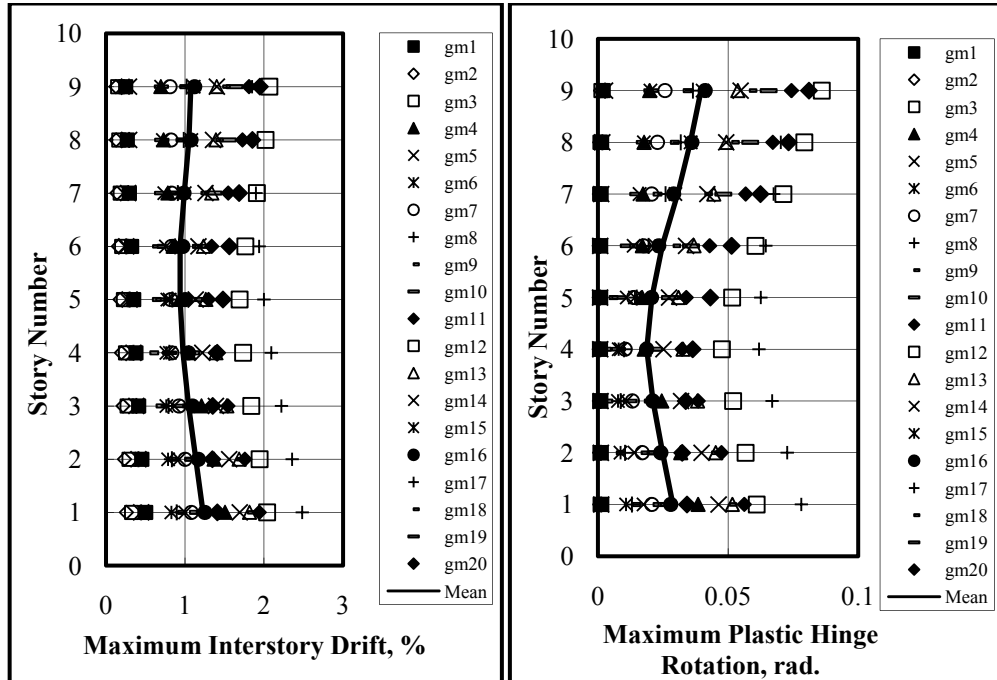


Figure 3.33: Response of 9 Story STMF-ED-IT

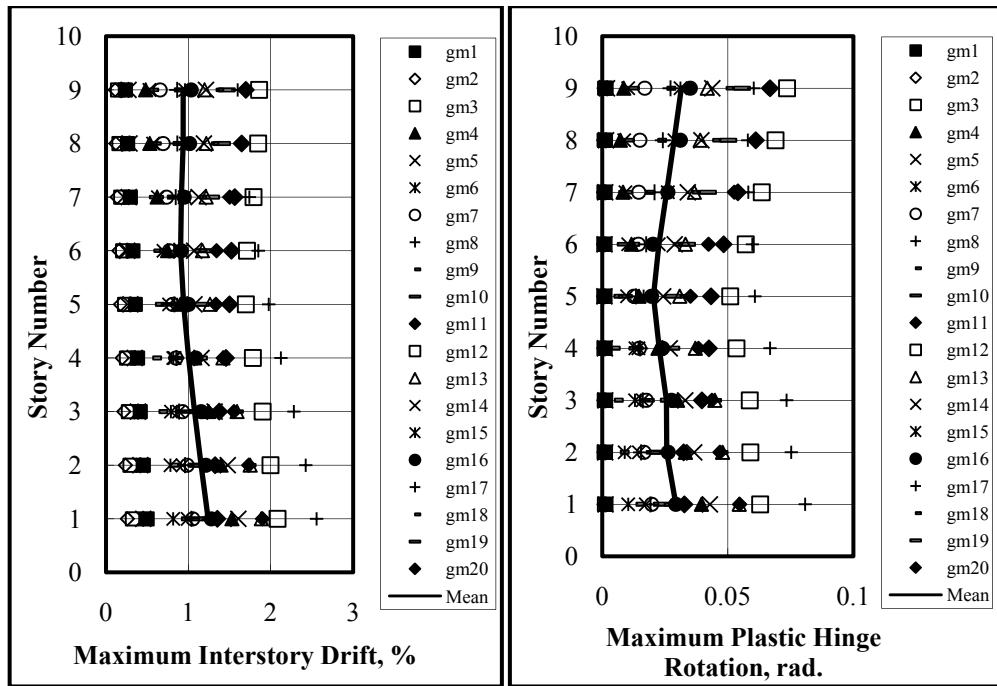


Figure 3.34: Response of 9 Story STMF-ED-CGL

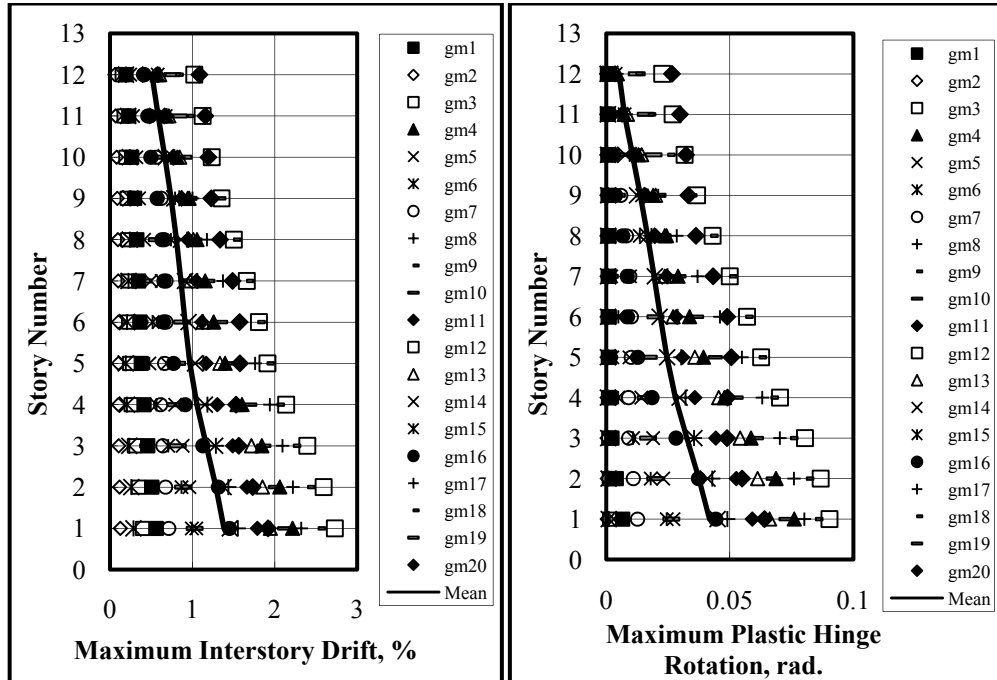


Figure 3.35: Response of 12 Story STMF-PD

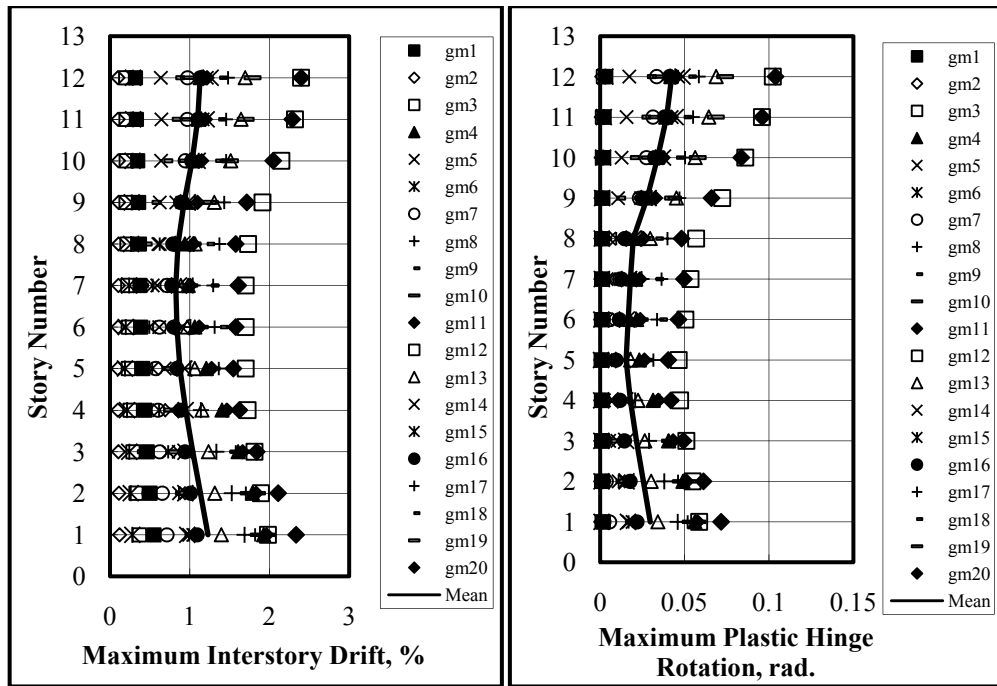


Figure 3.36: Response of 12 Story STMF-ED-IT

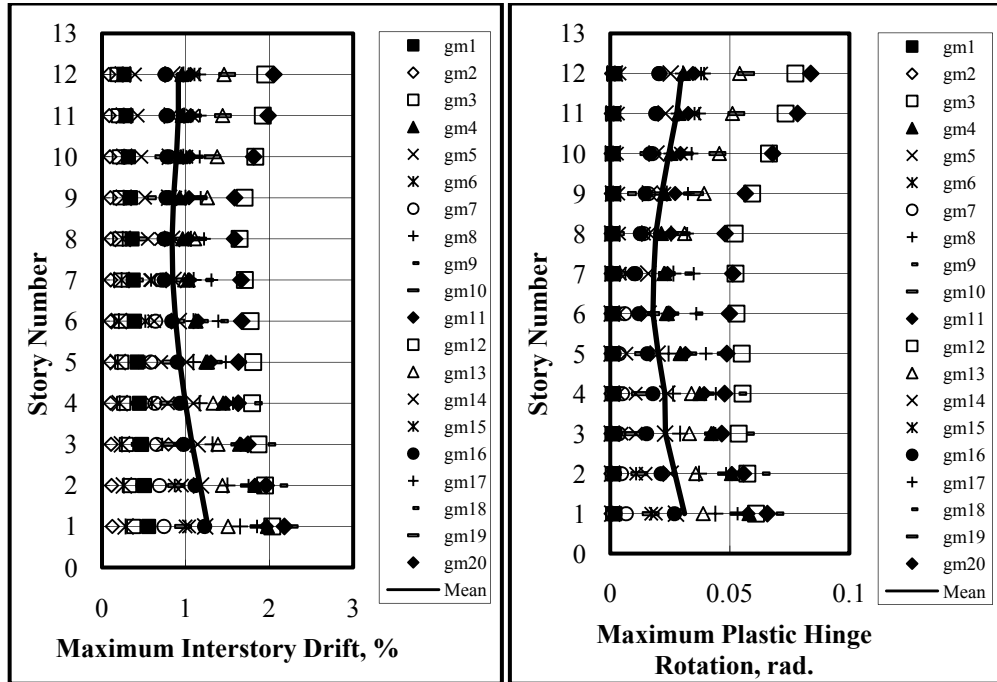


Figure 3.37: Response of 12 Story STMF-ED-CGL

The mean of the maximum quantities at every story was considered for comparison purposes. For all systems, the mean interstory drift and the mean plastic rotation are given in Figures 3.38 through 3.40 for the three different types of designs.

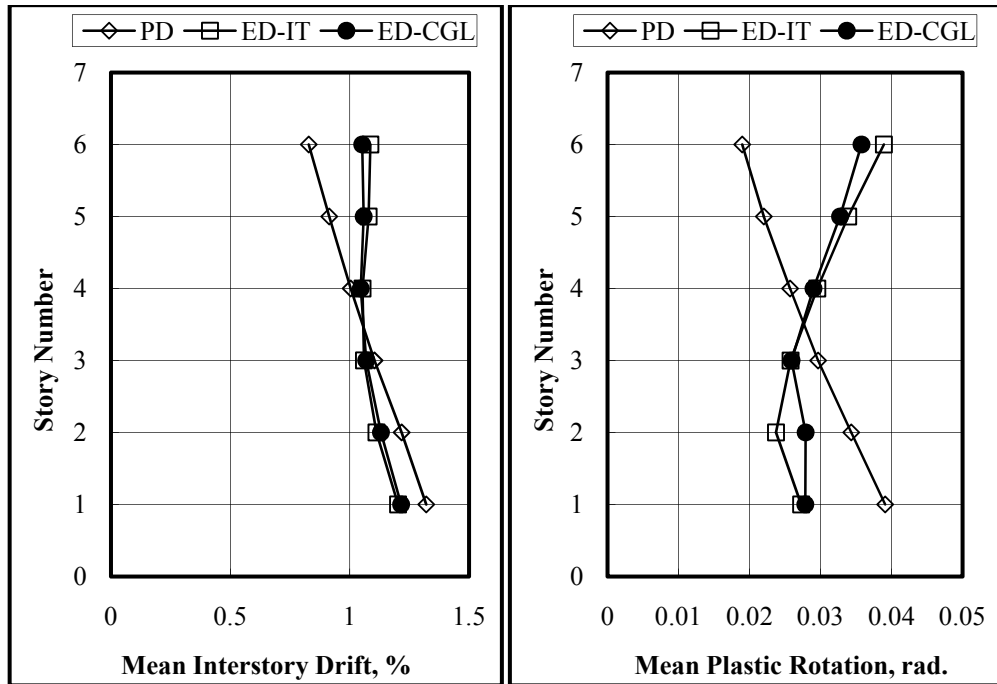


Figure 3.38: Comparisons of Different Designs – 6 Story Systems

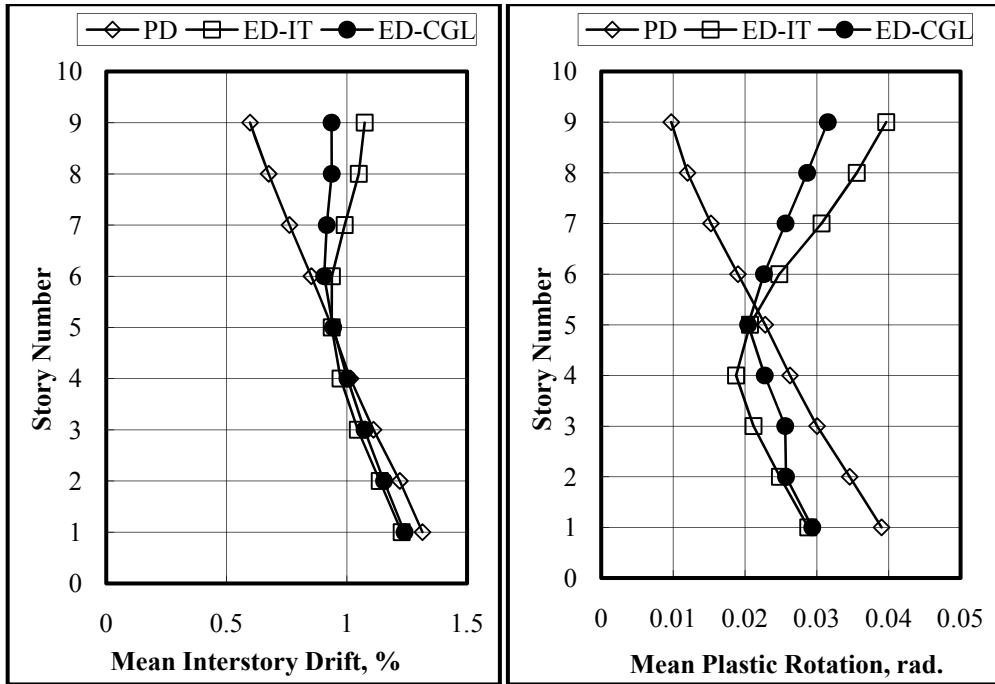


Figure 3.39: Comparisons of Different Designs – 9 Story Systems

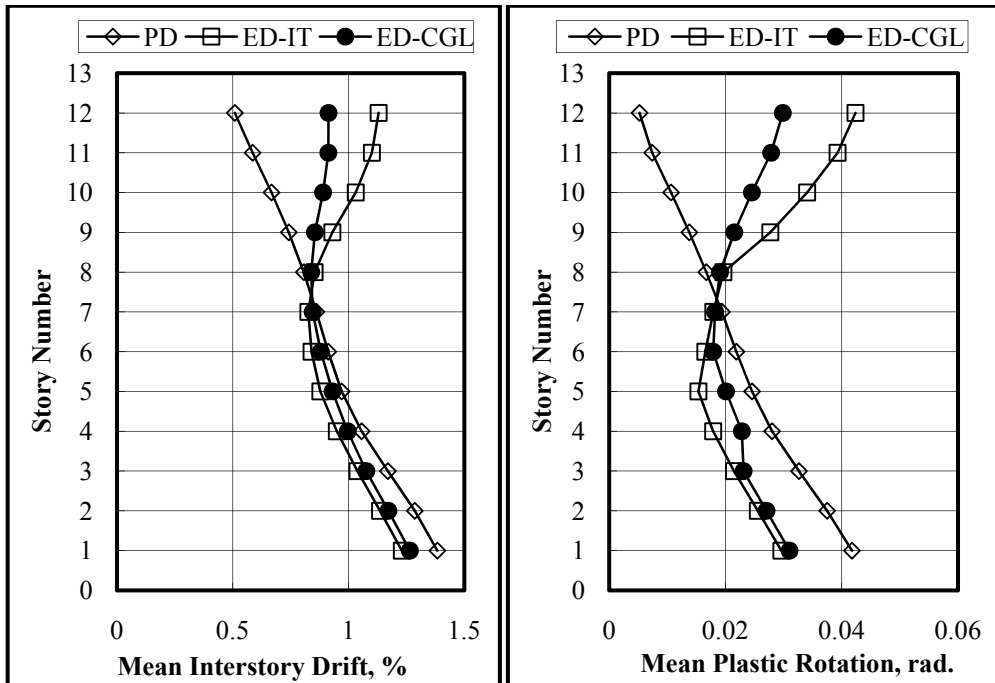


Figure 3.40: Comparisons of Different Designs – 12 Story Systems

In order to observe the level of change in the response quantities, normalized measures were used. Primarily, the response values for trusses designed based on PD and CGL were normalized by the response values of the truss designed based on IT. The ratios for interstory drifts and plastic rotations are given in Figures 3.41 through 3.43.

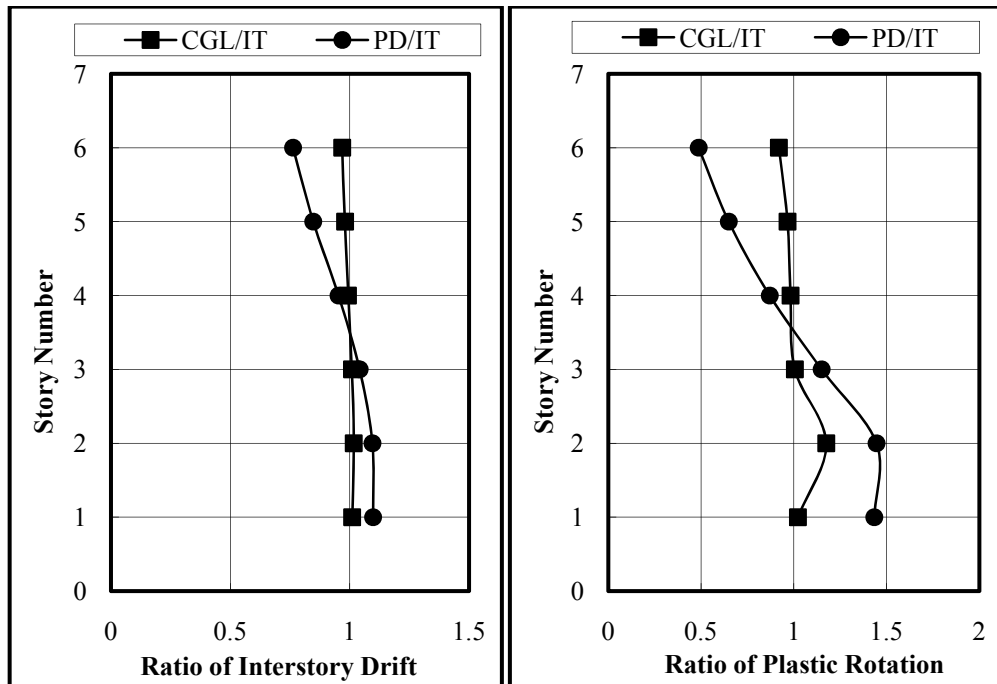


Figure 3.41: Ratio of Response Quantities – 6 Story Systems

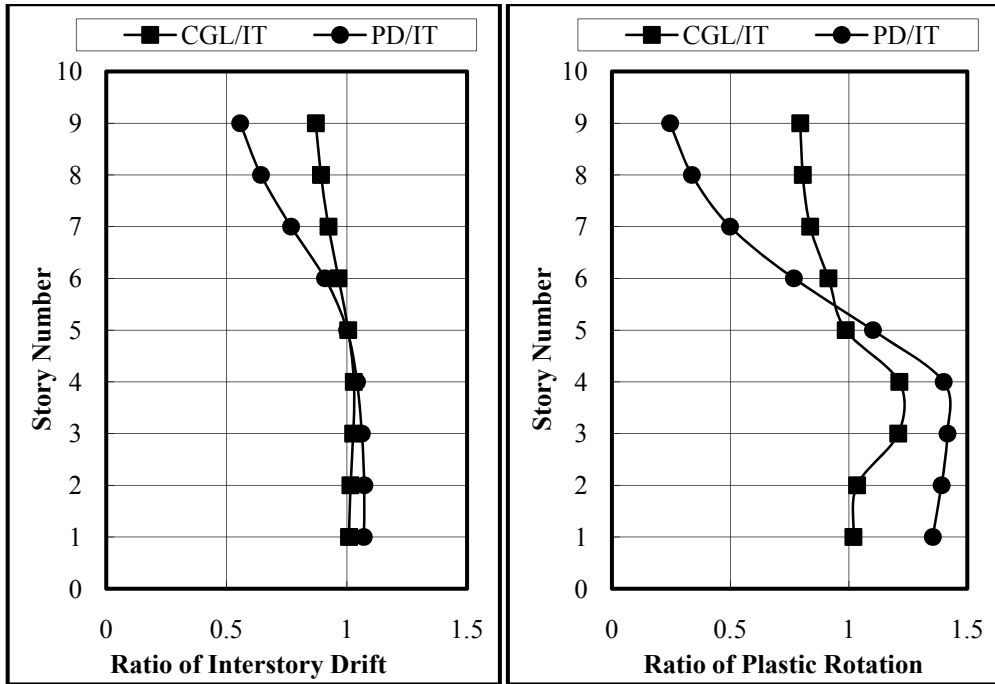


Figure 3.42: Ratio of Response Quantities – 9 Story Systems

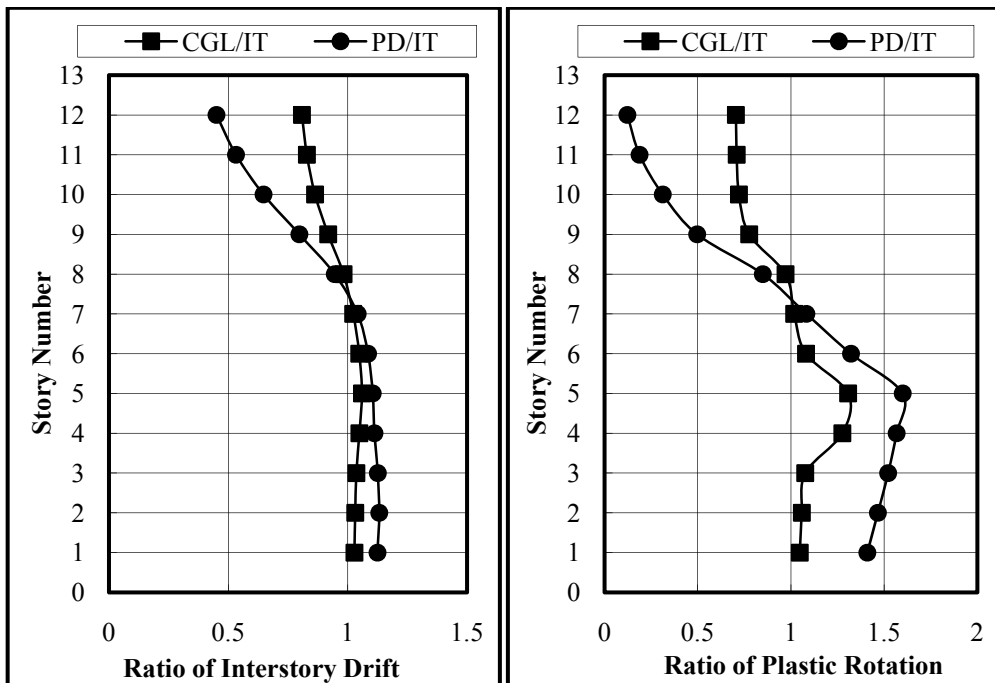


Figure 3.43: Ratio of Response Quantities – 12 Story Systems

These comparison graphs revealed that there are no significant changes in both response quantities between ED-IT and ED-CGL. Utilizing CGL distribution resulted in a 15 percent decrease in the lateral drifts at top stories. The drift levels for the bottom stories remained essentially the same. This is natural because both ED-IT and ED-CGL resulted in the same member sizes in these stories. When plastic rotations are considered, there is a reduction of 20 percent at top stories when ED-CGL is utilized. However, in some stories close to the base, increase in the plastic rotations on the order of 20 percent was observed. Therefore, the ED-CGL resulted in improvements at some levels and deterioration in others.

When the results for PD are considered, it can be observed that utilizing PD results in a minimal increase on the order of 7 percent in the lateral drifts at bottom stories. PD results in a decrease in drifts on the order of 45 percent at the top stories. Utilizing PD does not result in a significant increase in drift levels as expected. Naturally, utilization of the same type of truss resulted in an uneven distribution of lateral drifts along the height of the structure.

Contrary to the lateral drifts the plastic rotations increased by 40 percent at the bottom stories, as a result of PD. Reductions in plastic rotations as high as 75 percent were also observed at topmost stories. From a performance perspective utilizing PD does not have any detrimental effects as long as an increase in plastic rotations by 40 percent is tolerable. While plastic rotations increase at bottom stories PD has the beneficial effect of reducing the amount of rotations significantly at the top stories. In general, the increase and the reduction in percentage values of quantities are dependent on the number of story of STMF systems.

In conclusion, utilizing ED-IT and ED-CGL resulted in similar responses and no significant benefits of ED-CGL were observed. Because the use of ED-CGL is based on predicting the natural period before the design is finalized, it is more convenient to use ED-IT instead. The potential of utilizing PD is demonstrated. PD is a viable option that results in higher and lower plastic rotations at the bottom and top stories,

respectively. Future studies should explore the differences in results between ED-IT and PD in terms of final weight and cost of the systems.

## CHAPTER 4

### EVALUATION OF THE EXPECTED VERTICAL SHEAR STRENGTH FORMULATIONS

#### 4.1 The Expected Vertical Shear Strength Formulations

The design of STMF starts with the design of special segment. Since the inelastic activity is restrained in the special segment, shear strength at the fully yielded and strain hardened state should be known to design the members outside the special segment. This shear strength was named as, the expected vertical shear strength,  $V_{ne}$ . The expected vertical shear strength of the special segment,  $V_{ne}$ , is given in the AISC Seismic Specification (2005) as:

$$V_{ne} = \frac{3.75R_y M_{nc}}{L_s} + 0.075EI \frac{(L - L_s)}{L_s^3} + R_y (P_{nt} + 0.3P_{nc}) \sin \alpha \quad \text{Equation (4.1)}$$

Where;

$R_y$ : ratio of the expected yield stress to the specified minimum yield stress

$M_{nc}$ : nominal flexural strength of the chord members of the special segment

$EI$ : flexural elastic stiffness of a chord member of the special segment

$L$ : span length of the truss

$L_s$ : length of the special segment center-to-center support

$P_{nt}$ : nominal axial tension strength of diagonal members of the special segment

$P_{nc}$ : nominal axial compression strength of diagonal members of the special segment

$\alpha$ : angle of diagonal members with the horizontal.

The first two terms of Equation 4.1 are for the STMF systems with a vierendeel special segment. During the derivation of this formulation, Basha and Goel (1994) neglected the contribution of rotation in special segment member ends in finding the member end moments. This assumption leads to an overestimation of the elastic stiffness of the chord members. Afterwards, Chao and Goel (2008a) proposed a modification to Equation 4.1. They used the average of the two extreme cases for the elastic stiffness of the chord member in the special segment. If the chord member has fixed end conditions at two ends, then the elastic stiffness will be as follows:

$$\frac{M}{\theta} = k = \frac{6EI}{L_s} \quad \text{Equation (4.2)}$$

Where;

$\theta$ : relative vertical displacement at the chord ends divided by the length of the special segment.

If the chord member of the special segment is pinned at their ends, then the elastic stiffness of the chord member is equal to zero. By averaging the values for two extreme cases, Chao and Goel (2008a) proposed to use an elastic stiffness value as follows:

$$k = \frac{3EI}{L_s} \quad \text{Equation (4.3)}$$

By using the elastic stiffness of the chord member of the special segment as in Equation 4.3, the maximum elastic rotation can be expressed as follows:

$$\theta_e = \frac{M_p L_s}{3EI} \quad \text{Equation (4.4)}$$

Chao and Goel (2008a) obtained the maximum rotation of the chord member of the special segment by using a geometrical relation as:

$$\theta_u = \frac{L}{L_s} \left( \frac{\Delta}{h} \right) \quad \text{Equation (4.5)}$$

Where;

$\Delta/h$ : story drift.

Hence, the plastic rotation of the chord member was obtained as:

$$\theta_p = \theta_u - \theta_e = \frac{L}{L_s} \left( \frac{\Delta}{h} \right) - \frac{M_p L_s}{3EI} \quad \text{Equation (4.6)}$$

Finally, Chao and Goel (2008a) developed the expression for maximum moment as:

$$M_{\max} = M_p + \eta k \theta_p = (1 - \eta) R_y M_{nc} + 3EI \eta \left( \frac{L}{L_s^2} \right) \left( \frac{\Delta}{h} \right) \quad \text{Equation (4.7)}$$

Where;

$\eta$ : ratio of the post yield slope to the elastic slope of the assumed bilinear moment-rotation model of the chord member.

Chao and Goel (2008a) proposed to use  $\Delta/h=0.03$  and  $\eta=10\%$  and obtained  $V_{ne}$ , as:

$$V_{ne} = \frac{3.6 R_y M_{nc}}{L_s} + 0.036 EI \frac{L}{L_s^3} \quad \text{Equation (4.8)}$$

## 4.2 Details of the Numerical Modeling

To be able to evaluate the expected vertical shear strength formulations, a set of three dimensional finite element analyses was conducted. As shown in Figure 4.1, a one story and single bay frame was considered. The length of the special segment, the yield strength and the design of the truss were the parameters investigated.

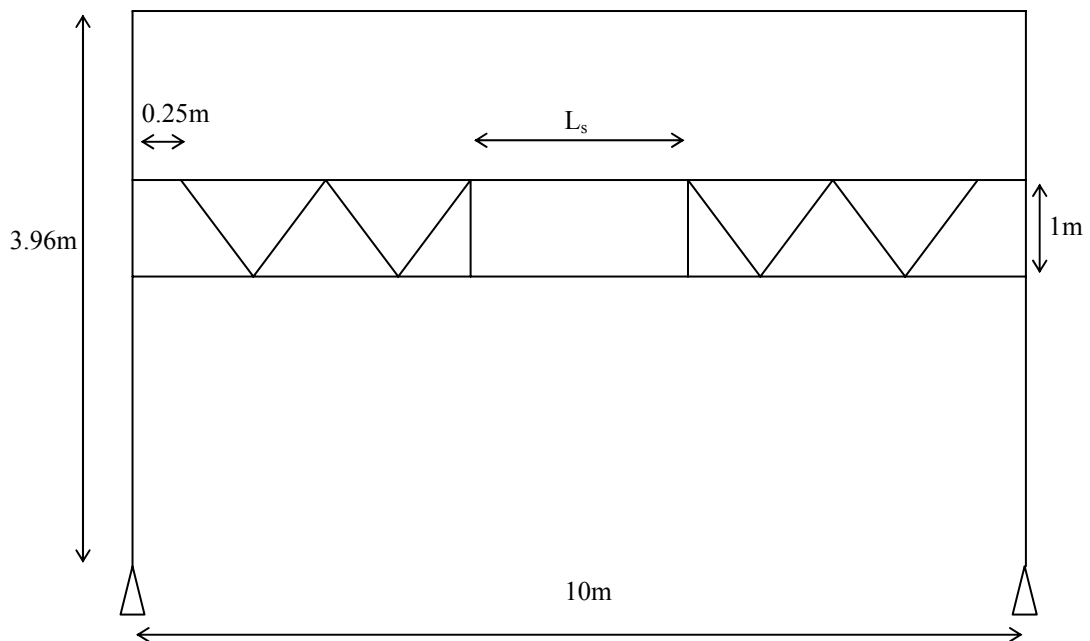


Figure 4.1: Dimensions of the Numerical Model

The section of the columns was W40x324 and the section of the link beam was W12x50 in all cases. These sections were not changed in order not to introduce any other parameters to the study. To explore the effect of the special segment length on the expected vertical shear strength of the special segment, the special segment length was taken as 2m, 2.5m, and 3m. Longer lengths were not considered because lengths in excess of 3m are impractical. Thirty five double channel sections were considered for the chord members of the truss along the span and same sections were used for the verticals as proposed by Chao and Goel (2008a). All the diagonals were

designed by using the expected vertical shear strength formulation proposed by Chao and Goel (2008a). The sections considered are tabulated in Table 4.1.

Table 4.1: The Chord and Diagonal Sections Considered

System Number	Chord Section	Diagonal Section
1	2C15x50	2L8x8x1
2	2C15x33.9	2L8x8x1
3	2C12x30	2L6x6x3/4
4	2C12x25	2L6x6x5/8
5	2C10x30	2L6x6x9/16
6	2C10x20	2L6x6x7/16
7	2C9x20	2L5x5x3/8
8	2C9x13.4	2L4x4x3/8
9	2C8x13.7	2L6x6x5/16
10	2C7x14.7	2L3-1/2x3-1/2x5/16
11	2C7x9.8	2L3-1/2x3-1/2x1/4
12	2C6x13	2L3x3x1/4
13	2C6x8.2	2L2x2x5/16
14	2C4x4.5	2L2x2x3/16
15	2C3x3.5	2L2x2x1/8
16	2MC18x58	2L8x8x1-1/8
17	2MC18x45.8	2L8x8x1-1/8
18	2MC13x50	2L8x8x1
19	2MC13x35	2L6x6x1
20	2MC12x50	2L8x8x7/8
21	2MC12x40	2L6x6x1
22	2MC12x31	2L6x6x7/8
23	2MC10x41.1	2L8x8x1/2
24	2MC10x28.5	2L6x6x5/8
25	2MC10x22	2L6x6x1/2
26	2MC10x6.5	2L3x3x1/4
27	2MC9x23.9	2L6x6x3/8
28	2MC8x22.8	2L4x4x1/2
29	2MC8x20	2L4x4x7/16
30	2MC8x8.5	2L3-1/2x3-1/2x1/4
31	2MC7x22.7	2L4x4x7/16
32	2MC6x18	2L3x3x3/8
33	2MC6x16.3	2L3x3x5/16
34	2MC6x6.5	2L2x2x3/8
35	2MC3x7.1	2L2x2x1/8

To be able to explore the extreme cases, A36 and A572-Gr50 steel grades were studied. The yield strengths of these materials are 248 MPa and 345 MPa, respectively.

The expected shear strength formulations presented by earlier researchers are based on a target story drift of 3 percent. To be able to make a fair assessment, pushover analyses were conducted using ANSYS and structures were subjected to 3 percent lateral drift. All elements were modeled as 8-node shell elements (shell 93) and the link beam was modeled with truss element (link 8). Bilinear kinematic hardening with a slope of 1 percent of the initial elastic slope was utilized in the models. The modeling details were similar to the ones adopted in Chapter 2.

The lateral drifts applied from the top of the models were 2%, 2.5%, and 3%. All the systems were analyzed for 2m, 2.5m and 3m special segment lengths and 248 MPa and 345 MPa yield strengths. A total of 210 analyses were completed.

The base shear values were monitored for all analysis. The vertical shear values of the special segment were obtained by using the following relation:

$$V_{ansys} = V_{base} \times \frac{H}{L} \quad \text{Equation (4.9)}$$

Where;

$V_{ansys}$ : the vertical shear value of the special segment obtained from analysis

$V_{base}$ : base shear obtained from analysis

$H$ : height of the model

$L$ : span length of the model.

### 4.3 Evaluation of the Formulation Proposed by Chao and Goel (2008a)

In order to evaluate the formulation of the expected vertical shear strength of the special segment proposed by Chao and Goel (2008a), their assumption for the elastic stiffness of the chord member was considered first. They assumed that the elastic stiffness ( $k_e$ ) of the chord member is the average of the two extreme cases, as in Equation 4.3.

To be able to calculate the elastic stiffness of the chord member in the special segment, the moment and the rotation values should be obtained. The moment at the end of the chord member in the special segment was calculated as:

$$M = \frac{V_{ansys} \times L_s}{4} \quad \text{Equation (4.10)}$$

The rotation of the chord member in the special segment was obtained as:

$$\theta = \frac{\Delta}{h} \times \frac{(L - L_s)}{L_s} \quad \text{Equation (4.11)}$$

After finding the moment and rotation values, the elastic stiffness of the chord member was calculated for six different systems and for 2m, 2.5m, and 3m lengths of the special segment. The results are illustrated in Tables 4.2 through 4.4.

Table 4.2: The Elastic Stiffness of the Chord Member for 2m  $L_s$

<b>System Number</b>	<b>EI/<math>L_s</math> kNm</b>	<b><math>k_e</math> kNm</b>	<b><math>k_e/(EI/L_s)</math></b>
1	33623	14904	0.44
3	13482	9567	0.71
5	8572	8510	0.99
12	1440	2832	1.97
16	56177	17608	0.31
33	2164	3439	1.59

Table 4.3: The Elastic Stiffness of the Chord Member for 2.5m  $L_s$

<b>System Number</b>	<b>EI/<math>L_s</math> kNm</b>	<b><math>k_e</math> kNm</b>	<b><math>k_e/(EI/L_s)</math></b>
1	26898	23117	0.86
3	10786	14230	1.32
5	6858	12230	1.78
12	1152	3647	3.17
16	44941	27887	0.62
33	1731	4533	2.62

Table 4.4: The Elastic Stiffness of the Chord Member for  $3m L_s$

System Number	$EI/L_s$ kNm	$k_e$ kNm	$k_e/(EI/L_s)$
1	22415	32571	1.45
3	8988	19162	2.13
5	5715	15881	2.78
12	960	4283	4.46
16	37451	40299	1.08
33	1443	5463	3.79

As can be seen from the results, the assumption proposed by Chao and Goel (2008a) is not appropriate for all cases. As the length of the special segment decreases and the depth of the section increases, the end conditions of the chord member in the special segment is closer to the pinned case, since the stiffness of the special panel is much larger than the stiffness of the neighboring panels. Therefore, the formulation for the expected vertical shear strength of the special segment proposed by Chao and Goel (2008a) overestimates the result for smaller lengths of special segment and deeper sections. The comparison of the formulations with the analysis results will be presented in the following section.

#### 4.4 The Proposed Formulation and Verification with the Analysis Results

Since the formulations proposed by the researchers are dependent on the elastic stiffness of the system and the end conditions of the chord in the special segment can not be predicted as discussed in the previous section, the proposed formulation can not be based on the elastic stiffness of the chord member in the special segment. Therefore, a curve fitting procedure was applied to the results of the finite element analysis. The moment values of the chord members in the special segment obtained from the analysis were normalized with the plastic moment values ( $M_p$ ) for both A572-Gr50 and A36 type of steel, as shown in Figure 4.2 and Figure 4.3.

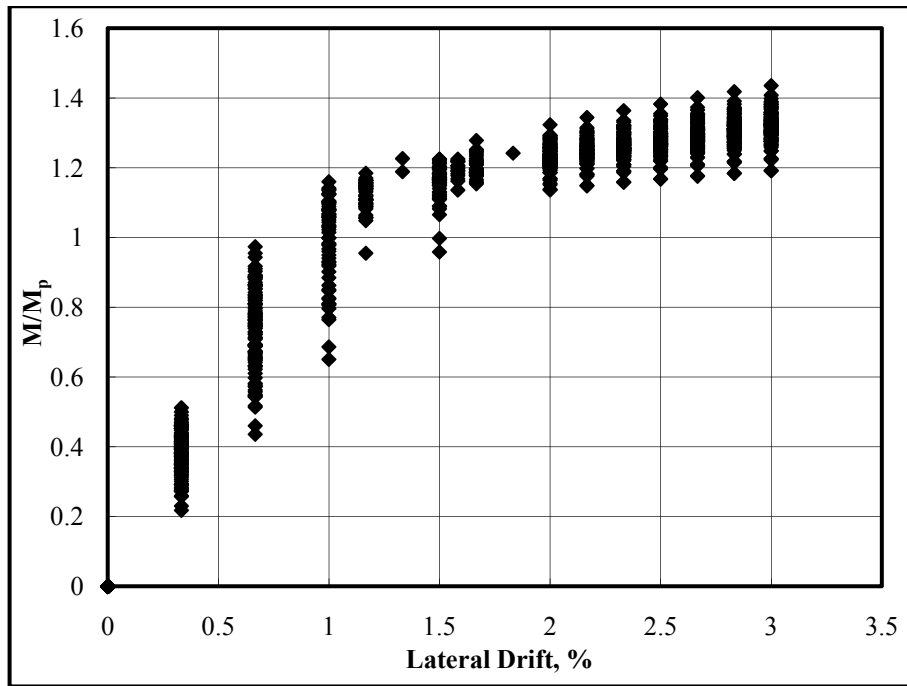


Figure 4.2: The Normalized Moment Values versus Lateral Drift for A572-Gr50 Type of Steel

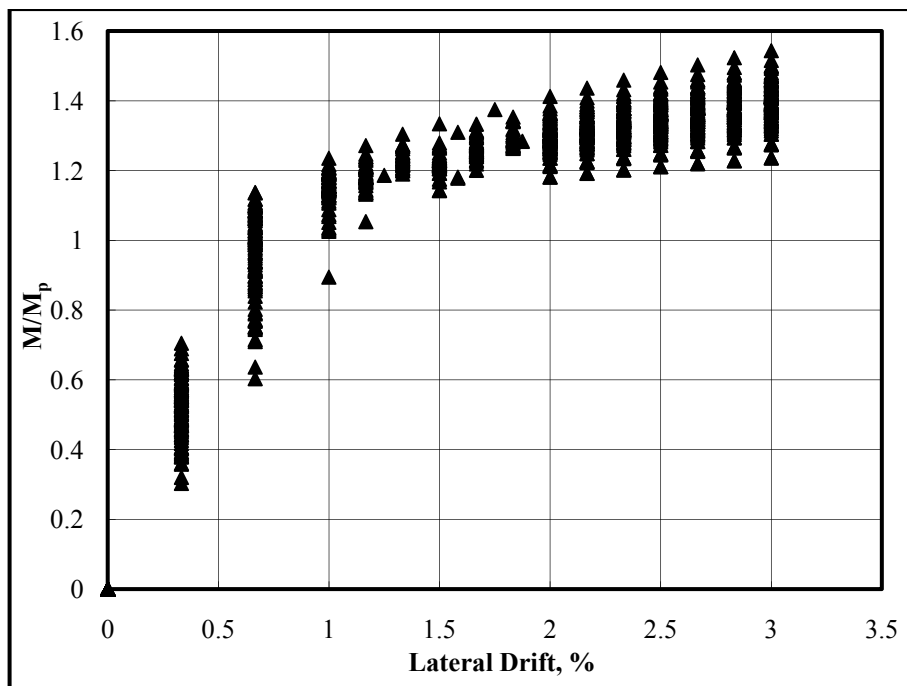


Figure 4.3: The Normalized Moment Values versus Lateral Drift for A36 Type of Steel

As shown in the Figures 4.2 and 4.3, the hardening of the material is based on the lateral drift of the system. As the system is exposed to larger lateral drift values, the rotation of the chord member in the special segment increases, as shown in Equation 4.11. This results in an increase in the hardening.

When Figures 4.2 and 4.3 are compared, it can be obviously seen that the yield strength of the material is also influential on the hardening. As the yield strength of the material is small, the lateral drift at which the chord member in the special segment yields, is also small. Therefore, the system, which has a material with smaller yield strength, has greater hardening.

For the curve fitting procedure the 84.1<sup>th</sup> percentile data were considered in order to calculate the vertical shear strength of the special segment conservatively. The formulation is based on the yield strength of the material, the lateral drift of the system, the plastic moment capacity of the chord member inside special segment, and special segment length. Moreover, the formulation is valid for STMFs having chord members with double channel sections.

The proposed formulation is as follows:

$$V_{ne} = H_f \frac{4M_p}{L_s} \quad \text{Equation (4.12)}$$

$$H_f = (1.25 - 0.000725F_y) \left( 10 \frac{\Delta}{h} + 1.05 \right)$$

Where;

$H_f$ : the hardening factor

$F_y$ : the yield strength of steel in MPa

$\Delta/h$ : story drift.

The formulation in the AISC Seismic Specification (2005) was named as  $V_{ne1}$ , the formulation proposed by Chao and Goel (2008a) was named as  $V_{ne2}$ , the proposed formulation indicated in Equation 4.12 was named as  $V_{ne3}$ , and the results obtained from finite element analysis was named as  $V_{ansys}$  in the Tables 4.5 through 4.10. Since story drift was used as 3% in past formulations, the same value was used in Equation 4.12 to calculate the expected vertical shear strength of the special segment. The expected vertical shear strength of the special segment obtained by the formulations are compared with the analysis results obtained for 3% story drift in the following tables. The graphical illustrations of these tables are given in Figures 4.4 through 4.9. The statistical quantities including all cases are tabulated in Table 4.11.

Table 4.5: Comparison of Results for 2m L<sub>s</sub> and A36 Type of Steel

System	V <sub>ne1</sub> kN	V <sub>ne2</sub> kN	V <sub>ne3</sub> kN	V <sub>ansys</sub> kN	V <sub>ne1</sub> /V <sub>ansys</sub> (Ratio 1)	V <sub>ne2</sub> /V <sub>ansys</sub> (Ratio 2)	V <sub>ne3</sub> /V <sub>ansys</sub> (Ratio 3)
1	6088.24	4029.08	1609.87	1637.56	3.72	2.46	0.98
2	4707.21	3103.27	1193.89	1176.97	4.00	2.64	1.01
3	2537.91	1708.34	794.36	824.93	3.08	2.07	0.96
4	2246.09	1509.09	690.95	707.94	3.17	2.13	0.98
5	1693.07	1162.46	627.50	658.28	2.57	1.77	0.95
6	1280.87	875.05	455.93	471.14	2.72	1.86	0.97
7	1018.03	703.62	397.18	411.86	2.47	1.71	0.96
8	788.91	542.53	296.12	298.14	2.65	1.82	0.99
9	618.44	431.47	258.52	262.95	2.35	1.64	0.98
10	488.27	346.50	229.14	233.65	2.09	1.48	0.98
11	374.32	264.07	168.98	168.45	2.22	1.57	1.00
12	327.16	236.33	171.33	173.12	1.89	1.37	0.99
13	242.24	173.68	121.27	120.45	2.01	1.44	1.01
14	77.90	58.38	49.82	47.10	1.65	1.24	1.06
15	38.51	29.92	29.14	26.82	1.44	1.12	1.09
16	9881.63	6452.82	2242.07	2169.29	4.56	2.97	1.03
17	8423.61	5489.06	1861.34	1764.27	4.77	3.11	1.06
18	4847.26	3242.21	1428.91	1451.79	3.34	2.23	0.98
19	3855.15	2568.43	1092.83	1070.86	3.60	2.40	1.02
20	4219.91	2842.19	1327.85	1338.99	3.15	2.12	0.99
21	3648.75	2451.17	1121.03	1112.48	3.28	2.20	1.01
22	3127.25	2094.34	933.02	897.56	3.48	2.33	1.04
23	2559.38	1751.43	923.62	923.80	2.77	1.90	1.00
24	2030.53	1383.05	705.05	688.84	2.95	2.01	1.02
25	1637.88	1113.97	561.69	542.31	3.02	2.05	1.04
26	375.87	257.92	138.66	148.16	2.54	1.74	0.94
27	1403.06	965.38	528.79	516.45	2.72	1.87	1.02
28	1087.79	757.55	448.88	439.06	2.48	1.73	1.02
29	929.26	647.61	385.43	382.44	2.43	1.69	1.01
30	396.88	276.29	163.34	166.83	2.38	1.66	0.98
31	841.88	595.18	385.43	376.05	2.24	1.58	1.02
32	549.23	393.78	274.97	262.50	2.09	1.50	1.05
33	483.21	347.03	244.42	234.26	2.06	1.48	1.04
34	202.60	145.06	100.59	99.01	2.05	1.47	1.02
35	68.12	53.17	52.64	48.37	1.41	1.10	1.09

Table 4.6: Comparison of Results for 2.5m L<sub>s</sub> and A36 Type of Steel

System	V <sub>ne1</sub> kN	V <sub>ne2</sub> kN	V <sub>ne3</sub> kN	V <sub>ansys</sub> kN	V <sub>ne1</sub> /V <sub>ansys</sub> (Ratio 1)	V <sub>ne2</sub> /V <sub>ansys</sub> (Ratio 2)	V <sub>ne3</sub> /V <sub>ansys</sub> (Ratio 3)
1	3256.70	2351.76	1287.90	1301.41	2.50	1.81	0.99
2	2507.41	1803.11	955.11	947.63	2.65	1.90	1.01
3	1383.17	1017.21	635.49	642.87	2.15	1.58	0.99
4	1221.62	896.64	552.76	554.98	2.20	1.62	1.00
5	943.00	707.78	502.00	506.70	1.86	1.40	0.99
6	709.51	529.84	364.75	364.66	1.95	1.45	1.00
7	571.14	431.52	317.74	317.29	1.80	1.36	1.00
8	440.18	330.91	236.90	231.47	1.90	1.43	1.02
9	350.54	267.30	206.82	202.30	1.73	1.32	1.02
10	281.96	218.53	183.31	178.80	1.58	1.22	1.03
11	214.77	165.53	135.18	129.94	1.65	1.27	1.04
12	192.62	151.74	137.06	132.20	1.46	1.15	1.04
13	141.46	110.68	97.02	92.58	1.53	1.20	1.05
14	47.74	38.83	39.86	36.24	1.32	1.07	1.10
15	24.54	20.55	23.31	20.60	1.19	1.00	1.13
16	5208.82	3706.16	1793.65	1781.81	2.92	2.08	1.01
17	4429.90	3144.39	1489.07	1460.08	3.03	2.15	1.02
18	2623.45	1916.41	1143.13	1144.53	2.29	1.67	1.00
19	2077.44	1511.13	874.27	856.19	2.43	1.76	1.02
20	2301.33	1693.47	1062.28	1052.16	2.19	1.61	1.01
21	1984.22	1456.16	896.83	879.54	2.26	1.66	1.02
22	1694.85	1239.72	746.42	718.30	2.36	1.73	1.04
23	1420.32	1062.46	738.90	722.58	1.97	1.47	1.02
24	1121.08	834.64	564.04	542.68	2.07	1.54	1.04
25	902.84	671.14	449.35	429.04	2.10	1.56	1.05
26	209.21	156.94	110.93	112.90	1.85	1.39	0.98
27	783.29	589.16	423.03	404.96	1.93	1.45	1.04
28	615.37	468.41	359.11	341.82	1.80	1.37	1.05
29	526.09	400.74	308.34	296.63	1.77	1.35	1.04
30	224.42	170.77	130.67	128.39	1.75	1.33	1.02
31	484.15	373.89	308.34	291.64	1.66	1.28	1.06
32	320.74	250.96	219.98	204.03	1.57	1.23	1.08
33	282.70	221.54	195.53	181.73	1.56	1.22	1.08
34	118.14	92.32	80.47	76.02	1.55	1.21	1.06
35	43.63	36.67	42.12	37.14	1.17	0.99	1.13

Table 4.7: Comparison of Results for 3m L<sub>s</sub> and A36 Type of Steel

System	V <sub>ne1</sub> kN	V <sub>ne2</sub> kN	V <sub>ne3</sub> kN	V <sub>ansys</sub> kN	V <sub>ne1</sub> /V <sub>ansys</sub> (Ratio 1)	V <sub>ne2</sub> /V <sub>ansys</sub> (Ratio 2)	V <sub>ne3</sub> /V <sub>ansys</sub> (Ratio 3)
1	2004.10	1565.30	1073.25	1060.02	1.89	1.48	1.01
2	1536.07	1194.99	795.93	778.04	1.97	1.54	1.02
3	868.02	689.48	529.57	519.69	1.67	1.33	1.02
4	765.02	606.58	460.63	449.90	1.70	1.35	1.02
5	604.86	489.23	418.33	407.10	1.49	1.20	1.03
6	452.63	364.49	303.96	294.18	1.54	1.24	1.03
7	368.95	300.13	264.79	255.27	1.45	1.18	1.04
8	282.83	229.08	197.41	187.30	1.51	1.22	1.05
9	228.69	187.50	172.35	162.90	1.40	1.15	1.06
10	187.18	155.54	152.76	143.54	1.30	1.08	1.06
11	141.73	117.24	112.65	104.90	1.35	1.12	1.07
12	130.12	109.56	114.22	106.04	1.23	1.03	1.08
13	94.87	79.44	80.85	74.62	1.27	1.06	1.08
14	33.37	28.80	33.22	29.30	1.14	0.98	1.13
15	17.69	15.59	19.43	16.62	1.06	0.94	1.17
16	3154.73	2429.33	1494.71	1470.48	2.15	1.65	1.02
17	2676.06	2055.91	1240.89	1213.61	2.21	1.69	1.02
18	1634.52	1290.39	952.60	930.35	1.76	1.39	1.02
19	1288.44	1013.20	728.55	701.43	1.84	1.44	1.04
20	1445.15	1148.54	885.23	854.69	1.69	1.34	1.04
21	1242.39	984.96	747.36	716.73	1.73	1.37	1.04
22	1057.47	835.85	622.01	589.41	1.79	1.42	1.06
23	907.76	732.08	615.75	585.53	1.55	1.25	1.05
24	712.86	572.49	470.04	441.88	1.61	1.30	1.06
25	573.15	459.68	374.46	350.27	1.64	1.31	1.07
26	134.11	108.42	92.44	90.15	1.49	1.20	1.03
27	503.57	408.06	352.53	329.19	1.53	1.24	1.07
28	400.71	328.04	299.26	277.19	1.45	1.18	1.08
29	342.83	280.83	256.95	240.05	1.43	1.17	1.07
30	146.08	119.56	108.89	103.42	1.41	1.16	1.05
31	320.18	265.29	256.95	236.03	1.36	1.12	1.09
32	215.10	180.13	183.31	165.47	1.30	1.09	1.11
33	189.90	159.23	162.95	147.10	1.29	1.08	1.11
34	79.12	66.19	67.06	61.27	1.29	1.08	1.09
35	31.58	27.90	35.10	30.03	1.05	0.93	1.17

Table 4.8: Comparison of Results for 2m L<sub>s</sub> and A572-Gr50 Type of Steel

System	V <sub>ne1</sub> kN	V <sub>ne2</sub> kN	V <sub>ne3</sub> kN	V <sub>ansys</sub> kN	V <sub>ne1</sub> /V <sub>ansys</sub> (Ratio 1)	V <sub>ne2</sub> /V <sub>ansys</sub> (Ratio 2)	V <sub>ne3</sub> /V <sub>ansys</sub> (Ratio 3)
1	6494.56	4419.15	2089.65	2092.32	3.10	2.11	1.00
2	5008.54	3392.55	1549.70	1518.62	3.30	2.23	1.02
3	2738.40	1900.81	1031.10	1060.50	2.58	1.79	0.97
4	2420.48	1676.51	896.87	912.51	2.65	1.84	0.98
5	1851.45	1314.50	814.51	849.43	2.18	1.55	0.96
6	1395.95	985.52	591.81	608.92	2.29	1.62	0.97
7	1118.28	799.85	515.55	533.85	2.09	1.50	0.97
8	863.65	614.28	384.37	386.64	2.23	1.59	0.99
9	683.69	494.11	335.56	341.92	2.00	1.45	0.98
10	546.11	402.02	297.43	304.62	1.79	1.32	0.98
11	416.97	305.02	219.34	219.86	1.90	1.39	1.00
12	370.40	277.84	222.39	226.40	1.64	1.23	0.98
13	272.85	203.06	157.41	157.71	1.73	1.29	1.00
14	90.48	70.45	64.67	62.23	1.45	1.13	1.04
15	45.87	36.98	37.83	35.57	1.29	1.04	1.06
16	10447.51	6996.07	2910.26	2786.88	3.75	2.51	1.04
17	8893.40	5940.06	2416.07	2283.82	3.89	2.60	1.06
18	5207.91	3588.43	1854.76	1859.90	2.80	1.93	1.00
19	4130.98	2833.22	1418.52	1383.25	2.99	2.05	1.03
20	4555.05	3163.92	1723.58	1717.91	2.65	1.84	1.00
21	3931.69	2722.80	1455.13	1433.08	2.74	1.90	1.02
22	3362.74	2320.41	1211.08	1163.59	2.89	1.99	1.04
23	2792.50	1975.22	1198.88	1194.23	2.34	1.65	1.00
24	2208.49	1553.89	915.18	893.31	2.47	1.74	1.02
25	1779.65	1250.06	729.09	705.26	2.52	1.77	1.03
26	410.87	291.52	179.98	191.35	2.15	1.52	0.94
27	1536.52	1093.51	686.38	671.03	2.29	1.63	1.02
28	1201.09	866.32	582.66	571.17	2.10	1.52	1.02
29	1026.54	741.00	500.30	497.43	2.06	1.49	1.01
30	438.10	315.87	212.02	216.92	2.02	1.46	0.98
31	939.16	688.57	500.30	491.04	1.91	1.40	1.02
32	618.63	460.41	356.92	344.26	1.80	1.34	1.04
33	544.90	406.25	317.26	307.21	1.77	1.32	1.03
34	227.99	169.44	130.57	129.62	1.76	1.31	1.01
35	81.41	65.93	68.33	64.06	1.27	1.03	1.07

Table 4.9: Comparison of Results for 2.5m L<sub>s</sub> and A572-Gr50 Type of Steel

System	V <sub>ne1</sub> kN	V <sub>ne2</sub> kN	V <sub>ne3</sub> kN	V <sub>ansys</sub> kN	V <sub>ne1</sub> /V <sub>ansys</sub> (Ratio 1)	V <sub>ne2</sub> /V <sub>ansys</sub> (Ratio 2)	V <sub>ne3</sub> /V <sub>ansys</sub> (Ratio 3)
1	3581.76	2663.82	1671.72	1676.09	2.14	1.59	1.00
2	2748.48	2034.53	1239.76	1228.61	2.24	1.66	1.01
3	1543.57	1171.19	824.88	835.19	1.85	1.40	0.99
4	1361.14	1030.57	717.50	721.67	1.89	1.43	0.99
5	1069.70	829.41	651.61	660.84	1.62	1.26	0.99
6	801.57	618.22	473.45	476.37	1.68	1.30	0.99
7	651.34	508.51	412.44	415.31	1.57	1.22	0.99
8	499.97	388.31	307.50	303.37	1.65	1.28	1.01
9	402.74	317.41	268.45	265.76	1.52	1.19	1.01
10	328.23	262.94	237.95	235.19	1.40	1.12	1.01
11	248.89	198.28	175.47	171.24	1.45	1.16	1.02
12	227.21	184.95	177.91	174.33	1.30	1.06	1.02
13	165.95	134.19	125.93	122.30	1.36	1.10	1.03
14	57.80	48.49	51.74	48.23	1.20	1.01	1.07
15	30.42	26.20	30.26	27.48	1.11	0.95	1.10
16	5661.53	4140.76	2328.21	2289.34	2.47	1.81	1.02
17	4805.74	3505.19	1932.85	1890.10	2.54	1.85	1.02
18	2911.96	2193.39	1483.81	1481.15	1.97	1.48	1.00
19	2298.10	1722.96	1134.82	1112.56	2.07	1.55	1.02
20	2569.44	1950.86	1378.87	1364.92	1.88	1.43	1.01
21	2210.58	1673.46	1164.11	1143.13	1.93	1.46	1.02
22	1883.24	1420.58	968.87	936.76	2.01	1.52	1.03
23	1606.82	1241.50	959.11	942.75	1.70	1.32	1.02
24	1263.45	971.30	732.14	709.27	1.78	1.37	1.03
25	1016.25	780.02	583.27	561.43	1.81	1.39	1.04
26	237.21	183.81	143.99	147.29	1.61	1.25	0.98
27	890.06	691.66	549.11	530.65	1.68	1.30	1.03
28	706.00	555.43	466.13	449.22	1.57	1.24	1.04
29	603.92	475.45	400.24	389.81	1.55	1.22	1.03
30	257.40	202.43	169.61	168.66	1.53	1.20	1.01
31	561.97	448.60	400.24	384.27	1.46	1.17	1.04
32	376.26	304.26	285.54	269.75	1.39	1.13	1.06
33	332.05	268.92	253.81	240.20	1.38	1.12	1.06
34	138.45	111.82	104.45	100.46	1.38	1.11	1.04
35	54.26	46.88	54.67	49.51	1.10	0.95	1.10

Table 4.10: Comparison of Results for 3m L<sub>s</sub> and A572-Gr50 Type of Steel

System	V <sub>ne1</sub> kN	V <sub>ne2</sub> kN	V <sub>ne3</sub> kN	V <sub>ansys</sub> kN	V <sub>ne1</sub> /V <sub>ansys</sub> (Ratio 1)	V <sub>ne2</sub> /V <sub>ansys</sub> (Ratio 2)	V <sub>ne3</sub> /V <sub>ansys</sub> (Ratio 3)
1	2274.98	1825.34	1393.10	1378.46	1.65	1.32	1.01
2	1736.96	1387.84	1033.13	1014.64	1.71	1.37	1.02
3	1001.68	817.80	687.40	680.78	1.47	1.20	1.01
4	881.28	718.19	597.92	589.77	1.49	1.22	1.01
5	710.45	590.59	543.01	535.29	1.33	1.10	1.01
6	529.35	438.13	394.54	387.12	1.37	1.13	1.02
7	435.78	364.29	343.70	336.52	1.29	1.08	1.02
8	332.66	276.92	256.25	247.29	1.35	1.12	1.04
9	272.19	229.26	223.71	215.37	1.26	1.06	1.04
10	225.73	192.56	198.29	190.02	1.19	1.01	1.04
11	170.16	144.53	146.22	139.10	1.22	1.04	1.05
12	158.95	137.23	148.26	140.70	1.13	0.98	1.05
13	115.27	99.03	104.94	99.14	1.16	1.00	1.06
14	41.75	36.84	43.12	39.15	1.07	0.94	1.10
15	22.59	20.30	25.22	22.26	1.01	0.91	1.13
16	3531.99	2791.49	1940.18	1902.63	1.86	1.47	1.02
17	2989.25	2356.58	1610.71	1575.76	1.90	1.50	1.02
18	1874.95	1521.20	1236.51	1214.70	1.54	1.25	1.02
19	1472.33	1189.72	945.68	917.88	1.60	1.30	1.03
20	1668.58	1363.04	1149.06	1118.40	1.49	1.22	1.03
21	1431.02	1166.05	970.09	939.18	1.52	1.24	1.03
22	1214.46	986.56	807.39	773.47	1.57	1.28	1.04
23	1063.17	881.27	799.25	769.58	1.38	1.15	1.04
24	831.49	686.38	610.12	582.04	1.43	1.18	1.05
25	667.67	550.41	486.06	461.61	1.45	1.19	1.05
26	157.44	130.82	119.99	118.63	1.33	1.10	1.01
27	592.55	493.48	457.59	434.58	1.36	1.14	1.05
28	476.24	400.55	388.44	366.77	1.30	1.09	1.06
29	407.69	343.09	333.53	317.54	1.28	1.08	1.05
30	173.57	145.94	141.34	136.74	1.27	1.07	1.03
31	385.03	327.55	333.53	312.78	1.23	1.05	1.07
32	261.36	224.54	237.95	220.00	1.19	1.02	1.08
33	231.03	198.71	211.51	195.51	1.18	1.02	1.08
34	96.05	82.44	87.04	81.42	1.18	1.01	1.07
35	40.44	36.41	45.56	40.20	1.01	0.91	1.13

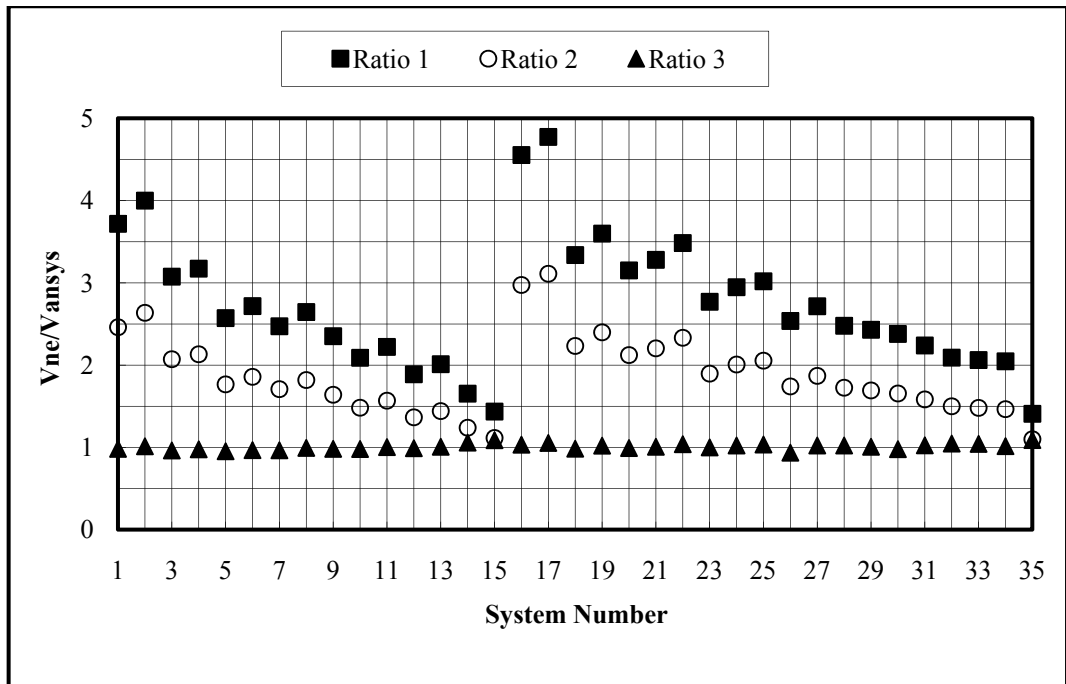


Figure 4.4: Ratio of Predicted to the Results of Analysis for Systems with A36 Type of Steel – 2m  $L_s$

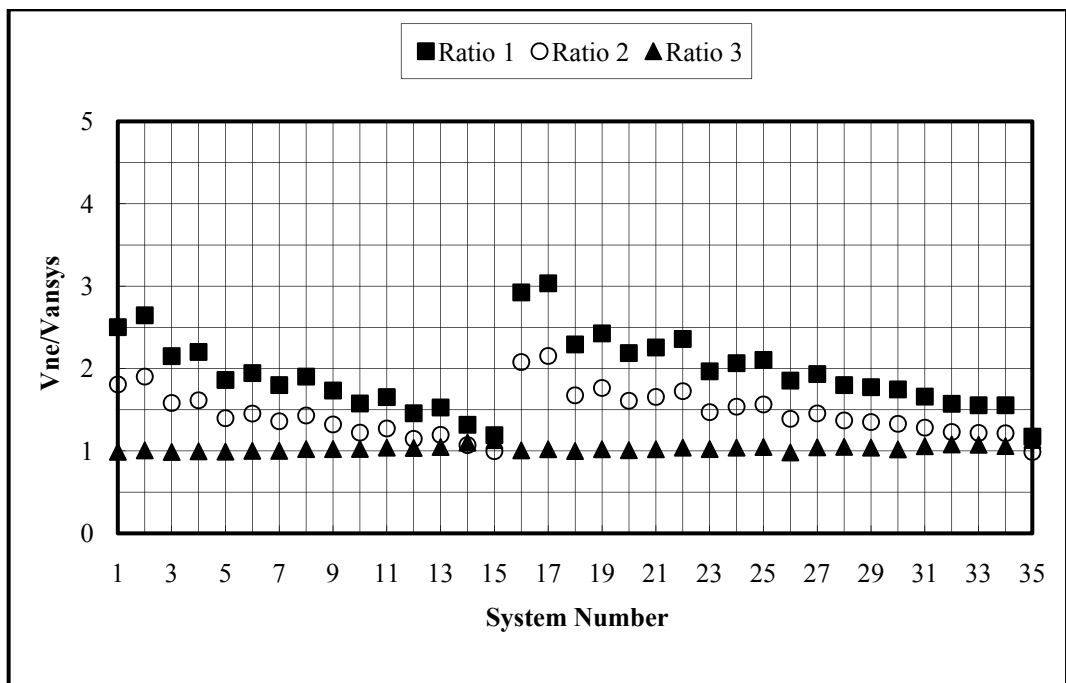


Figure 4.5: Ratio of Predicted to the Results of Analysis for Systems with A36 Type of Steel – 2.5m  $L_s$

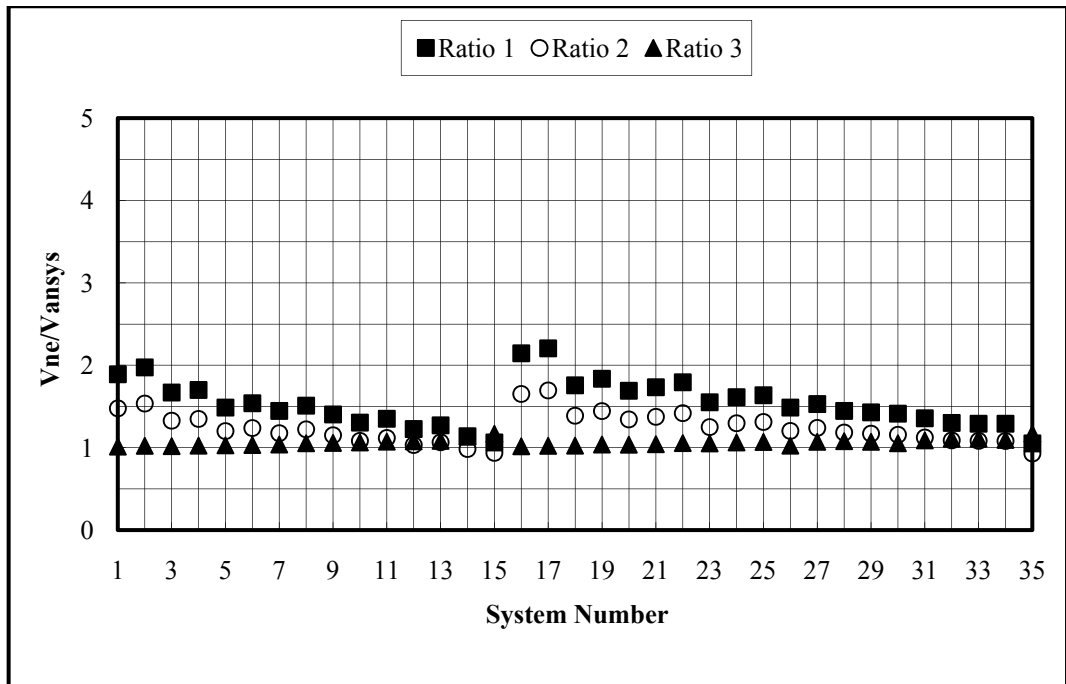


Figure 4.6: Ratio of Predicted to the Results of Analysis for Systems with A36 Type of Steel – 3m  $L_s$

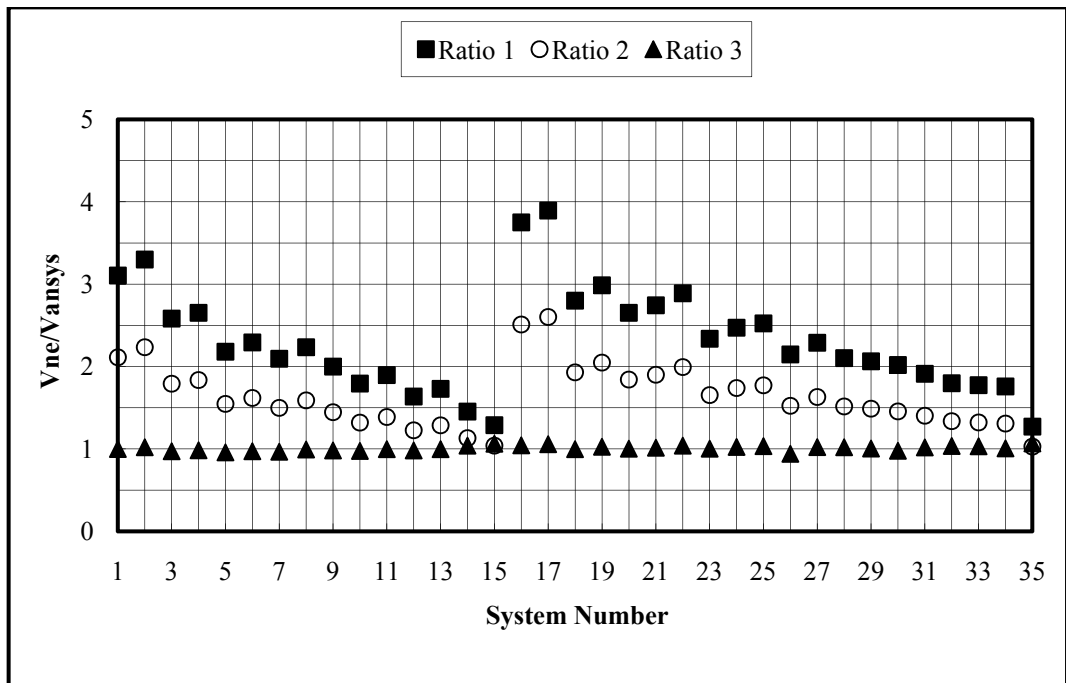


Figure 4.7: Ratio of Predicted to the Results of Analysis for Systems with A572-Gr50 Type of Steel – 2m  $L_s$

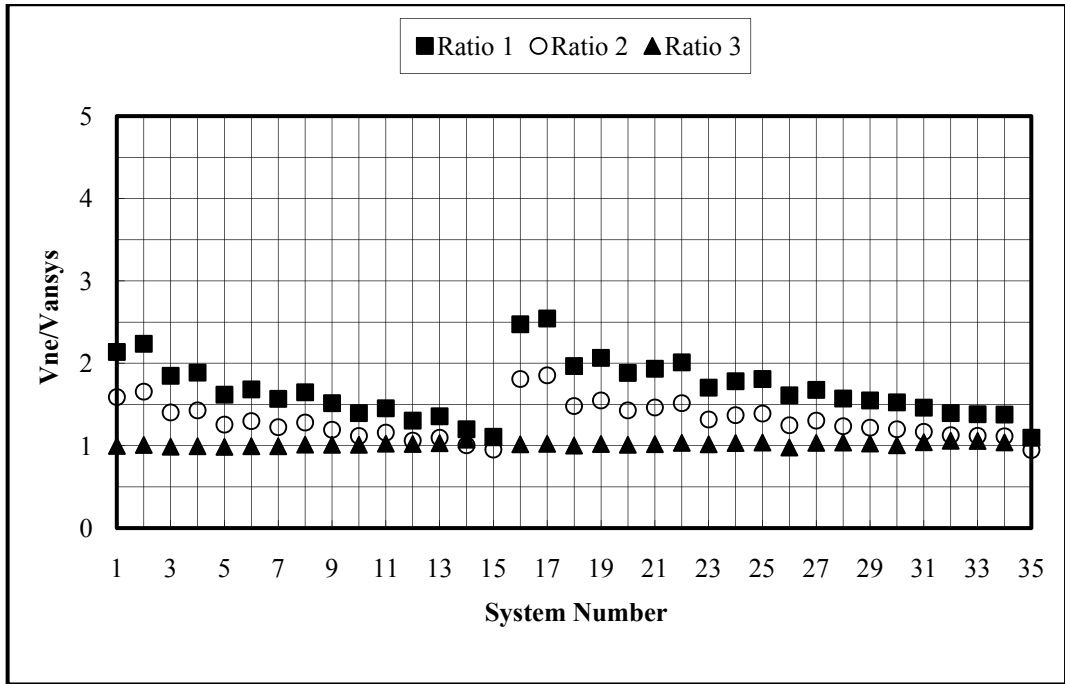


Figure 4.8: Ratio of Predicted to the Results of Analysis for Systems with A572-Gr50 Type of Steel – 2.5m  $L_s$

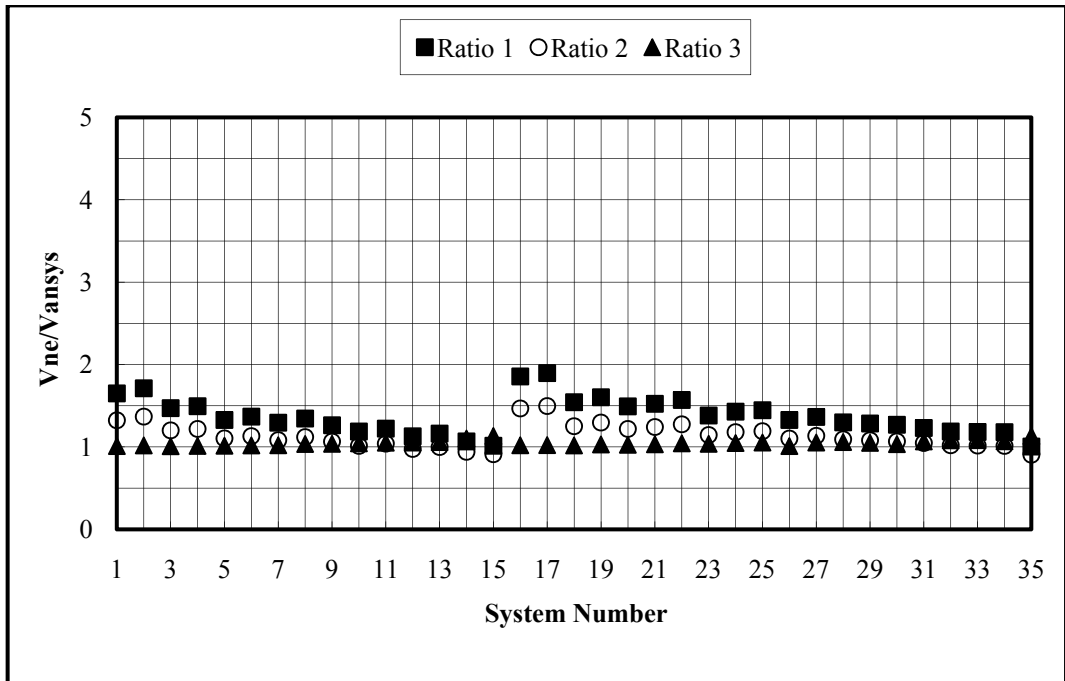


Figure 4.9: Ratio of Predicted to the Results of Analysis for Systems with A572-Gr50 Type of Steel – 3m  $L_s$

Table 4.11: Statistical Values for All Cases

Statistical Quantity	$V_{ne1}/V_{ansvs}$	$V_{ne2}/V_{ansvs}$	$V_{ne3}/V_{ansvs}$
Maximum	4.77	3.11	1.17
Minimum	1.01	0.91	0.94
Average	1.92	1.44	1.03
Standard Deviation	0.68	0.39	0.04

The formulation in the AISC Seismic Specification (2005) significantly overestimated the results. However, the updated version of this formulation, which was proposed by Chao and Goel (2008a), estimated the results better, as can be observed from the Tables 4.5 through 4.10. As the length of the special segment increases and the moment of inertia of the chord section decreases, the result of the formulation proposed by Chao and Goel (2008a) is closer to the result of the finite element analysis. As the length of the special segment increases and the moment of inertia of the section decreases, the stiffness of the chord member in the special segment decreases. Therefore, the stiffness of the chord member in the special segment is significantly lower than the stiffness of the neighboring chord members. As a result of this, the end conditions of the chord member in the special segment approaches to the fixed-end case and the elastic stiffness assumption of Chao and Goel (2008a), as discussed in the first section, is appropriate. However, for smaller lengths of the special segment and chord sections with higher moment of inertia, the proposed formulation by Chao and Goel (2008a) significantly overestimated the results.

The proposed formulation in this chapter, Equation 4.12, showed a good agreement with the analysis results, as shown from the Figure 4.4 through 4.9. This proposed formulation is only 6 percent unconservative, as shown from the Table 4.11. This value is tolerable for design purposes. Moreover, the accuracy of the proposed formulation is the best when compared with the other formulations, as indicated in Table 4.11.

## CHAPTER 5

### AN EVALUATION OF SHEAR CONTRIBUTION BY X-DIAGONALS FOR STMF SYSTEMS

The special segments in STMF systems can include X-braces. The design of the special segments with X-bracing is similar to the design of vierendeel segments. First of all, the required shear strength of the special segment is determined by considering all possible load combinations. The AISC Seismic Specification (2005) mandates that the shear resistance of the X-diagonals be limited to 75 percent of the total shear resistance. In other words, at least 25 percent of the shear force should be resisted by the chord members.

Unlike the provisions for braced frames there are no specific brace slenderness requirements for the X-braces in STMF systems. In fact the use of flat bars as X-bracing is recommended in the AISC Seismic Specification (2005). Therefore, engineers can choose very slender members that have low energy dissipating capacity.

In this chapter, the shear contribution of the X-diagonals to the total required shear strength, named as the load share, as well as the influence of brace slenderness are evaluated from a performance-based point of view.

#### 5.1 Methodology and Design of the Systems

To be able to compare X-diagonals with different load shares, five different systems were considered. The load shares of these systems were 10%, 25%, 50%, 75%, and 90%. Moreover, for each load share of the X-diagonals, the diagonal elements in the special segment were designed by using two extreme values of slenderness, which

were zero and infinity. For the systems having X-diagonals with zero slenderness, the diagonals can develop their yield strength capacity under compression. For the systems having X-diagonals with infinite slenderness, the diagonals have no compression strength. The extreme slenderness values were considered to study the effects of the slenderness of the X-diagonals on the performance of the whole system.

The model studied is a one story frame, which has a span length of 10m, a panel length of 1m, a special segment consisted of two panels and a height of 3.5m, as shown in Figure 5.1.

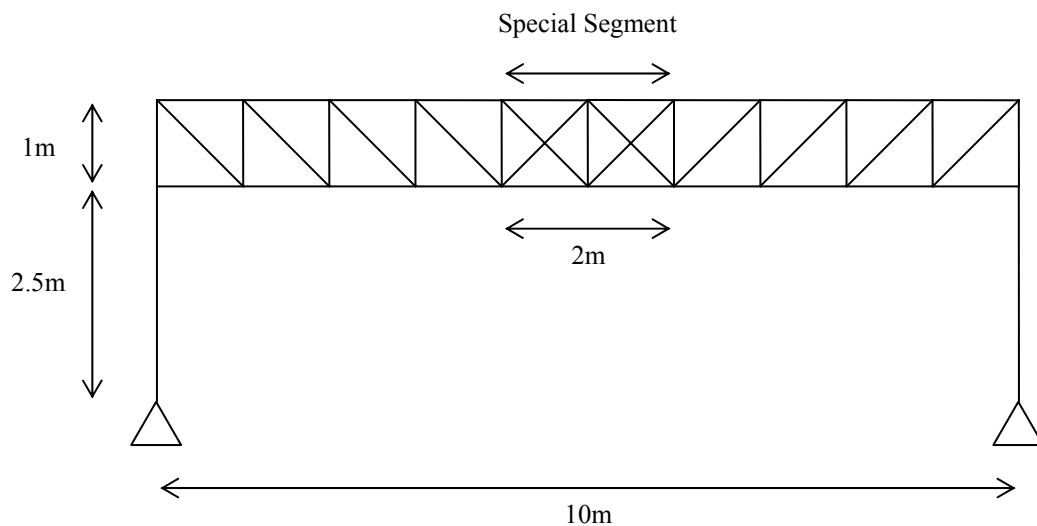


Figure 5.1: Geometrical Properties of the Systems

The member sections outside the special segment were the same in order not to introduce any other parameters to the study. All the members outside the special segment were modeled with elastic elements, as given in Table 5.1.

The members inside the special segment, namely the chord members and the X-diagonals, were selected by considering the load share and the slenderness of the X-diagonals. The shear strength of the special segment was taken as 360 kN and kept

constant for each case to be able to make a fair comparison between the different systems. The cross-section types, material properties, and element types for each case are given in Table 5.2.

Table 5.1: The Members outside the Special Segment

Load Share %	Slenderness of X-Diagonals inside the S.S.	Element	Section	Element Model
For All Load Shares	For All Slenderness Values	Columns	W14x370	Elastic Beam-Column
		Chords outside the S.S.	2MC12x35	Elastic Beam-Column
		Diagonals outside the S.S.	2L5x5x5/16	Truss
		Verticals	2L3x3x1/2	Truss

A bilinear kinematic hardening with 1 percent of the initial elastic modulus of the material, as verified in Chapter 2, was used for the modeling material behavior of the chords. However, for the material of the diagonals of the special segment, elastic perfectly plastic material was used. The diagonals with zero slenderness were modeled with ordinary two node truss elements. For diagonals with infinite slenderness, tension-only truss elements were utilized. It should be mentioned that certain amount of inaccuracy is introduced by modeling the braces as tension-only elements. Basically, from a strength point of view these elements are capable of representing the loss of strength under compressive forces. However, from a stiffness point of view the loss of stiffness due to buckling is not adequately addressed. In earlier stages of research, the braces were modeled with beam-column elements as recommended by Uriz, Fillipou, and Mahin (2008). The recommended formulation failed to capture the response of the braces under earthquake excitation. Therefore, an alternative modeling technique was adopted in this study.

Table 5.2: The Members inside the Special Segment

Load Share %	Slenderness of X-Diagonals inside the S.S.	Element	Section	$Z_x$ mm <sup>3</sup>	A mm <sup>2</sup>	Element Model	$F_y$ MPa
10	Zero	Chords inside the S.S.	2C10x15.3	$5.21 \times 10^5$	2890.32	Nonlinear Beam-Column	310
		Diagonals inside the S.S.	-	-	72.73	Truss	310
	Infinity	Chords inside the S.S.	2C10x15.3	$5.21 \times 10^5$	2890.32	Nonlinear Beam-Column	310
		Diagonals inside the S.S.	-	-	145.46	Truss	310
25	Zero	Chords inside the S.S.	2C9x13.4	$4.13 \times 10^5$	5083.86	Nonlinear Beam-Column	335
		Diagonals inside the S.S.	-	-	181.83	Truss	335
	Infinity	Chords inside the S.S.	2C9x13.4	$4.13 \times 10^5$	5083.86	Nonlinear Beam-Column	335
		Diagonals inside the S.S.	-	-	363.66	Truss	335
50	Zero	Chords inside the S.S.	2C7x12.2	$2.77 \times 10^5$	4645.15	Nonlinear Beam-Column	350
		Diagonals inside the S.S.	-	-	363.66	Truss	350
	Infinity	Chords inside the S.S.	2C7x12.2	$2.77 \times 10^5$	4645.15	Nonlinear Beam-Column	350
		Diagonals inside the S.S.	-	-	727.32	Truss	350
75	Zero	Chords inside the S.S.	2C5x9	$1.44 \times 10^5$	3406.45	Nonlinear Beam-Column	360
		Diagonals inside the S.S.	-	-	545.48	Truss	360
	Infinity	Chords inside the S.S.	2C5x9	$1.44 \times 10^5$	3406.45	Nonlinear Beam-Column	360
		Diagonals inside the S.S.	-	-	1090.96	Truss	360

Table 5.2 (continued)

Load Share %	Slenderness of X-Diagonals inside the S.S.	Element	Section	$Z_x$ mm <sup>3</sup>	A mm <sup>2</sup>	Element Model	$F_y$ MPa
90	Zero	Chords inside the S.S.	2C3x6	$0.57 \times 10^5$	2270.96	Nonlinear Beam-Column	370
		Diagonals inside the S.S.	-	-	654.58	Truss	370
	Infinity	Chords inside the S.S.	2C3x6	$0.57 \times 10^5$	2270.96	Nonlinear Beam-Column	370
		Diagonals inside the S.S.	-	-	1309.16	Truss	370

## 5.2 Static Pushover Analysis and Natural Periods

A set of pushover analysis was conducted to verify the designs in terms of a strength point of view. The idea was to prove that the systems selected essentially provide the same amount of lateral strength at a lateral drift of 3%. The pushover characteristic of the systems having the X-diagonal members inside the special segment with zero slenderness and infinite slenderness are given in Figure 5.2 and Figure 5.3, respectively.

As shown from the Figures 5.2 and 5.3, the capacities of the models are close to each other and reach to 1100 kN at 3 percent lateral drift. Moreover, as the load share of X-diagonals increase, the stiffness of the system also increases. This is natural because as the load share increases, the behavior shifts from a moment frame behavior to a braced frame behavior.

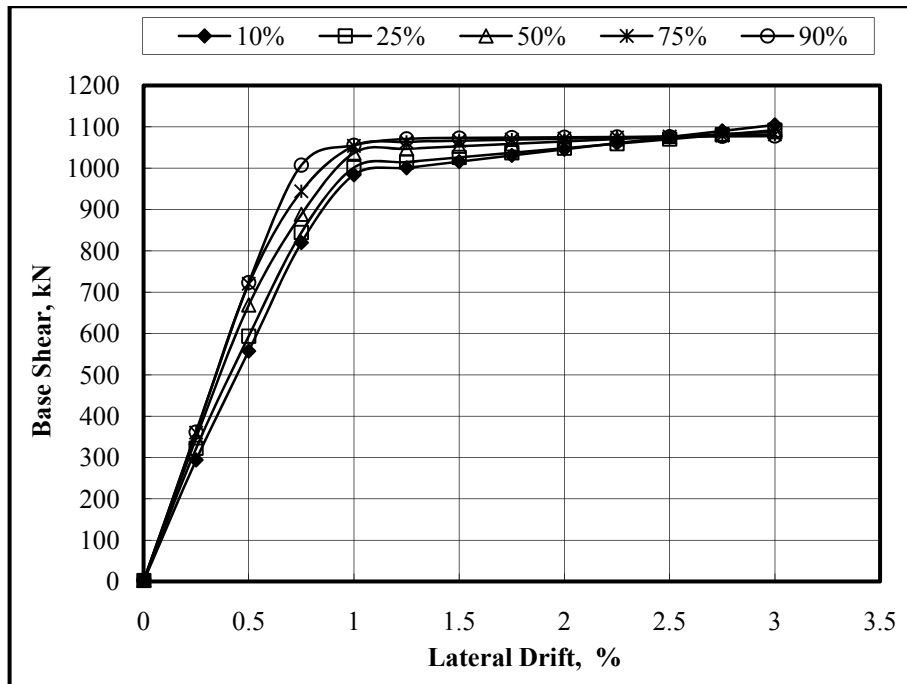


Figure 5.2: Pushover Analysis Results for Systems Having X-Diagonals with Zero Slenderness

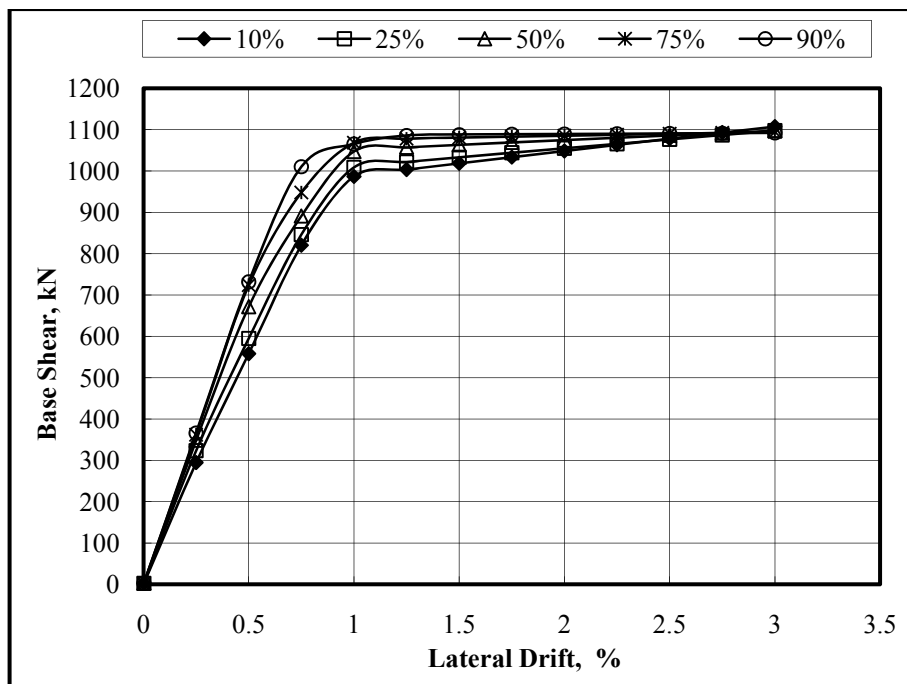


Figure 5.3: Pushover Analysis Results for Systems Having X-Diagonals with Infinite Slenderness

The responses of the systems for cyclic pushover analysis are needed to evaluate the effect of different slenderness values on the strength of the systems. The results of the cyclic pushover analysis are given in Figure 5.4 and Figure 5.5, for the systems having X-diagonals with zero slenderness and with infinite slenderness, respectively. For systems having X-diagonals with zero slenderness, there is no degradation in the strength and stiffness, as shown in Figure 5.4. However, for systems having X-diagonals with infinite slenderness, the pinching of system takes place, as shown in Figure 5.5. The degree of pinching significantly increases, when the load share of X-diagonals increases, as expected, since the X-diagonal members in the special segment do not carry compressive forces.

Apart from pushover analysis, an eigenvalue analysis was conducted for each STMF to obtain the natural period of the systems. The natural period and the mass properties of the systems are given in Table 5.3.

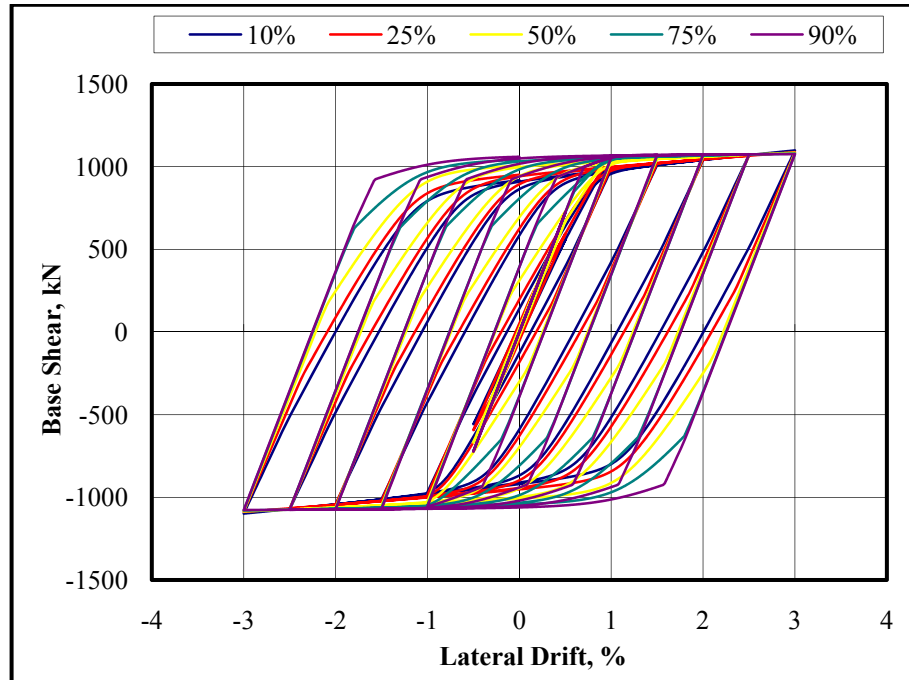


Figure 5.4: Cyclic Pushover Analysis Results for Systems Having X-Diagonals with Zero Slenderness

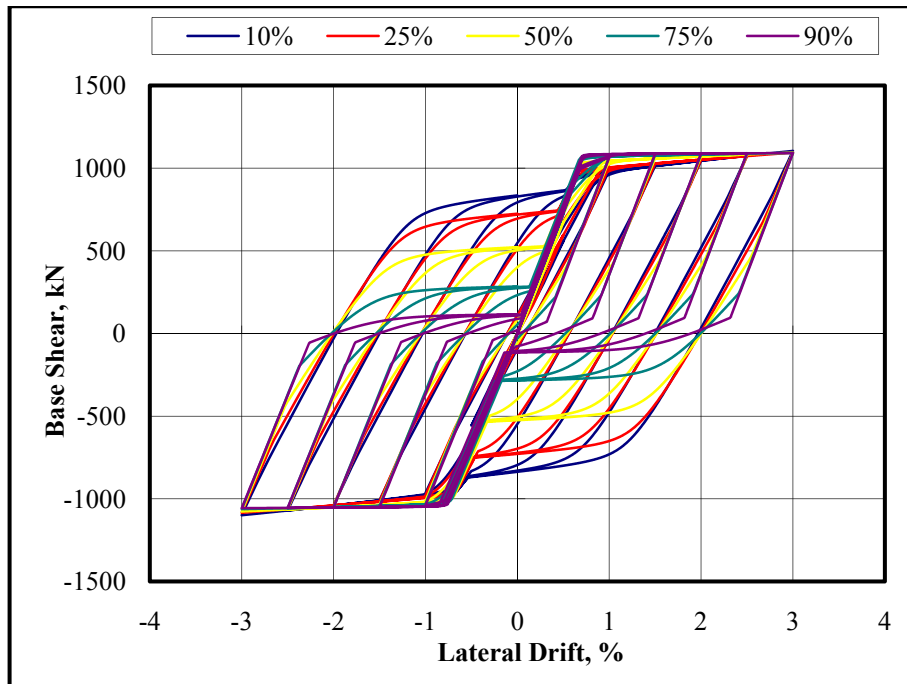


Figure 5.5: Cyclic Pushover Analysis Results for Systems Having X-Diagonals with Infinite Slenderness

Table 5.3: Natural Period and Mass of the STMF Systems

Load Share %	Slenderness of X-Diagonals inside the S.S.	Mass ton	T sec
10	Zero	125	0.376
	Infinity	125	0.363
25	Zero	125	0.360
	Infinity	125	0.344
50	Zero	125	0.346
	Infinity	125	0.333
75	Zero	125	0.339
	Infinity	125	0.328
90	Zero	125	0.336
	Infinity	125	0.327

As shown in Table 5.3, as the load share of the X-diagonals increases, the natural period decreases, in other words, the stiffness of the system increases. For a particular load share, the natural period of the system having X-diagonals with infinite slenderness is slightly lower than the natural period of the system having X-diagonals with zero slenderness, as shown in Table 5.3. This is because the area of X-diagonals with infinite slenderness needs to be twice the area of its counterpart to keep the same level of strength. Therefore, the stiffness of the systems having X-diagonals with infinite slenderness is greater than the other one, in other words, these systems have a lower natural periods than the others. However, in a general sense, the natural periods of the systems are close to each other.

### **5.3 Time-History Analysis**

A set of time-history analysis were conducted to study the behavior of systems under earthquake loading. All structures were subjected to a suite of ground motions listed in Table 3.4, except the twentieth ground motion. The twentieth ground motion was excluded from the set because it produced numerical instabilities in the solution process. A stiffness proportional damping equal to 2 percent of the critical damping was considered in all analysis.

During a typical analysis, story drift, curvatures at the chords of the special segment, the base shear, and the axial strain at the X-diagonals were recorded.

#### **5.3.1 Results of Time-History Analysis**

In order to compare the performance of the systems, the average values of the recorded maximum responses obtained from the analysis of nineteen different ground motions were considered. In Table 5.4, the average values of the results of time-history analysis are tabulated. In this table, curvature at the chords of the special segment and axial strain at the X-diagonals are normalized with the plastic curvature and yield axial strain, respectively. These normalizations were used for expressing the curvatures and the axial strains in terms of demands and provided a fair

comparison tool between different designs. Moreover, the graphical illustrations of the time-history analysis results are given in Figures 5.6 through 5.9.

Table 5.4: The Average Values of the Results of Time History Analysis

Load Share	10%		25%		50%		75%		90%	
	0	$\infty$	0	$\infty$	0	$\infty$	0	$\infty$	0	$\infty$
$(k/k_p)_{\text{average}}$	40.5	36.6	30.0	31.0	18.8	20.7	10.9	13.6	4.5	7.1
$(\varepsilon/\varepsilon_y)_{\text{average}}$	19.3	18.0	16.2	16.5	13.8	14.6	11.9	13.5	10.5	13.1
$(V_b)_{\text{average}}$ kN	931	931	939	946	969	988	981	1035	1007	1042
$(\Delta/h)_{\text{average}}$ %	1.40	1.34	1.32	1.34	1.25	1.30	1.17	1.27	1.12	1.28

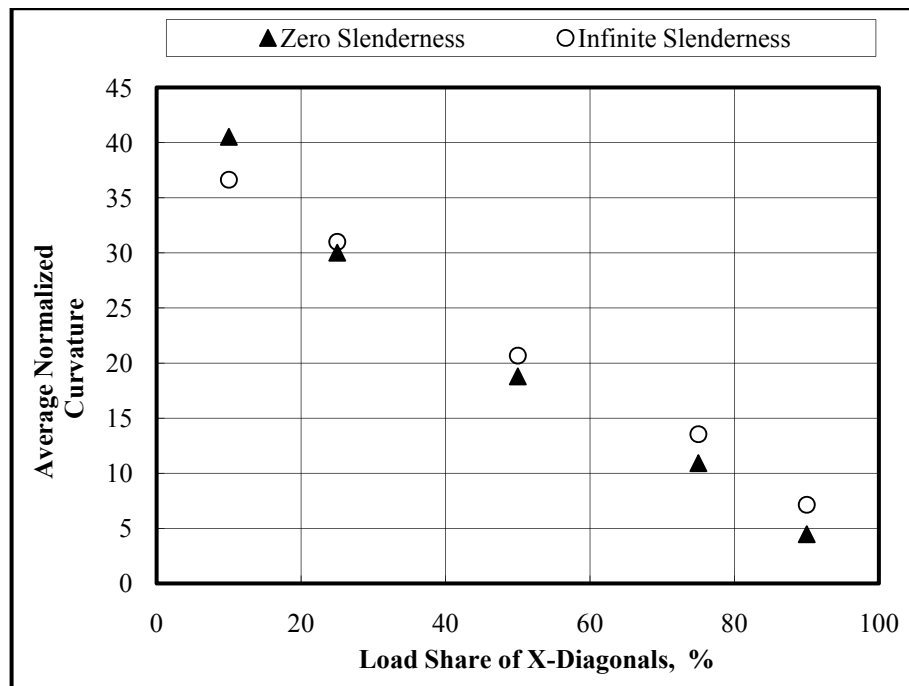


Figure 5.6: Average Normalized Curvature Values for Different Design Types

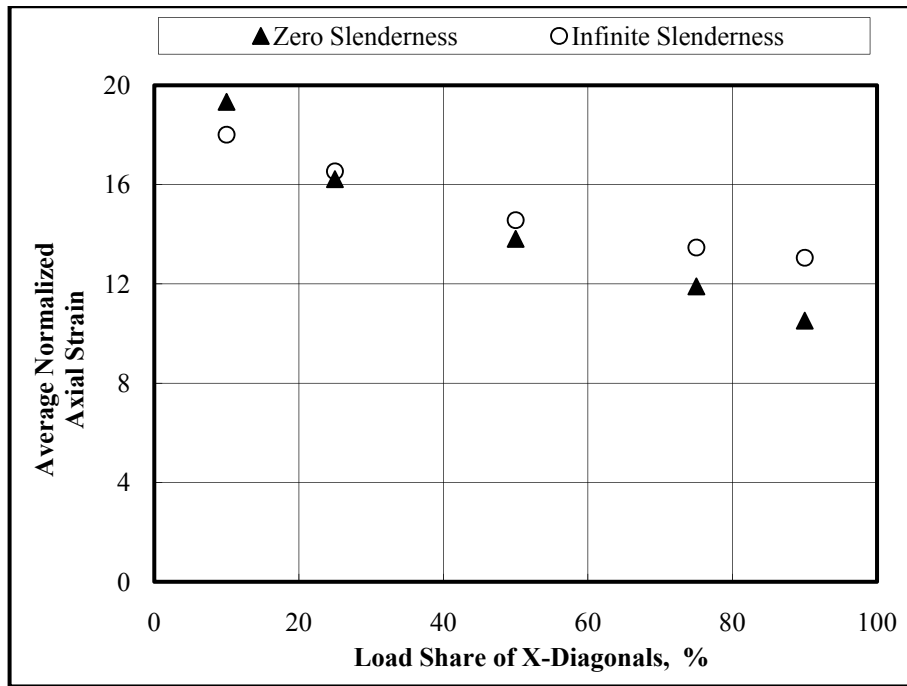


Figure 5.7: Average Normalized Axial Strain Values for Different Design Types

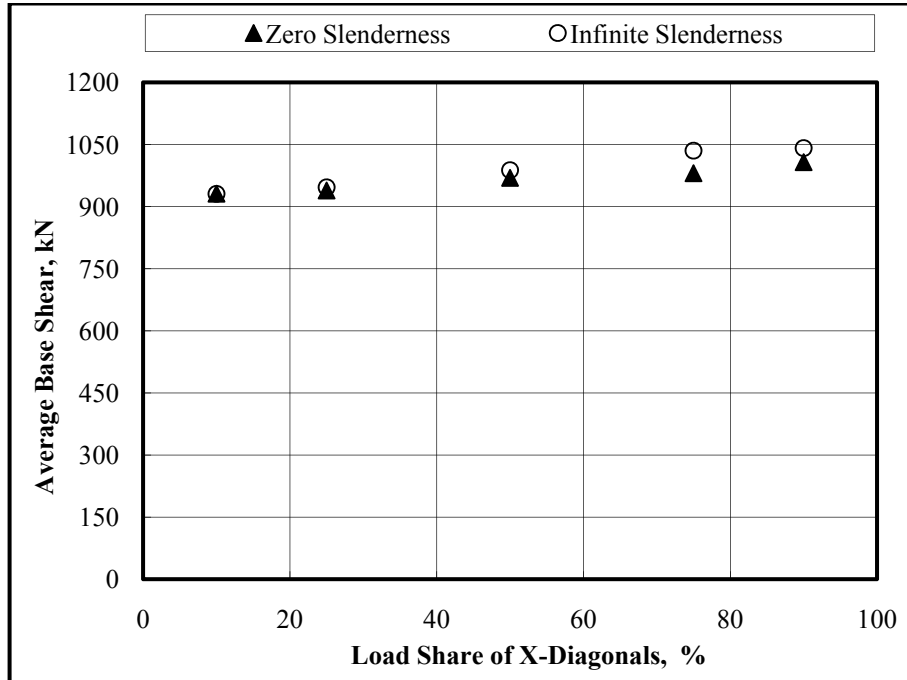


Figure 5.8: Average Base Shear Values for Different Design Types

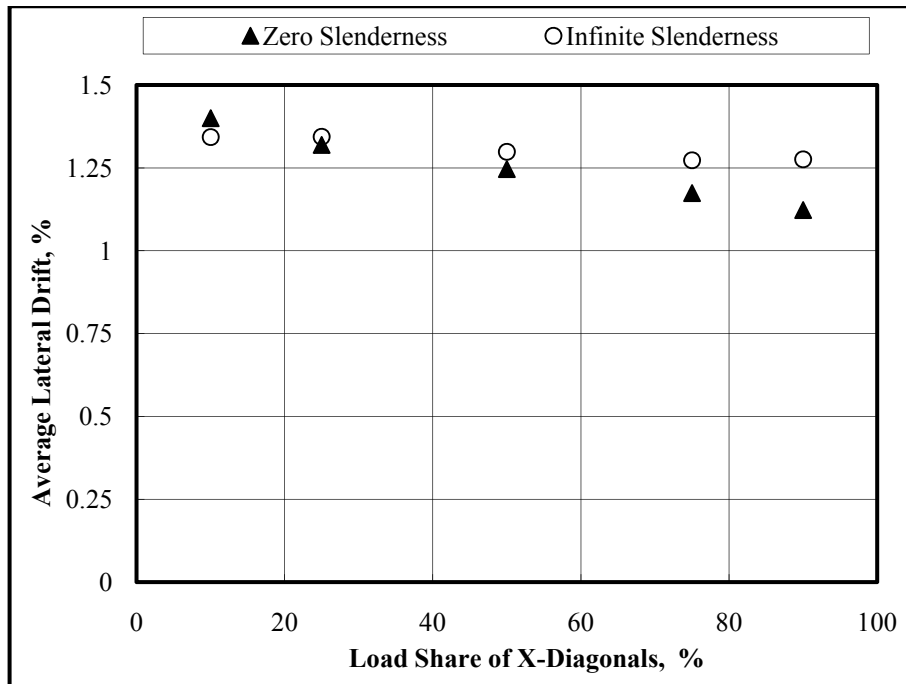


Figure 5.9: Average Lateral Drift Values for Different Design Types

As the load share of the X-diagonals increases, the average normalized curvature decreases, as shown from Figure 5.6. This is due to the fact that the behavior of the system switches from Moment Resisting Frame (MRF) to Concentrically Braced Frame (CBF), as the load share of the X-diagonals increases. Moreover, the average normalized axial strain reduces with increasing load share of the X-diagonals, as shown from Figure 5.7, since less deformation take place when the system behaves like a CBF.

The average drift values decrease for systems having X-diagonals with zero slenderness and these values are almost constant for infinite slenderness case, as the load share of the X-diagonals increases, as shown from Figure 5.9. For a particular load share greater than 10 percent, average base shear and average drift values of the infinite slenderness case are greater than the values of the zero slenderness case, as shown from Figure 5.8 and Figure 5.9, respectively. Moreover, for a particular load share, the average normalized axial strains are similar for systems with different slenderness values, as shown from Figure 5.7. The average normalized curvatures are

similar for systems with different slenderness values for a particular load distribution up to 90 percent load share, as shown from Figure 5.6.

To conclude, the amount of the load share of the X-diagonals has a significant effect on the behavior of the system. If this amount increases then the system behavior switches from MRF to CBF. However, although two theoretically extreme slenderness values were used, the slenderness value of the X-diagonals does not have any significant effects on the seismic performance of the system.

## CHAPTER 6

### CONCLUSIONS

The thesis work consisted of a three phase of numerical study on STMF systems. The numerical analyses of phase 1 and 3 was conducted using OPENSEES, while 3-D finite element analyses of phase 2 was performed using ANSYS.

For the first phase of the study, the seismic behavior of STMF system with a vierendeel special segment designed using three different methodologies was explored. Six, nine, and twelve story frames were designed using plastic and elastic design methods. Elastic design of frames was conducted using IT (inverted triangular) and CGL (proposed by Chao, Goel, and Lee (2008b)) lateral load distributions. The results of static pushover analysis and time-history analysis were utilized in order to compare the strength and the seismic performance of the systems.

For the second phase of the study, the expected vertical shear strength formulations were evaluated using three dimensional finite element analysis results. A single story STMF system with vierendeel special segment was considered. The parameters were the chord section in the special segment and the length of the special segment. For thirty five double channel sections and three different lengths of special segment, pushover analyses up to 3 percent lateral drift were conducted. The earlier formulations and the formulation developed in this phase, Equation 4.12, were compared with the finite element analysis results.

For the third phase of the study, single story STMF systems with X-diagonal special segment were evaluated in terms of the shear contribution and the slenderness of the

X-diagonals. To accomplish this, the frames were designed considering five different load shares of X-diagonals. For each load share, X-diagonals were designed with zero and infinite slenderness values. In order to compare the strength and the seismic performance of the frames, static pushover and time-history analyses were conducted.

The following can be concluded from the first phase of the study:

- For all types of design and all heights, the maximum base shear and maximum top story drift relation obtained from time-history analysis results can be best predicted using the static pushover analysis with the equal lateral load distribution.
- For ED-IT and ED-CGL, there were no significant changes in plastic rotations and story drifts. The ED-CGL improved the behavior at some levels and deteriorated in others. Since the use of the ED-CGL is based on predicting the natural period of the system before the design is finalized, the ED-IT is more useful.
- Utilizing PD increased the lateral drifts at bottom stories, however, decreased the lateral drifts at the top stories. While the use of PD increased the plastic rotations at bottom stories, significantly reduced them at the top stories. As long as the increases in the lateral drift and in the plastic rotation at bottom stories are tolerable, using PD is a viable option.

The following can be concluded from the second phase of the study:

- The elastic stiffness of the chord member in the special segment assumption proposed by Chao and Goel (2008a) was not appropriate for all lengths of special segment and chord sections.
- The expected vertical shear strength of the special segment formulation in the AISC Seismic Specification (2005) was found to be overly conservative.
- The expected vertical shear strength formulation developed by Chao and Goel (2008a) is better than the AISC formulation, however, overestimated the

results of the finite element analysis for smaller special segment lengths and chord sections with higher moment of inertia.

- The proposed formulation in this phase of the study, Equation 4.12, was derived for STMFs having double channel chord members. This formulation showed a good agreement with the analysis results and was only 6 percent unconservative.

The following can be concluded from the third phase of the study:

- As the load share of the X-diagonals increased, the average drift values decreased for systems having X-diagonals with zero slenderness and these values were almost constant for infinite slenderness case. Moreover, with increasing load share of the X-diagonals, average base shear values increased and average normalized curvature and axial strain values decreased.
- As the load share of X-diagonals increased, the behavior of the system switched from MRF to CBF. Therefore, fewer deformations took place.
- The slenderness of the X-diagonals in the special segment did not have any significant effects on the seismic response of the system.

### **Future Research Needs**

- The final steel weight of the STMF systems with a vierendeel opening designed using ED-IT and PD can be compared for economical point of view.
- The expected vertical shear strength at vierendeel opening formulation can be examined for multistory STMFs and more experimental research is needed to further verify the accuracy of it.
- The effects of the slenderness and the load share of the X-diagonals on the behavior of multistory systems can be evaluated.
- The existing and newly developed provisions for STMFs can take place in Eurocodes.

## REFERENCES

- AISC, 2005. Seismic Provisions for Structural Steel Buildings, ANSI/AISC 341-05, American Institute of Steel Construction, Chicago, Ill.
- ANSYS. Version 8.1 on-line user's manual; 2006.
- Aslani, H.O. (1998). Special truss moment frames under combined gravity and lateral loads. Dissertation, The University of Michigan, Ann Arbor, MI.
- Basha, H.S., and Goel, S.C. (1994). Seismic resistant truss moment frames with ductile vierendeel segment. *Report No. UMCEE 94-29*, Department of Civil and Environmental Engineering, The University of Michigan, Ann Arbor, MI.
- Chao, S., and Goel, S.C. (2006). Performance based plastic design of special truss moment frames. *Report No. UMCEE 06-03*, Department of Civil and Environmental Engineering, The University of Michigan, Ann Arbor, MI.
- Chao, S., and Goel, S.C. (2008a). A modified equation for expected maximum shear strength of the special segment for design of special truss moment frames. *Engineering Journal*; **45**(2): 117-125.
- Chao, S., and Goel, S.C. (2008b). Performance-based plastic design of special truss moment frames. *Engineering Journal*; **45**(2): 127-150.
- Chao, S., Goel, S.C., and Lee, S.S. (2007). A seismic design lateral force distribution based on inelastic state of structures. *Earthquake Spectra*; **23**(3): 547-569.
- Goel, S.C., and Itani, A.M. (1994a). Seismic behavior of open-web truss-moment frames. *Journal of Structural Engineering*; **120**(6): 1763-1780.
- Goel, S.C., and Itani, A.M. (1994b). Seismic-resistant special truss-moment frames. *Journal of Structural Engineering*; **120**(6): 1781-1797.
- Goel S.C., Leelataviwat S., and Stojadinovic B. (1997). Steel moment frames with ductile girder web openings. *AISC Engineering Journal*; Fourth Quarter: 115-125.
- Goel, S.C., Rai, D.C., and Basha, H.S. (1998). Special truss moment frames design guide. *Report No. UMCEE 98-44*, Department of Civil and Environmental Engineering, The University of Michigan, Ann Arbor, MI.

Ireland, R.C. (1997). Special truss moment frames in low to moderate seismic regions with wind. Dissertation, The University of Michigan, Ann Arbor, MI.

OPENSEES. Version 2.0 user command-language manual; 2009.

Parra-Montesinos, G.J., Goel, S.C., and Kim, K.Y. (2006). Behavior of steel double-channel built-up chords of special truss moment frames under reversed cyclic loading. *Journal of Structural Engineering*; **132**(9): 1343-1351.

Uriz, P., Filippou, F.C., and Mahin, S.A. (2008). Model for cyclic inelastic buckling of steel braces. *Journal of Structural Engineering*; **134**(4): 619-628.